AD-A078 434 YALE UNIV NEW HAVEN CT SYSTEMS AND INFORMATION SCIENCES F/G 20/1
SURFACE SCATTERING STUDIES.(U)
AUG 79 J G ZORNIG , P M SCHULTHEISS N00014-75-C-1014
UNCLASSIFIED S/IS-7905 NL

1 OF 2
AD A078434

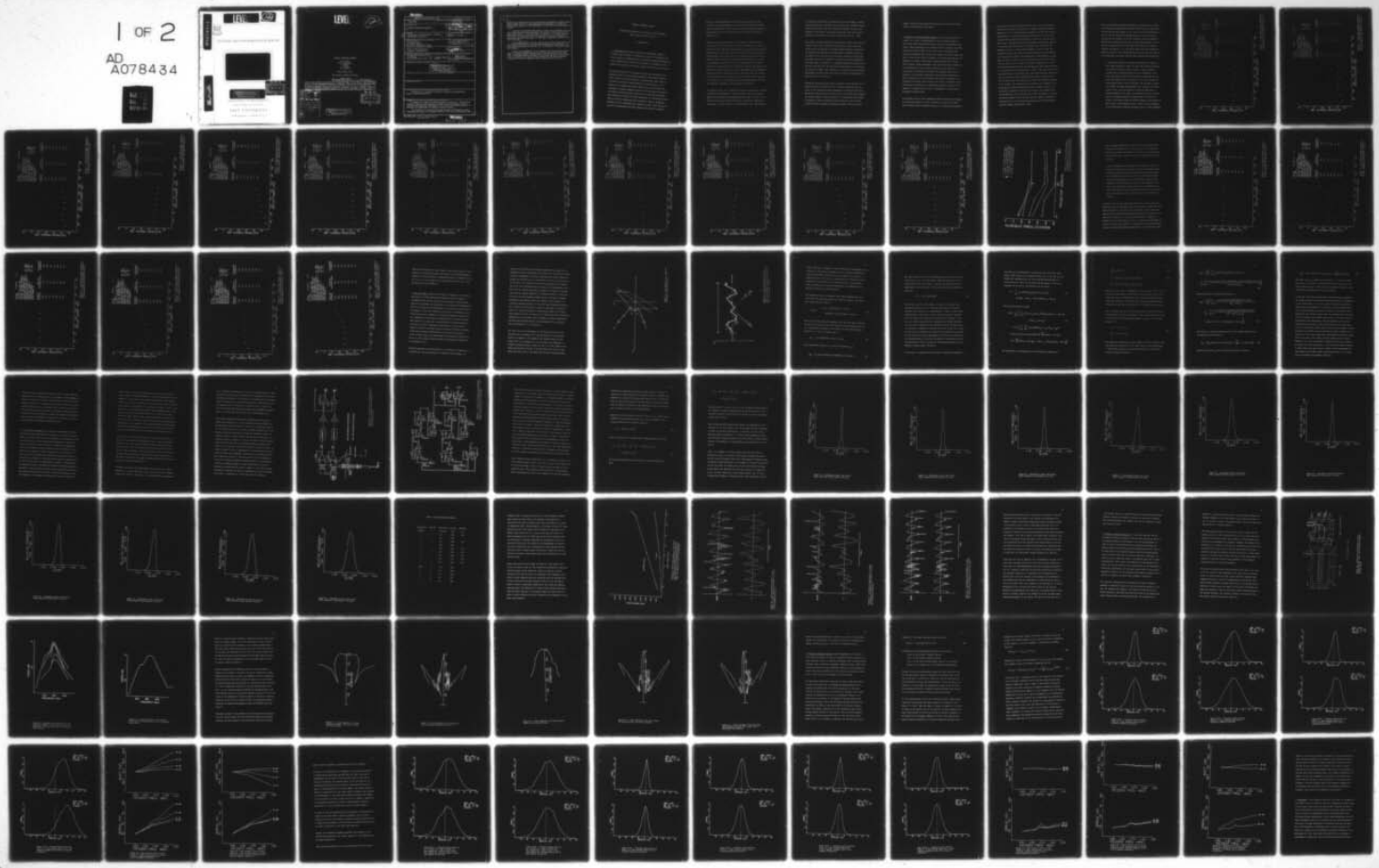

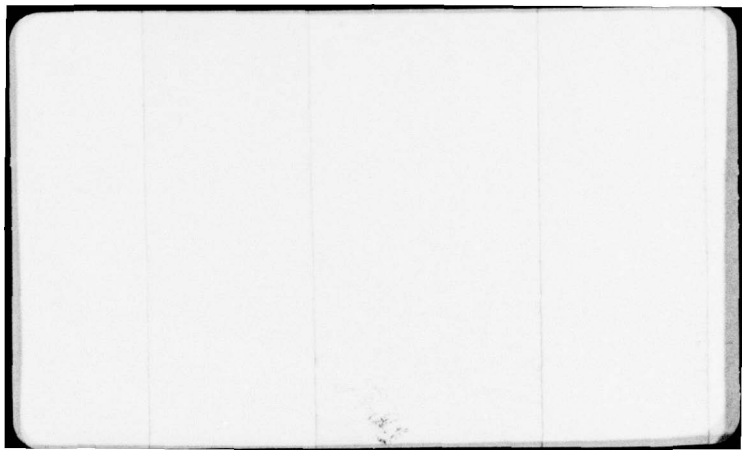

LEVEL II

12

SURFACE SCATTERING STUDIES

J.G. Zornig
P.M. Schultheiss
J. Snyder
S. Singhal
D.C. Gilbert

Final Report #7905

ONR Contract #N00014-75-C-1014

August 1979

UNCLASSIFIED

REPORT DOCUMENTATION PAGE	READ INSTRUCTIONS BEFORE COMPLETING FORM
1. REPORT NUMBER: S&IS 7905 / 2. GOVT ACCESSION NO	3. RECIPIENT'S CATALOG NUMBER: (Rept.)
4. TITLE (and Subtitle): (6) SURFACE SCATTERING STUDIES,	5. TYPE OF REPORT & PERIOD COVERED: (9) Final / Apr[redacted]78-Jun[redacted]79
	6. PERFORMING ORG. REPORT NUMBER: 7905
7. AUTHOR(s): (10) J.G. Zornig, P.M. Schultheiss, J. Snyder, S. Singhal, D.C. Gilbert	8. CONTRACT OR GRANT NUMBER(s): (15) N00014-75-C-1014
9. PERFORMING ORGANIZATION NAME AND ADDRESS: Yale University, 15 Prospect Street, New Haven, Connecticut 06520	10. PROGRAM ELEMENT, PROJECT, TASK AREA & WORK UNIT NUMBERS: NRL Req. N000173-75-RQ-6410/3-14-75 (12) 99
11. CONTROLLING OFFICE NAME AND ADDRESS: (11) Office of Naval Research, Arlington, Virginia 22217	12. REPORT DATE: Aug[redacted]979
	13. NUMBER OF PAGES: 90
14. MONITORING AGENCY NAME & ADDRESS (if different from Controlling Office): ONR Resident Representative, 715 Broadway, New York, New York 10003 (14) S/IS-7905	15. SECURITY CLASS. (of this report): U UNCLASSIFIED
	15a. DECLASSIFICATION/DOWNGRADING SCHEDULE

16. DISTRIBUTION STATEMENT (of this Report) The cont

DISTRIBUTION STATEMENT A
Approved for public release;
Distribution Unlimited

17. DISTRIBUTION STATEMENT (of the abstract entered in Block 20, if different from Report)

18. SUPPLEMENTARY NOTES

19. KEY WORDS (Continue on reverse side if necessary and identify by block number)

Communication, Underwater Acoustics, Scattering, Reverberation, Doppler, Surface Statistics.

20. ABSTRACT (Continue on reverse side if necessary and identify by block number)

Progress in a number of ongoing projects is reported. These include studies of bistatic and monostatic surface scattering strength, surface reverberation modelling, measurement of slope and correlation statistics of surfaces, and measurement of Doppler shifts and spread.

The extension of previous scattering strength measurements to lower frequencies has shown the strengths observed to be 10 to 15 dB higher under

DD FORM 1 JAN 73 1473 EDITION OF 1 NOV 65 IS OBSOLETE
S/N 0102-014-6601

UNCLASSIFIED

410 225

similar wind conditions but with wavelengths approximately 8 times longer. These studies have led to the beginning of development of a model for reverberation based on a characterization of the surface as an ensemble of facets.

A method for precision measurement of model tank waveheight and wave slope time series has been developed. The system is based on fine wire capacitance probes. It has been used to compile a set of slope measurements which is consistent with data reported by other investigators. A system for automatic measurement of time-space waveheight correlation has been developed.

A seventeen element, 320 kHz. linear array having a beam width of 4^{o} and sidelobe ejection of 23 dB. has been designed and constructed. The array uses foam backed PZT elements and is intended for low grazing angle measurements.

Additional measurements of the alignment and wind direction dependence of frequency spread and mean shift in forward scatter have been made. These measurements indicate that shift and spread are quite sensitive to alignment error in crosswind orientations but that even under conditions of precise alignment, some frequency shift does occur.

SURFACE SCATTERING STUDIES

Final Report Submitted to the Office of Naval Research

Under Contract N00014-75-C-1014

10 August 1979

1. Introduction: During the contract year as amended a number of projects were initiated or continued in support of the general contract objective, characterization of acoustic scattering strength from wind roughened water surfaces. This document is a statement of progress as of the end of the contract period for each of these projects.

The principal effort of the program has been the continuation of an empirical study of the scattering strength of wind driven surfaces under bistatic as well as monostatic configurations. This study was initiated to provide a characterization of this statistic in the absence of any working theoretical formulation so as to permit the refinement of global propagation models to include surface reverberation effects. During previous contract years a precision goniometer was constructed to permit efficient measurement of scattering strength under a variety of geometries and an extensive study of scattering strength at short wavelengths was conducted [Zornig, 1978]. During the past year the goniometer has been improved and a series of measure-

ments of scattering strength at much longer wavelengths has been conducted. These measurements have revealed some substantial differences in the behavior of the statistic at these wavelengths which will be described later in this report and which indicate the need for further study.

Motivated in part by the results of the empirical studies at this facility and in part by the work of other investigators, a basis for a theoretical model has been formulated during the past few months which shows promise of explaining some or all of the results of the experimental program. This work, which is an extension of previous work of Patterson [1964] and Novarini and Medwin [1978], attempts to explain the reverberant field of an insonified rough surface as the result diffractive interactions with an idealized piecewise plane surface the statistics of which can be derived from measurements of the height and slope statistics of the actual surface. The model, while by no means fully developed, does incorporate effects which are clearly important in reverberation at low grazing angles and long wavelengths but which are neglected in Helmholtz integral based formulations.

In a separate study also continuing previously reported work, a number of additional measurements of Doppler spread in the high roughness domain have been made. These measurements were made in order to clarify the relationship between beam pattern orientation, orientation with respect to wind direction, and mean Doppler shift. The results of

this series of experiments, reported later in this document, indicate that the prediction of Doppler shift and spread will probably require a more precise model than those presently available. This work has motivated a theoretical investigation supported under other auspices which will be published in the near future [Tuteur et al., 1979].

The acoustic studies conducted during previous contract years have all indicated that a more thorough characterization of the scattering surface would be required if any general model capable of explaining the phenomena observed were to be developed. Accordingly studies of the surface slope statistics and time-space covariance function were undertaken and will be documented in this report. These measurements were made using a refinement of a waveheight measuring apparatus which has been developed over the past several years based on a capacitance wire detection scheme. They exemplify a very high precision waveheight measurement capability which will used to extend the documentation of water surfaces in the future.

During past discussions with project sponsors of the direction of the modelling project at this facility, a recurrent theme has been the issue of very low grazing angle measurement of scattering statistics. During the contract period covered by this report funds were requested for partial support of the development of an ultrasonic array capable of producing a narrow sidelobeless beam pattern for use in future studies of heavily shadowed scattering processes. The array was de-

signed, constructed and characterized during the past year with success and is described in this report.

2. Bistatic Scattering Strength Studies: This section describes the results of a series of measurements of the scattering strength of short fetch model tank surfaces under a variety of experimental situations. These measurements were conducted using a technique described previously [Zornig, 1978] for the case of short wavelengths. The acoustic wavelengths used in this case, however, were much longer than those of the earlier study. In addition, scattering strengths were not measured for bistatic differential azimuths greater than 105 deg. (near forward). These measurements were omitted because of difficulty in obtaining data in near forward orientations that were free of direct path contributions and because the conceptual basis of the statistic is of doubtful usefulness in near-forward orientations in which contributions to the scattered field cannot be assumed to be uniformly distributed over the area of the surface insonified. These orientations are difficult to characterize primarily because of the absence of a simple statistic that is independent of the projector/hydrophone characteristics.

The procedure used in these experiments remains essentially unchanged. A directional projector is used to insonify a portion of the wind driven surface from a specified direction at a specified wavelength at

a relatively well defined frequency (more than 20 cycles per pulse). The projector used was a piezoelectric transducer having an effective aperture of 7.7 cm. and a principal resonance of 90 kHz. The transducer exhibited a reasonably piston-like beam pattern at the principal resonance and had sufficient response to be useful at 180 kHz and 360 kHz as well. The beam patterns at these harmonic frequencies appeared to be piston-like as well, but were somewhat less ideal than that measured at 90 kHz. A directional hydrophone is used to sense the scattered field at some other orientation during a precisely defined and constant time interval. The combination of beam patterns and time gate are used to compute, for each orientation, an effective insonification pattern on the surface. This pattern together with a calibration measurement made with the same apparatus from a smooth surface in a specular reflection orientation is used to calculate from the raw measured returns, the scattered power that would have been received at one yard from a uniformly insonified square yard of surface due to unit incident power. This statistic is called the scattering strength of the surface. The calculation of the statistic also depends on the spreading law governing reradiation from the surface. However, the experimental geometry was such that an error in the assumed form of the spreading law would have made only a small difference in computed scattering strength. There has been and still remains considerable controversy over the law governing spreading from rough scattering surfaces [Mikeska and McKinney, 1978].

Using this procedure scattering strengths were measured for a number of differential azimuths (the difference between projector and receiver orientations with respect to the center of the scattering area) at each of two wind speeds, two grazing angles, and three projector orientations with respect to the wind (upwind, crosswind, downwind). The surface statistics are the same as those used previously and are further documented later in this report. This basic set of data is presented as Figures 1 - 12. The plots differ from those presented in previous reports in that the backscatter direction is at the left end of the abscissa. From these data two basic observations are apparent:

a. Scattering strengths are apparently substantially higher at this longer wavelength. Figure 13. shows the scattering strength for backscatter from the Wind 4 surface at three projector orientations, two grazing angles and four wavelengths. It is clear from these results that the change of wavelength has produced what appears to be a consistent 10 to 15 dB. increase in scattering strength at all orientations. The increase is apparently higher at higher grazing angles, but whether it is proportional or not is an open question. As will be seen below, a recurring theme in this report is the speculation that reverberation at low grazing angles is primarily due to diffractive effects. If we believe that the surface behaves as an ensemble of plane facets, each reradiating with a pattern that is dependent on its size and the incident wavelength, then it seems reasonable

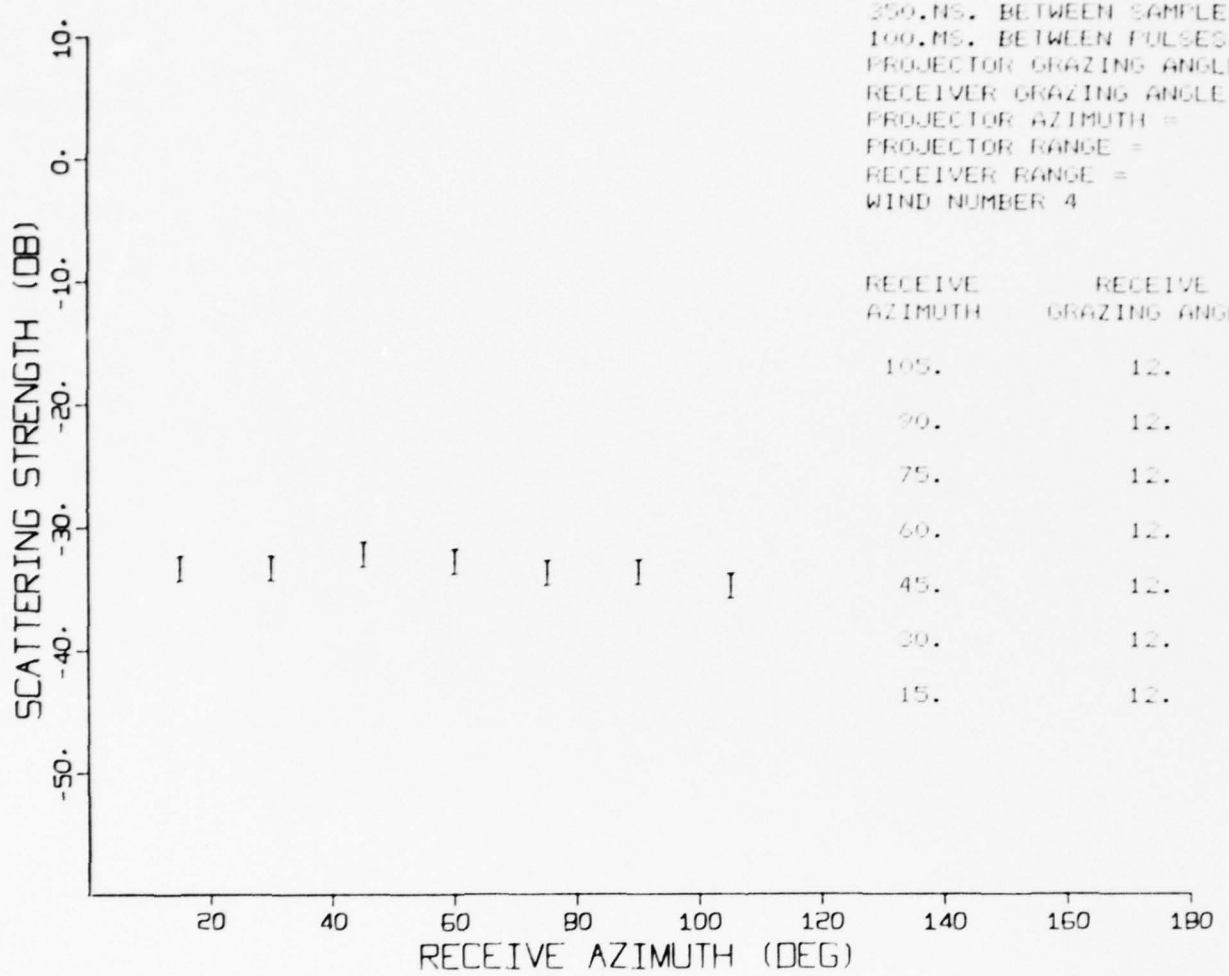

E0003 25MAY79 Z803.8IN
LF PWR
0.175 TO 0.180 MHZ.
350.MS. BETWEEN SAMPLES
100.MS. BETWEEN PULSES
PROJECTOR GRAZING ANGLE = 12. DEG.
RECEIVER GRAZING ANGLE = 12. DEG.
PROJECTOR AZIMUTH = 0.DEG.
PROJECTOR RANGE = 36. IN.
RECEIVER RANGE = 59. IN.
WIND NUMBER 4

RECEIVE AZIMUTH	RECEIVE GRAZING ANGLE	SCATTERING STRENGTH
105.	12.	-35.
90.	12.	-34.
75.	12.	-34.
60.	12.	-33.
45.	12.	-32.
30.	12.	-33.
15.	12.	-33.

Figure 1. - Scattering strength measured at 177 kHz., 12 deg. grazing angle, projector facing downwind, wind speed 8.3 m./sec.

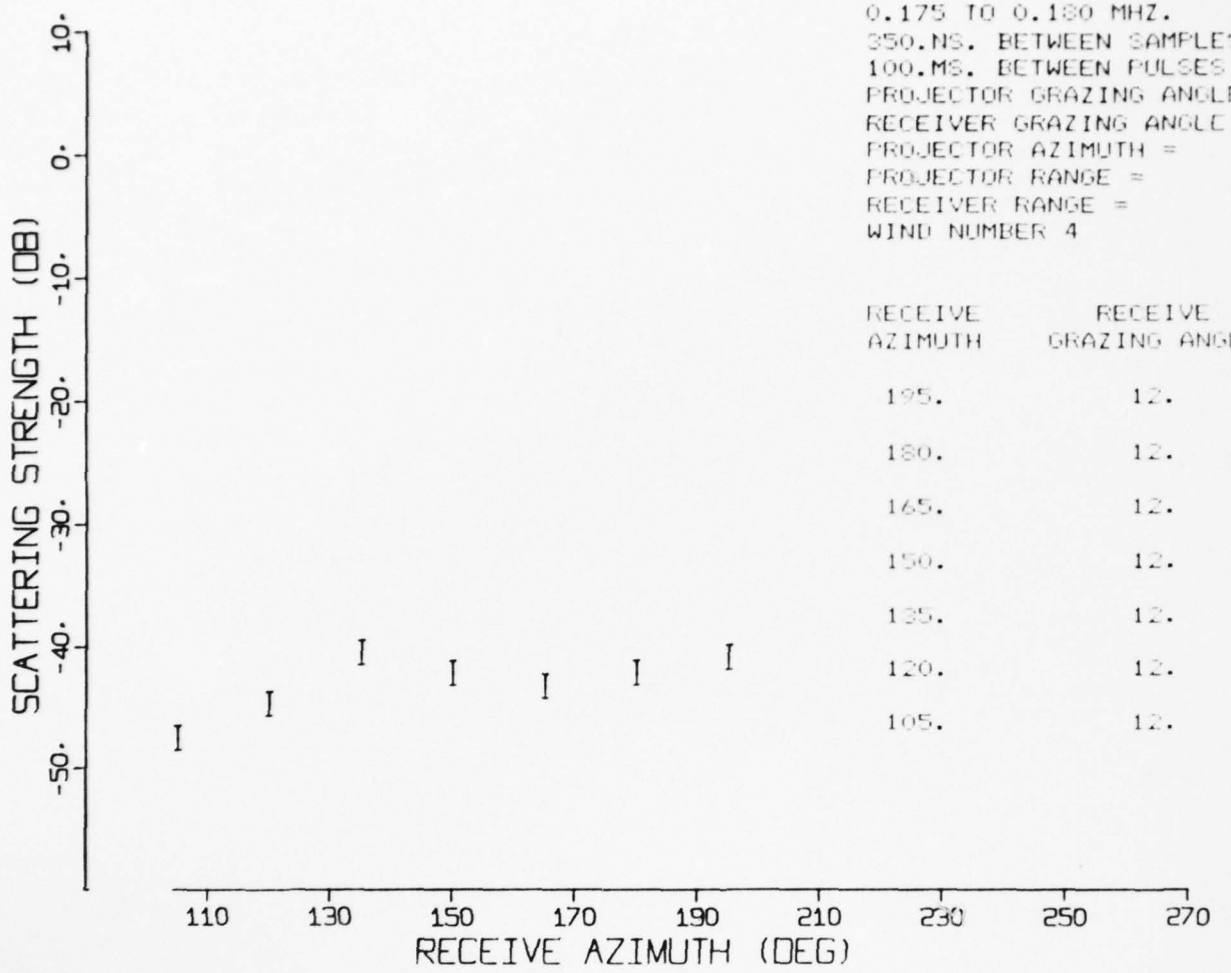

E0002 24MAY79 Z803.8IN
LF PWR
0.175 TO 0.180 MHZ.
350.NS. BETWEEN SAMPLES
100.MS. BETWEEN PULSES
PROJECTOR GRAZING ANGLE = 12. DEG.
RECEIVER GRAZING ANGLE = 12. DEG.
PROJECTOR AZIMUTH = 90.DEG.
PROJECTOR RANGE = 36. IN.
RECEIVER RANGE = 59. IN.
WIND NUMBER 4

RECEIVE AZIMUTH	RECEIVE GRAZING ANGLE	SCATTERING STRENGTH
195.	12.	-41.
180.	12.	-42.
165.	12.	-43.
150.	12.	-42.
135.	12.	-40.
120.	12.	-45.
105.	12.	-48.

Figure 2. - Scattering strength measured at 177 kHz., 12 deg. grazing angle, projector facing crosswind, wind speed 8.3 m./sec.

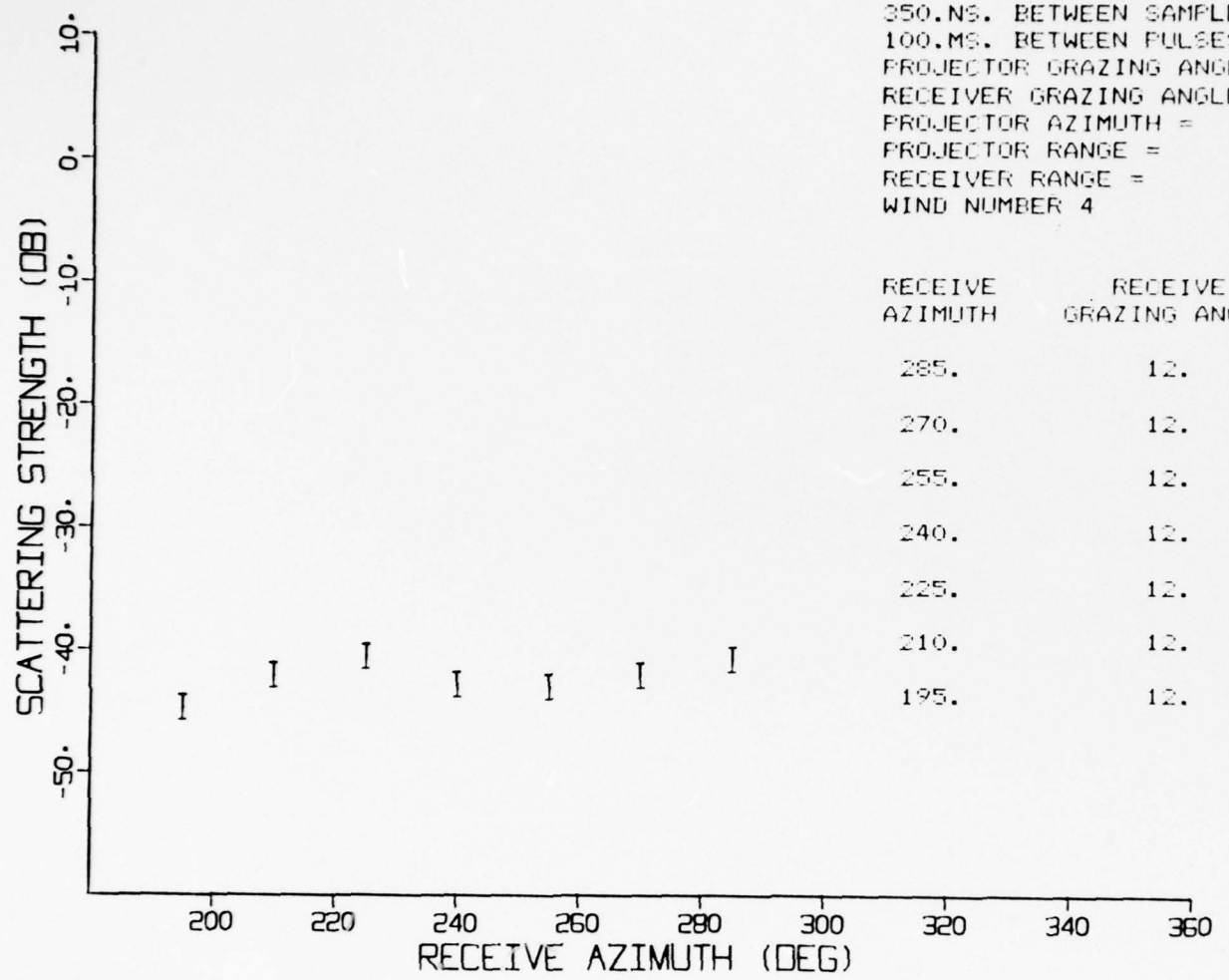

E0004 25MAY79 Z803,8IN
LF PWR
0.175 TO 0.180 MHZ.
350.NS. BETWEEN SAMPLES
100.MS. BETWEEN PULSES
PROJECTOR GRAZING ANGLE = 12. DEG.
RECEIVER GRAZING ANGLE = 12. DEG.
PROJECTOR AZIMUTH = 180.DEG.
PROJECTOR RANGE = 36. IN.
RECEIVER RANGE = 59. IN.
WIND NUMBER 4

RECEIVE AZIMUTH	RECEIVE GRAZING ANGLE	SCATTERING STRENGTH
285.	12.	-41.
270.	12.	-42.
255.	12.	-43.
240.	12.	-43.
225.	12.	-41.
210.	12.	-42.
195.	12.	-45.

Figure 3. - Scattering strength measured at 177 kHz., 12 deg. grazing angle, projector facing upwind, wind speed 8.3 m./sec.

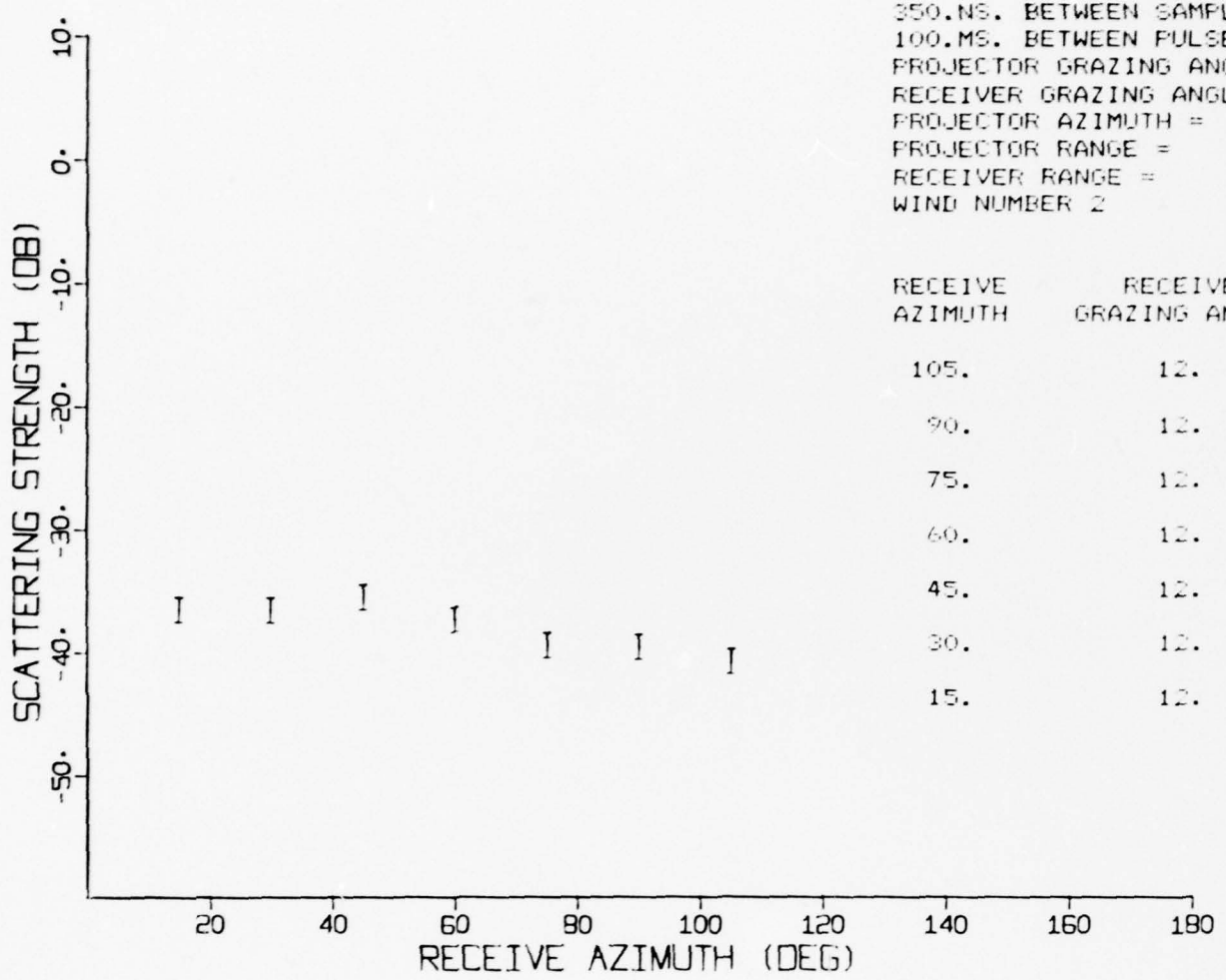

E0007 26MAY79 Z803.8IN
LF PWR
0.175 TO 0.180 MHZ.
350.NS. BETWEEN SAMPLES
100.MS. BETWEEN PULSES
PROJECTOR GRAZING ANGLE = 12. DEG.
RECEIVER GRAZING ANGLE = 12. DEG.
PROJECTOR AZIMUTH = 0.DEG.
PROJECTOR RANGE = 36. IN.
RECEIVER RANGE = 59. IN.
WIND NUMBER 2

RECEIVE AZIMUTH	RECEIVE GRAZING ANGLE	SCATTERING STRENGTH
105.	12.	-41.
90.	12.	-39.
75.	12.	-39.
60.	12.	-37.
45.	12.	-35.
30.	12.	-37.
15.	12.	-36.

Figure 4. - Scattering strength measured at 177 kHz., 12 deg. grazing angle, projector facing downwind, wind speed 5.4 m./sec.

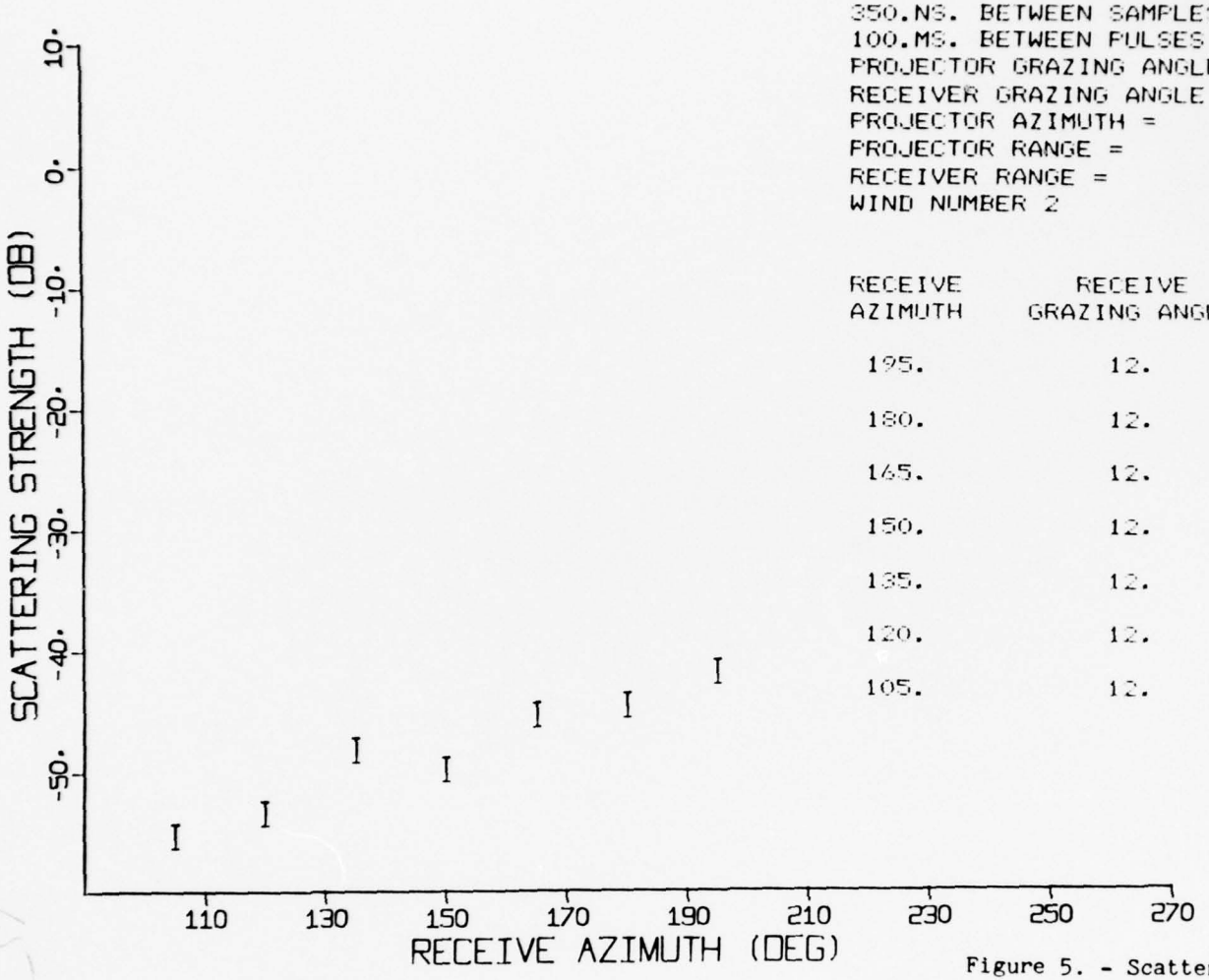

E0006 26MAY79 Z803,8IN
LF PWR
0.175 TO 0.180 MHZ.
350.NS. BETWEEN SAMPLES
100.MS. BETWEEN PULSES
PROJECTOR GRAZING ANGLE = 12. DEG.
RECEIVER GRAZING ANGLE = 12. DEG.
PROJECTOR AZIMUTH = 90.DEG.
PROJECTOR RANGE = 36. IN.
RECEIVER RANGE = 59. IN.
WIND NUMBER 2

RECEIVE AZIMUTH	RECEIVE GRAZING ANGLE	SCATTERING STRENGTH
195.	12.	-42.
180.	12.	-45.
165.	12.	-45.
150.	12.	-50.
135.	12.	-48.
120.	12.	-53.
105.	12.	-55.

Figure 5. - Scattering strength measured at 177 kHz., 12 deg. grazing angle, projector facing crosswind, wind speed 5.4 m./sec.

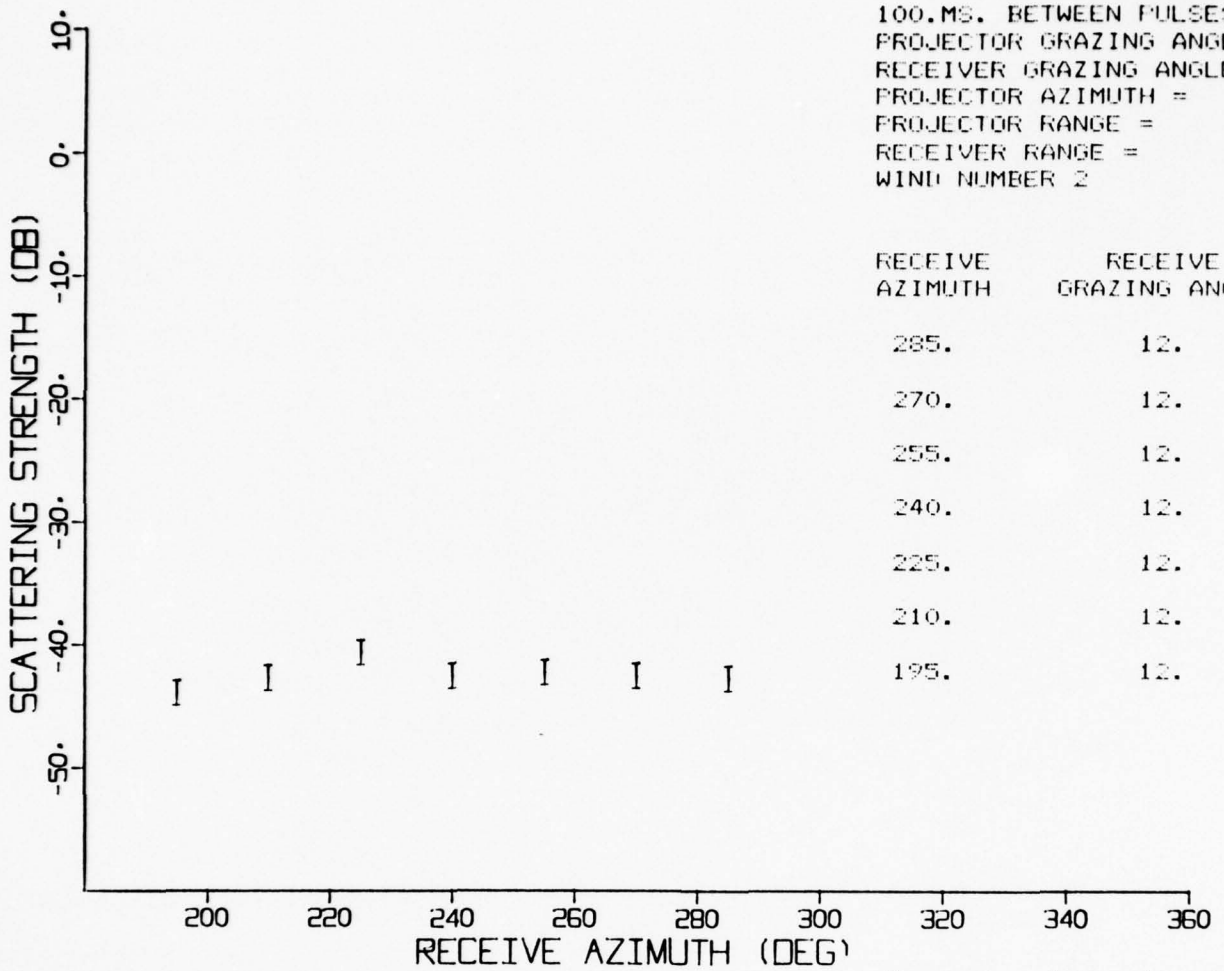

E0005 26MAY79 Z803,8IN
LF PWR
0.175 TO 0.180 MHZ.
350.NS. BETWEEN SAMPLES
100.MS. BETWEEN PULSES
PROJECTOR GRAZING ANGLE = 12. DEG.
RECEIVER GRAZING ANGLE = 12. DEG.
PROJECTOR AZIMUTH = 180.DEG.
PROJECTOR RANGE = 36. IN.
RECEIVER RANGE = 59. IN.
WIND NUMBER 2

RECEIVE AZIMUTH	RECEIVE GRAZING ANGLE	SCATTERING STRENGTH
285.	12.	-43.
270.	12.	-42.
255.	12.	-42.
240.	12.	-42.
225.	12.	-41.
210.	12.	-43.
195.	12.	-44.

Figure 6. - Scattering strength measured at 177 kHz., 12 deg. grazing angle, projector facing upwind, wind speed 5.4 m./sec.

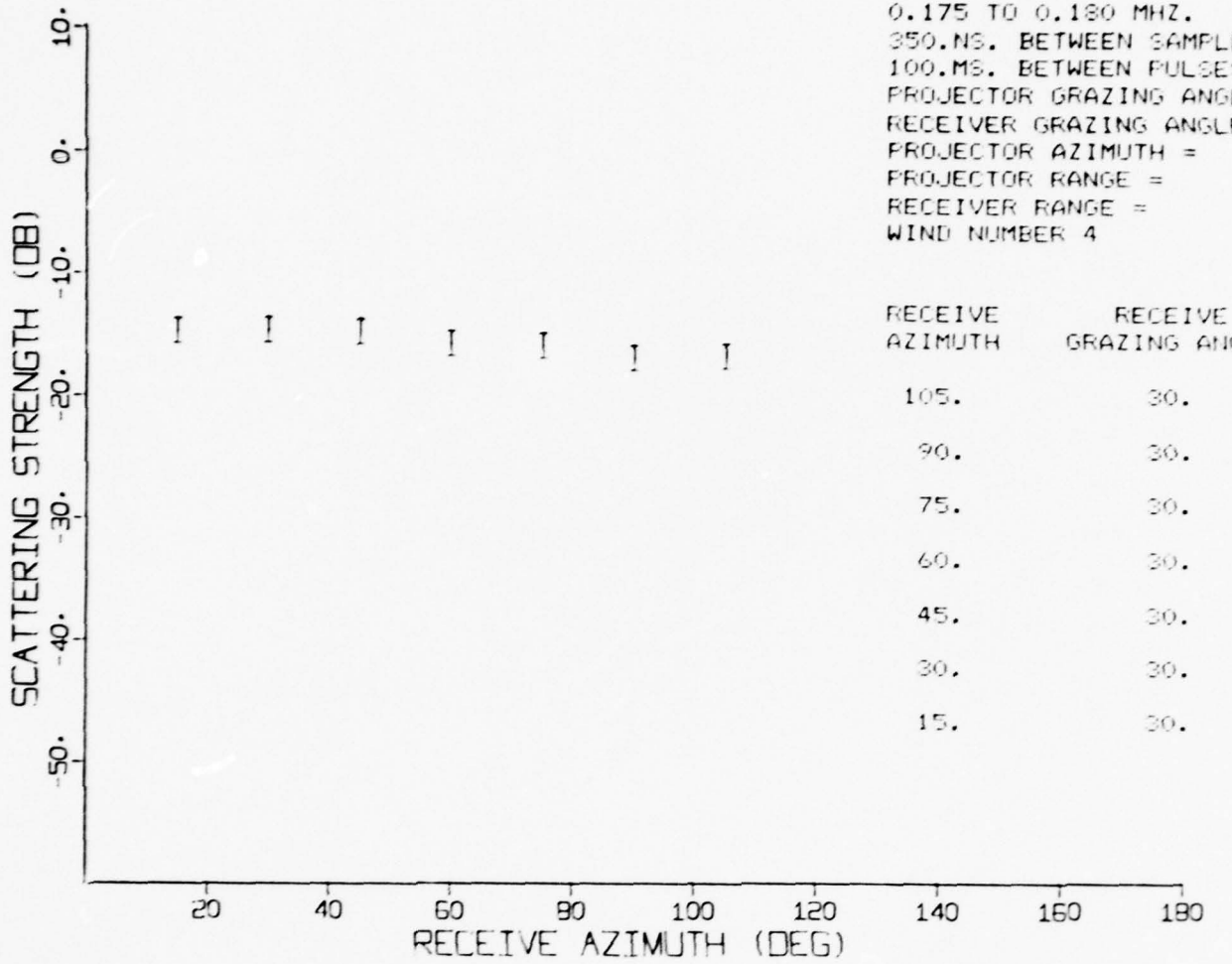

RUN3
0.175 TO 0.180 MHZ.
350.NS. BETWEEN SAMPLES
100.MS. BETWEEN PULSES
PROJECTOR GRAZING ANGLE = 30. DEG.
RECEIVER GRAZING ANGLE = 30. DEG.
PROJECTOR AZIMUTH = 0.DEG.
PROJECTOR RANGE = 36. IN.
RECEIVER RANGE = 36. IN.
WIND NUMBER 4

RECEIVE AZIMUTH	RECEIVE GRAZING ANGLE	SCATTERING STRENGTH
105.	30.	-17.
90.	30.	-17.
75.	30.	-16.
60.	30.	-16.
45.	30.	-15.
30.	30.	-15.
15.	30.	-15.

Figure 7. - Scattering strength measured at 177 kHz., 30 deg. grazing angle, projector facing downwind, wind speed 8.3 m./sec.

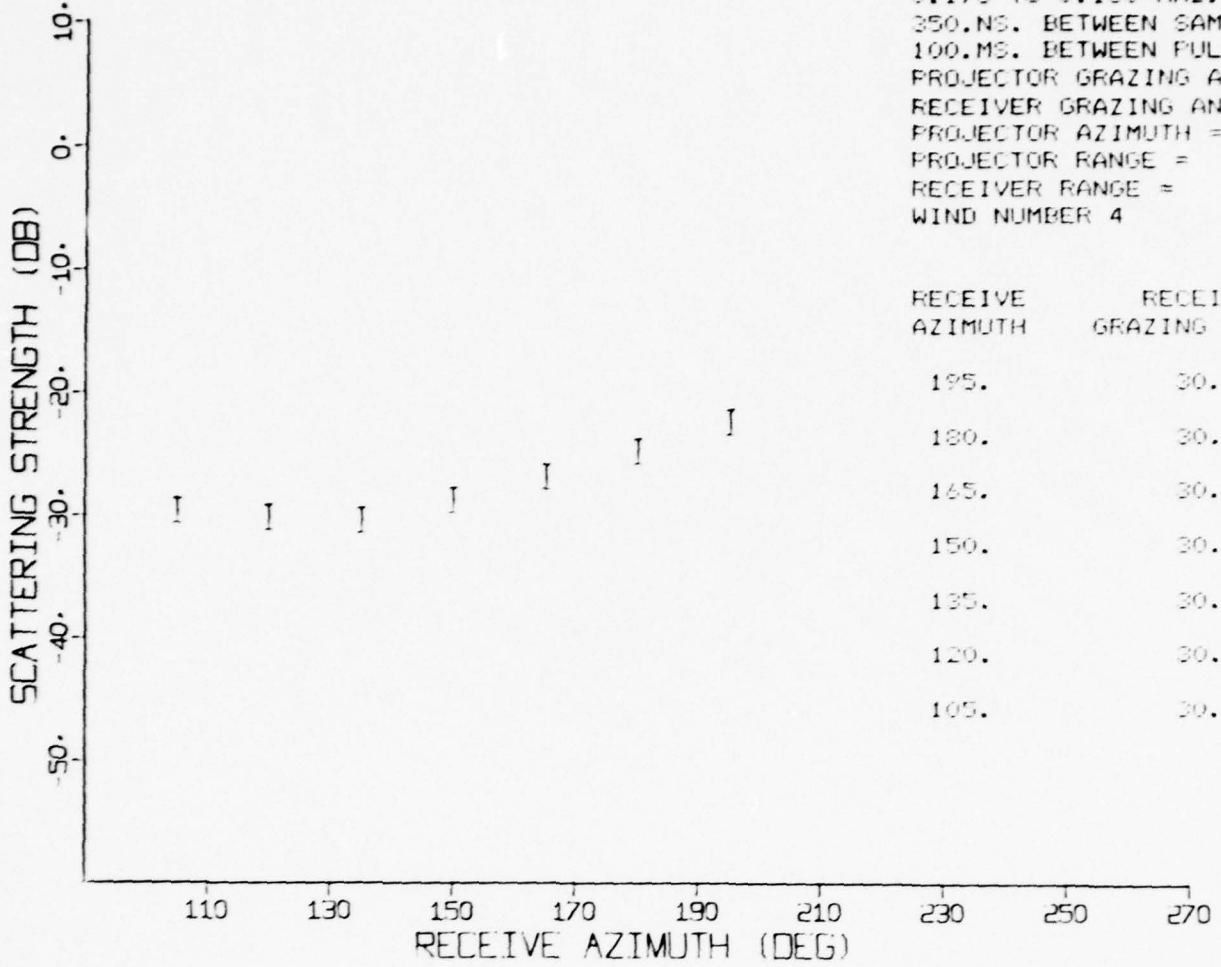

E0012 28MAY79 Z803.8IN
LF PWR
0.175 TO 0.180 MHZ.
350.NS. BETWEEN SAMPLES
100.MS. BETWEEN PULSES
PROJECTOR GRAZING ANGLE = 30. DEG.
RECEIVER GRAZING ANGLE = 30. DEG.
PROJECTOR AZIMUTH = 90.DEG.
PROJECTOR RANGE = 36. IN.
RECEIVER RANGE = 36. IN.
WIND NUMBER 4

RECEIVE AZIMUTH	RECEIVE GRAZING ANGLE	SCATTERING STRENGTH
195.	30.	-22.
180.	30.	-25.
165.	30.	-27.
150.	30.	-29.
135.	30.	-30.
120.	30.	-30.
105.	30.	-30.

Figure 8. - Scattering strength measured at 177 kHz., 30 deg. grazing angle, projector facing crosswind, wind speed 8.3 m./sec.

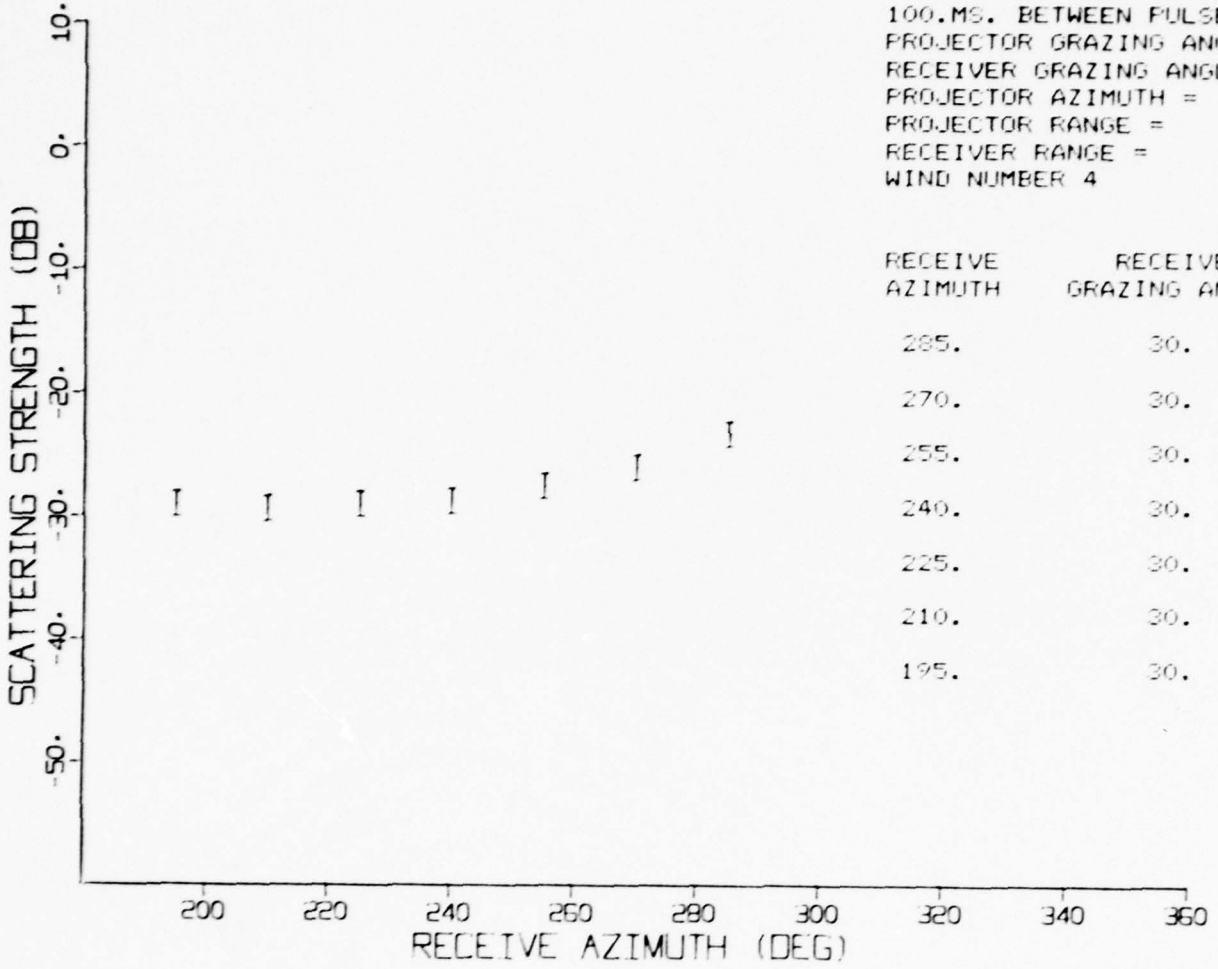

E0011 27MAY79 Z803.8IN
LF PWR
0.175 TO 0.180 MHZ.
350.NS. BETWEEN SAMPLES
100.MS. BETWEEN PULSES
PROJECTOR GRAZING ANGLE = 30. DEG.
RECEIVER GRAZING ANGLE = 30. DEG.
PROJECTOR AZIMUTH = 180.DEG.
PROJECTOR RANGE = 36. IN.
RECEIVER RANGE = 36. IN.
WIND NUMBER 4

RECEIVE AZIMUTH	RECEIVE GRAZING ANGLE	SCATTERING STRENGTH
285.	30.	-23.
270.	30.	-26.
255.	30.	-27.
240.	30.	-29.
225.	30.	-29.
210.	30.	-29.
195.	30.	-29.

Figure 9. - Scattering strength measured at 177 kHz., 30 deg. grazing angle, projector facing upwind, wind speed 8.3 m./sec.

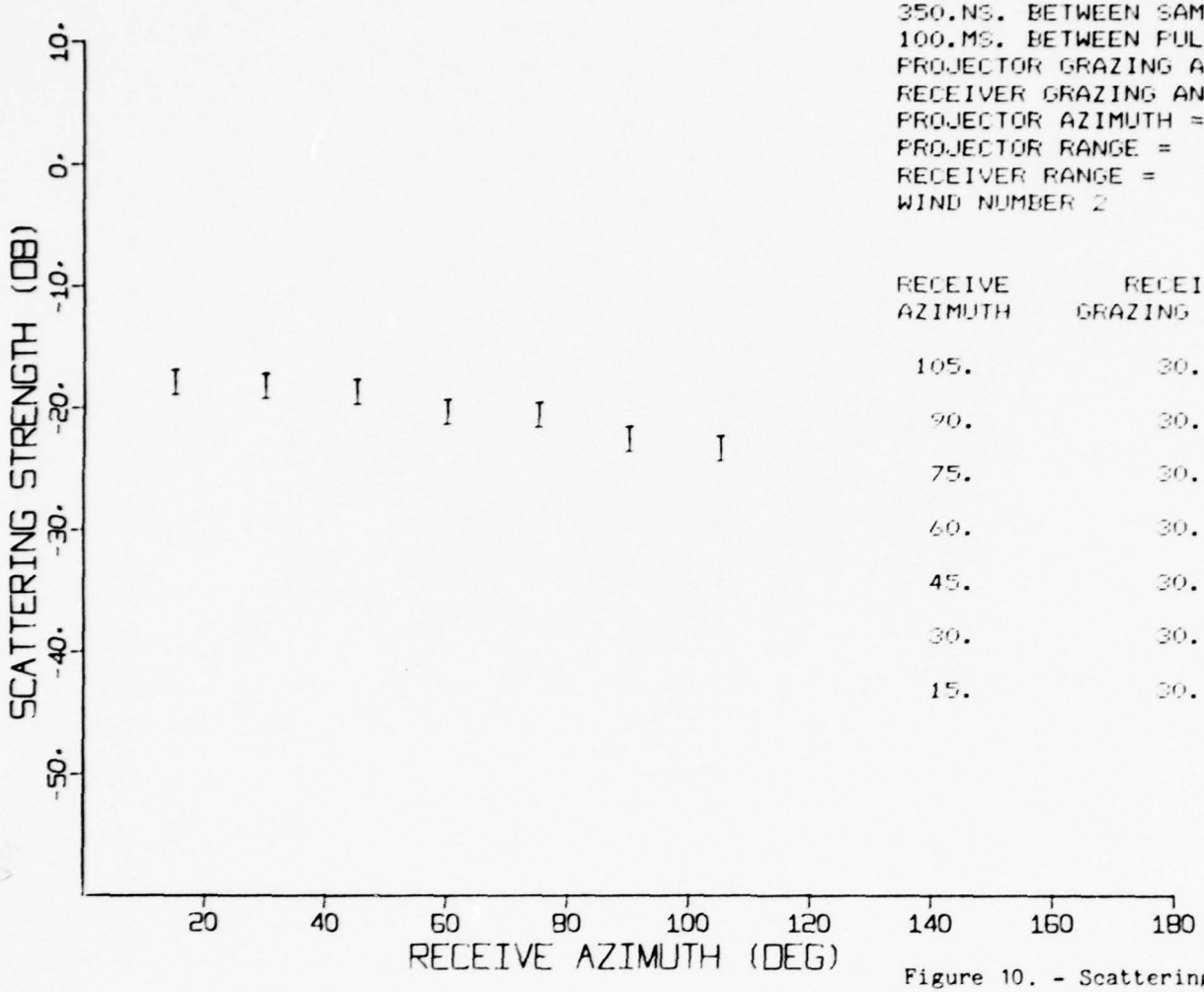

E0008 27MAY79 Z803,8IN
LF PWR
0.175 TO 0.180 MHZ.
350.NS. BETWEEN SAMPLES
100.MS. BETWEEN PULSES
PROJECTOR GRAZING ANGLE = 30. DEG.
RECEIVER GRAZING ANGLE = 30. DEG.
PROJECTOR AZIMUTH = 0.DEG.
PROJECTOR RANGE = 36. IN.
RECEIVER RANGE = 36. IN.
WIND NUMBER 2

RECEIVE AZIMUTH	RECEIVE GRAZING ANGLE	SCATTERING STRENGTH
105.	30.	-23.
90.	30.	-22.
75.	30.	-21.
60.	30.	-20.
45.	30.	-19.
30.	30.	-18.
15.	30.	-18.

Figure 10. - Scattering strength measured at 177 kHz., 30 deg. grazing angle, projector facing downwind, wind speed 5.4 m./sec.

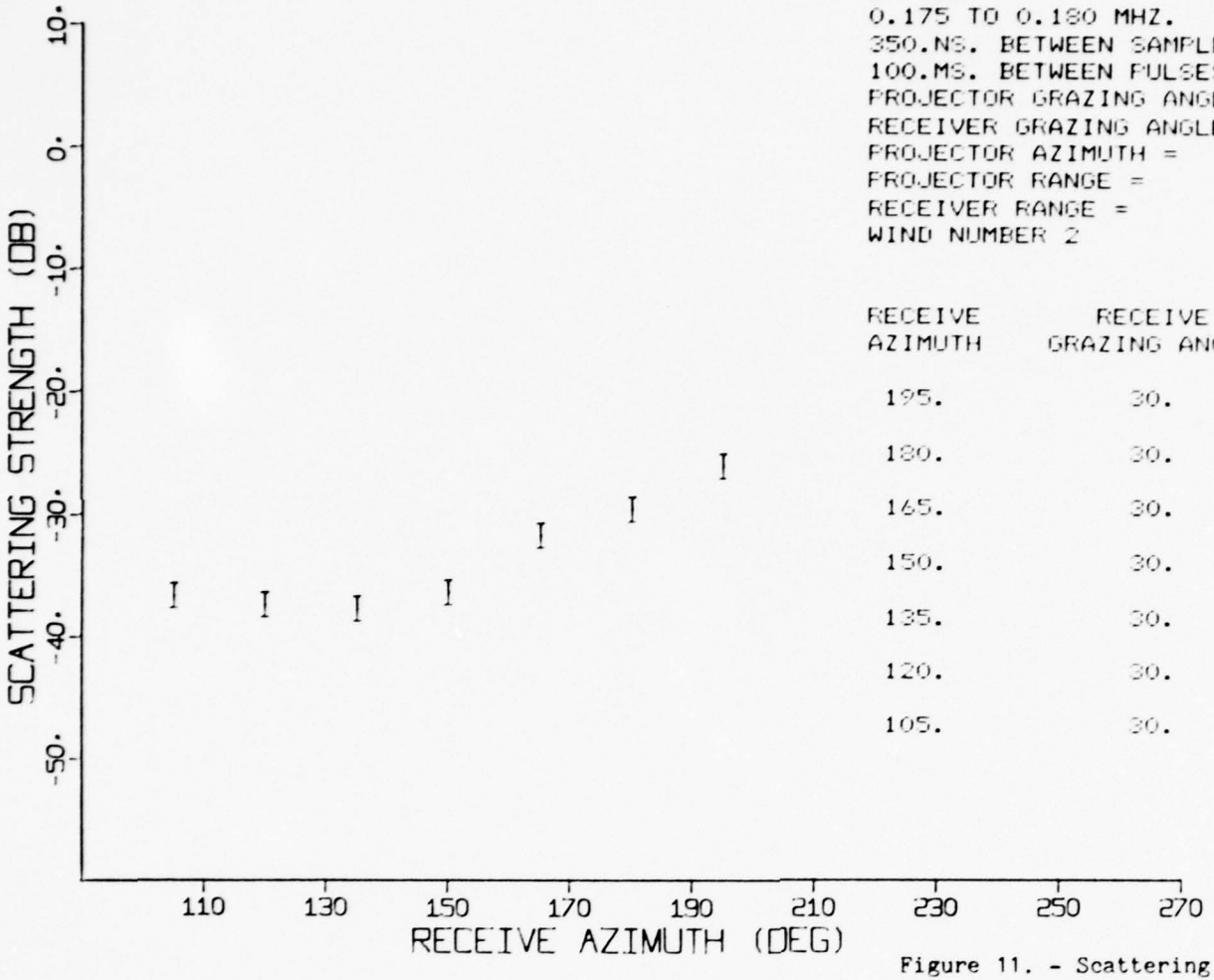

E0009 27MAY79 Z803.8IN
LF PWR
0.175 TO 0.180 MHZ.
350.NS. BETWEEN SAMPLES
100.MS. BETWEEN PULSES
PROJECTOR GRAZING ANGLE = 30. DEG.
RECEIVER GRAZING ANGLE = 30. DEG.
PROJECTOR AZIMUTH = 90.DEG.
PROJECTOR RANGE = 36. IN.
RECEIVER RANGE = 36. IN.
WIND NUMBER 2

RECEIVE AZIMUTH	RECEIVE GRAZING ANGLE	SCATTERING STRENGTH
195.	30.	-26.
180.	30.	-30.
165.	30.	-32.
150.	30.	-36.
135.	30.	-38.
120.	30.	-37.
105.	30.	-37.

Figure 11. - Scattering strength measured at 177 kHz., 30 deg. grazing angle, projector facing crosswind, wind speed 5.4 m./sec.

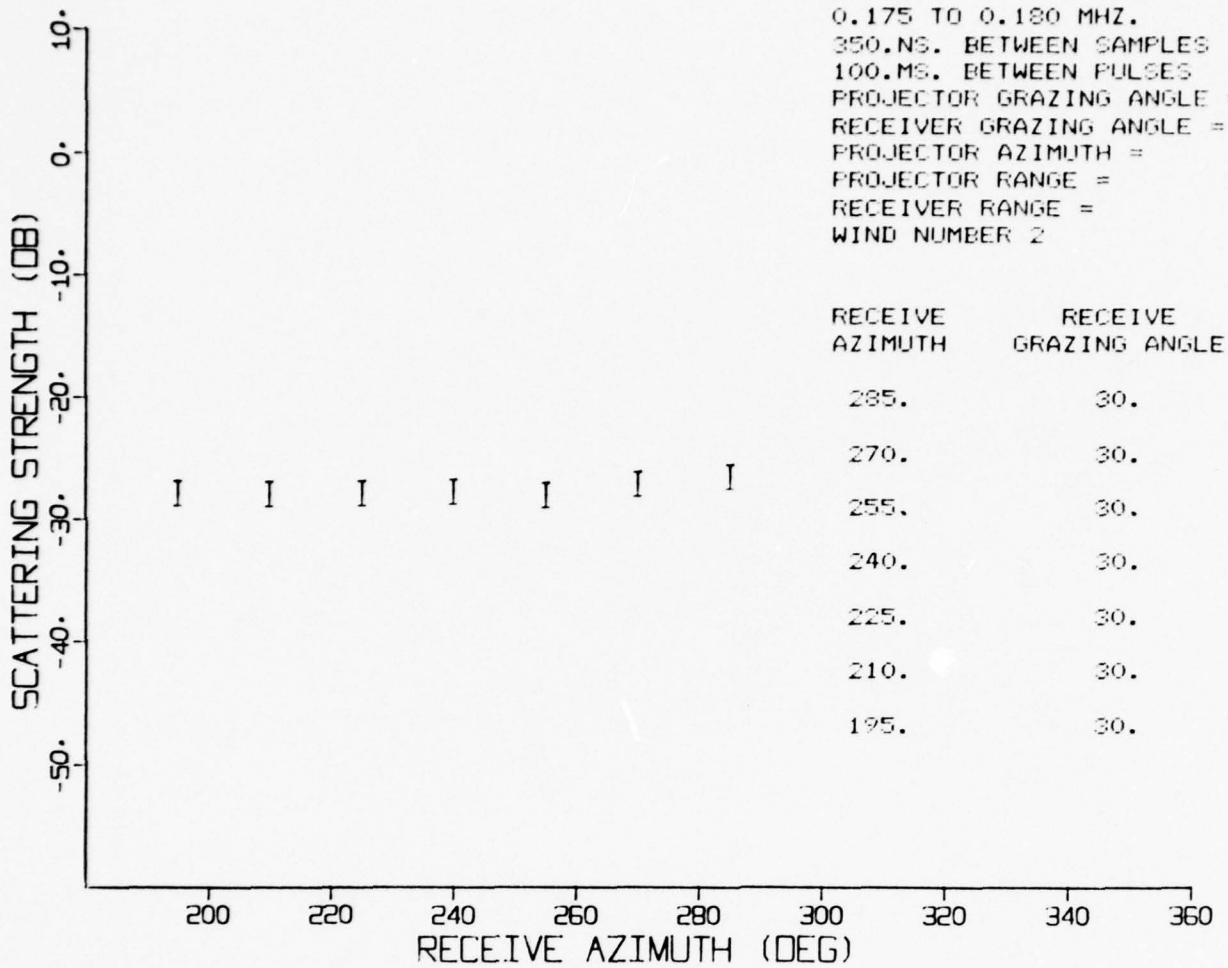

E0010 27MAY79 Z803,8IN
LF PWR
0.175 TO 0.180 MHZ.
350.NS. BETWEEN SAMPLES
100.MS. BETWEEN PULSES
PROJECTOR GRAZING ANGLE = 30. DEG.
RECEIVER GRAZING ANGLE = 30. DEG.
PROJECTOR AZIMUTH = 180.DEG.
PROJECTOR RANGE = 36. IN.
RECEIVER RANGE = 36. IN.
WIND NUMBER 2

RECEIVE AZIMUTH	RECEIVE GRAZING ANGLE	SCATTERING STRENGTH
285.	30.	-26.
270.	30.	-27.
255.	30.	-28.
240.	30.	-28.
225.	30.	-28.
210.	30.	-28.
195.	30.	-28.

Figure 12. - Scattering strength measured at 177 kHz., 30 deg. grazing angle, projector facing upwind, wind speed 5.4 m./sec.

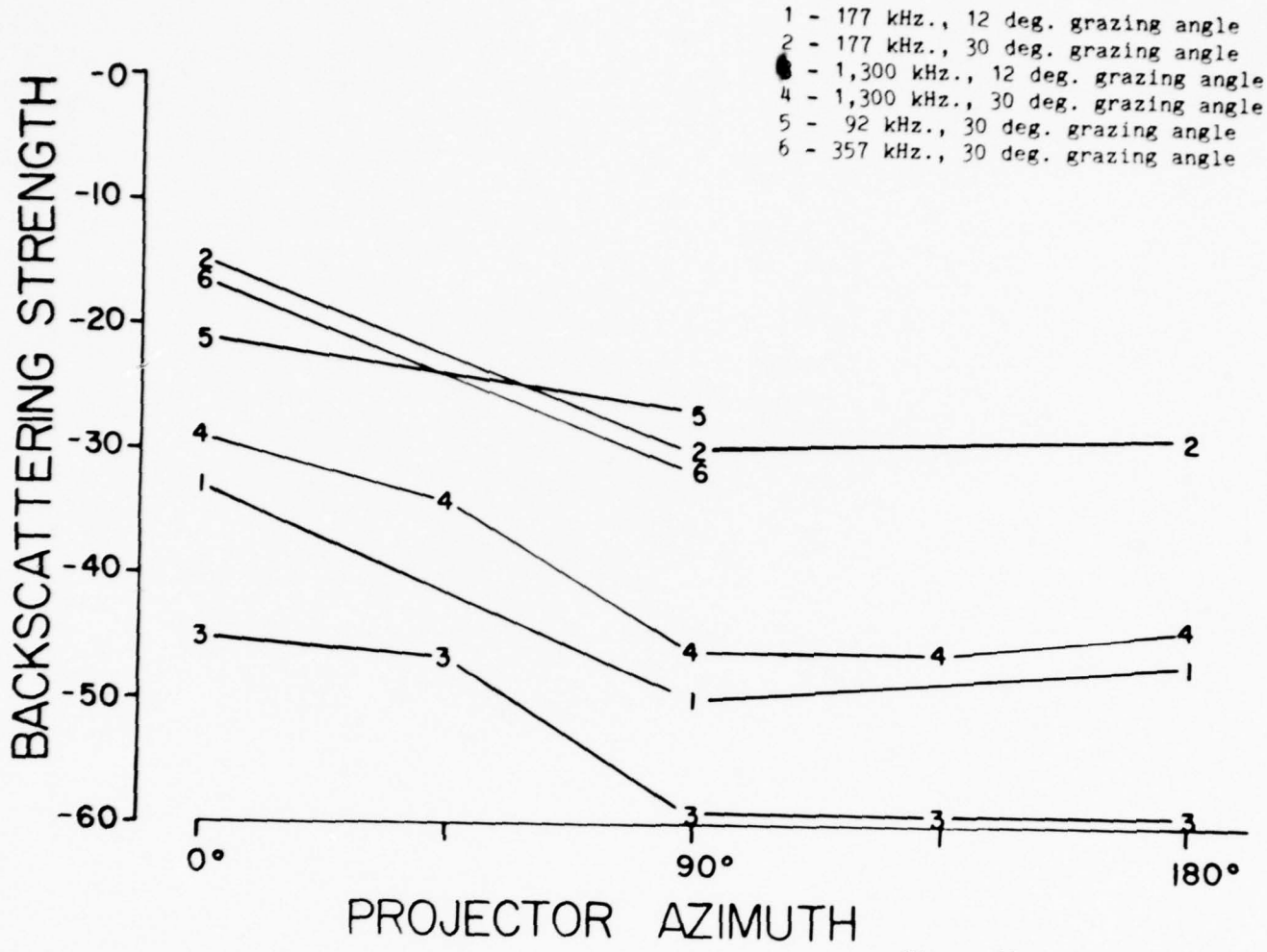

Figure 13. - Backscattering strength (extrapolated) for various conditions of projector orientation, grazing angle, and wavelength. Wind speed: 8.3 m./sec.

that at longer wavelengths the patterns would become more omni-directional and would tend to cast more power in non-specular directions. However, the degree to which this is the case would depend on the sizes of such facets and the distribution of their occurance.

b. At this wavelength the dependence of scattering strength on projector orientation with respect to the wind remains the same. It was noted during the short wavelength series of experiments that a difference of as much as 15 dB. in scattering strength could be observed between upwind and downwind backscattering strengths. This was supposed to be due to the asymmetry of the short fetch wind-driven surface used in these experiments. One could speculate that at some wavelength the effect of this asymmetry might diminish, but at this point there is apparently no change.

In addition to the basic series described above, several additional scans were made at wavelengths twice and one half as large. These runs were exploratory in the sense that no extensive scan at these wavelengths was contemplated unless anomalous behavior was observed. They are given as Figures 14 - 19. As can be seen from a comparison of Figures 14 and 15 with Figures 10 and 11, reducing the wavelength by a factor of two had only the effect of reducing the scattering strength at both crosswind and downwind orientations. On the other hand doub-

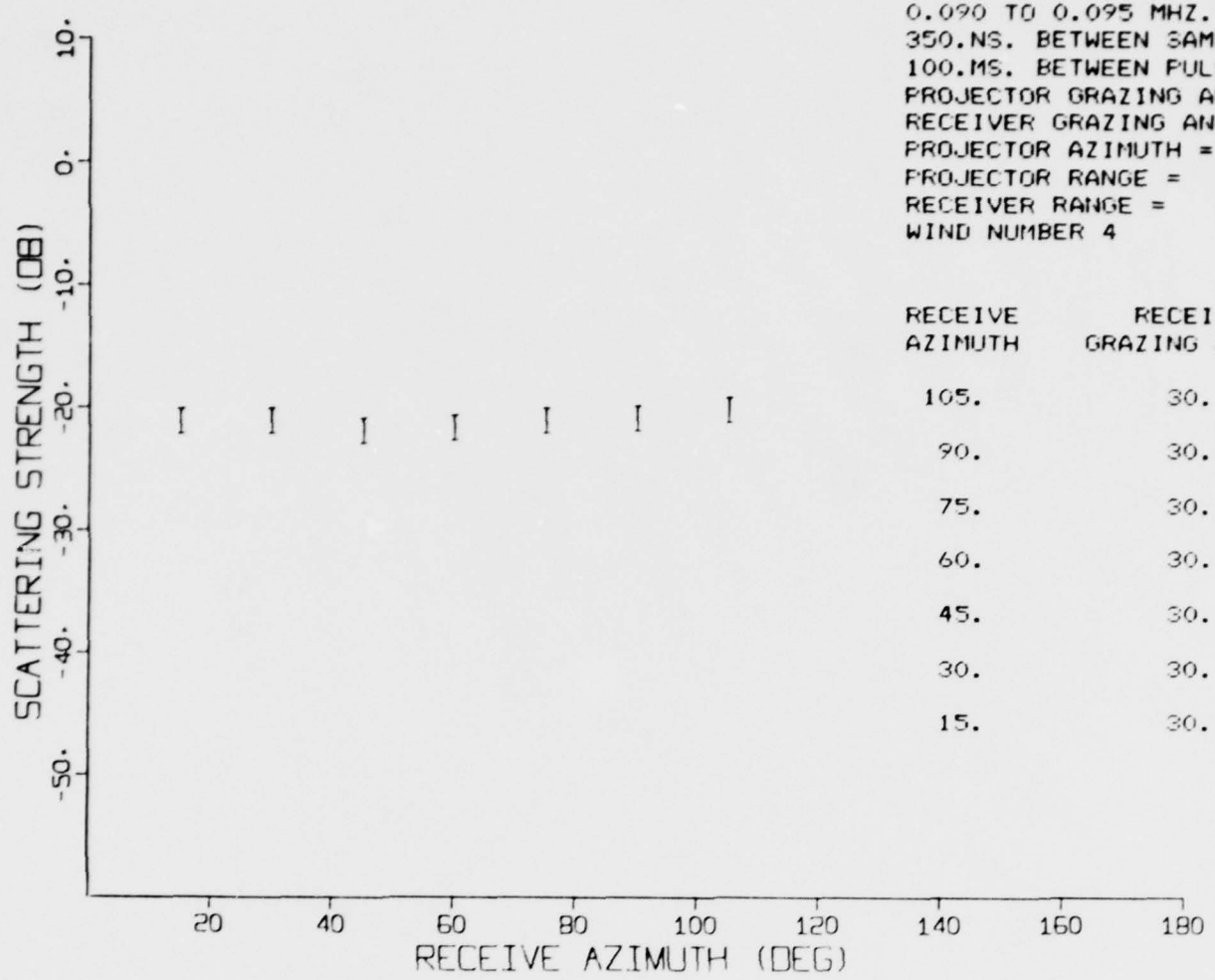

E0014 31JUL79 1 3
LF PWR
0.090 TO 0.095 MHZ.
350.NS. BETWEEN SAMPLES
100.MS. BETWEEN PULSES
PROJECTOR GRAZING ANGLE = 30. DEG.
RECEIVER GRAZING ANGLE = 30. DEG.
PROJECTOR AZIMUTH = 0.DEG.
PROJECTOR RANGE = 36. IN.
RECEIVER RANGE = 36. IN.
WIND NUMBER 4

RECEIVE AZIMUTH	RECEIVE GRAZING ANGLE	SCATTERING STRENGTH
105.	30.	-20.
90.	30.	-21.
75.	30.	-21.
60.	30.	-22.
45.	30.	-22.
30.	30.	-21.
15.	30.	-21.

Figure 14. - Scattering strength measured at 92 kHz., 30 deg. grazing angle, projector facing downwind, wind speed 8.3 m./sec.

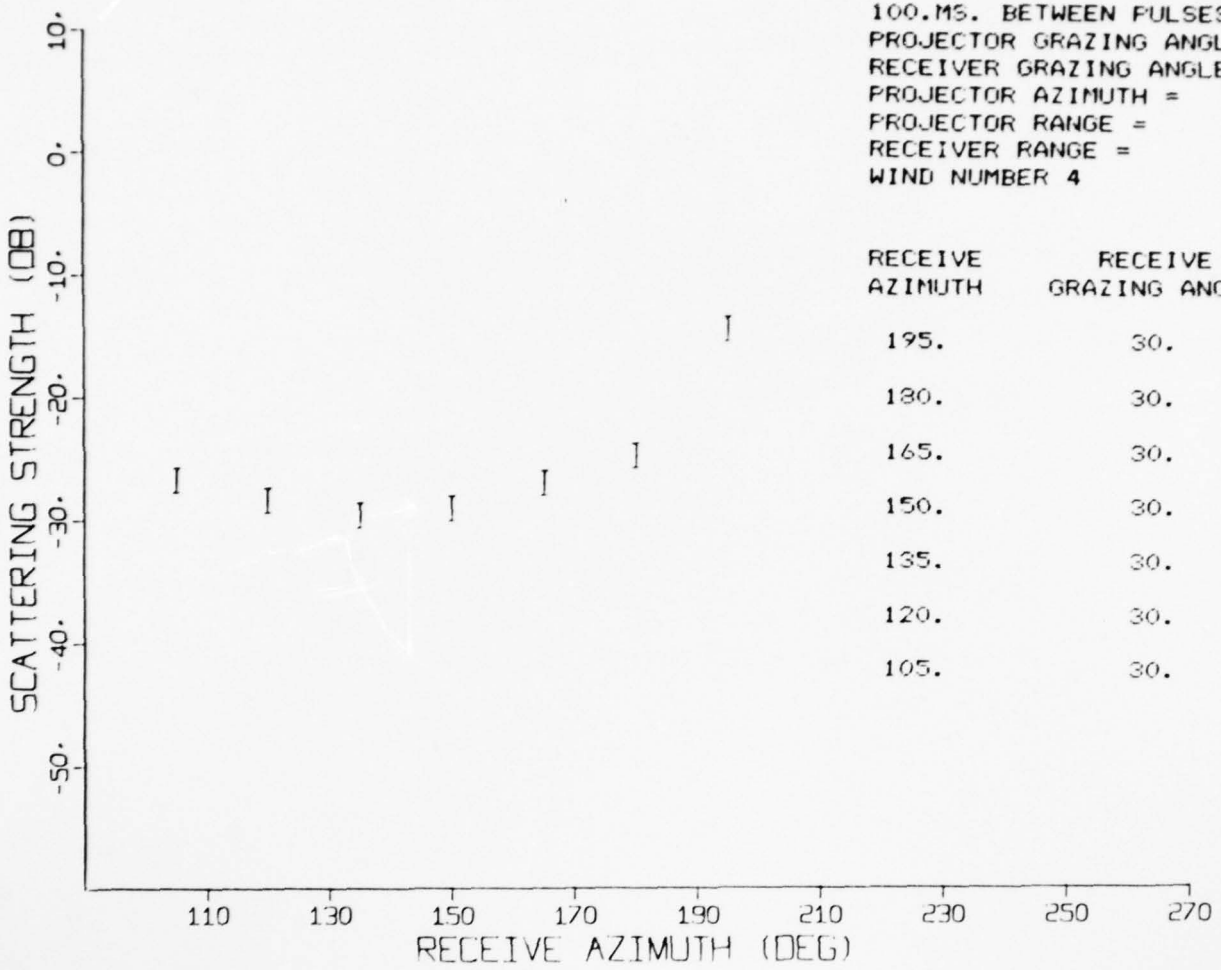

E0018 25-JUL-7 1 3
LF PWR
0.090 TO 0.095 MHZ.
350.NS. BETWEEN SAMPLES
100.MS. BETWEEN PULSES
PROJECTOR GRAZING ANGLE = 30. DEG.
RECEIVER GRAZING ANGLE = 30. DEG.
PROJECTOR AZIMUTH = 90.DEG.
PROJECTOR RANGE = 36. IN.
RECEIVER RANGE = 36. IN.
WIND NUMBER 4

RECEIVE AZIMUTH	RECEIVE GRAZING ANGLE	SCATTERING STRENGTH
195.	30.	-15.
180.	30.	-25.
165.	30.	-27.
150.	30.	-29.
135.	30.	-30.
120.	30.	-28.
105.	30.	-27.

Figure 15. - Scattering strength measured at 92 kHz., 30 deg. grazing angle, projector facing crosswind, wind speed 8.3 m./sec.

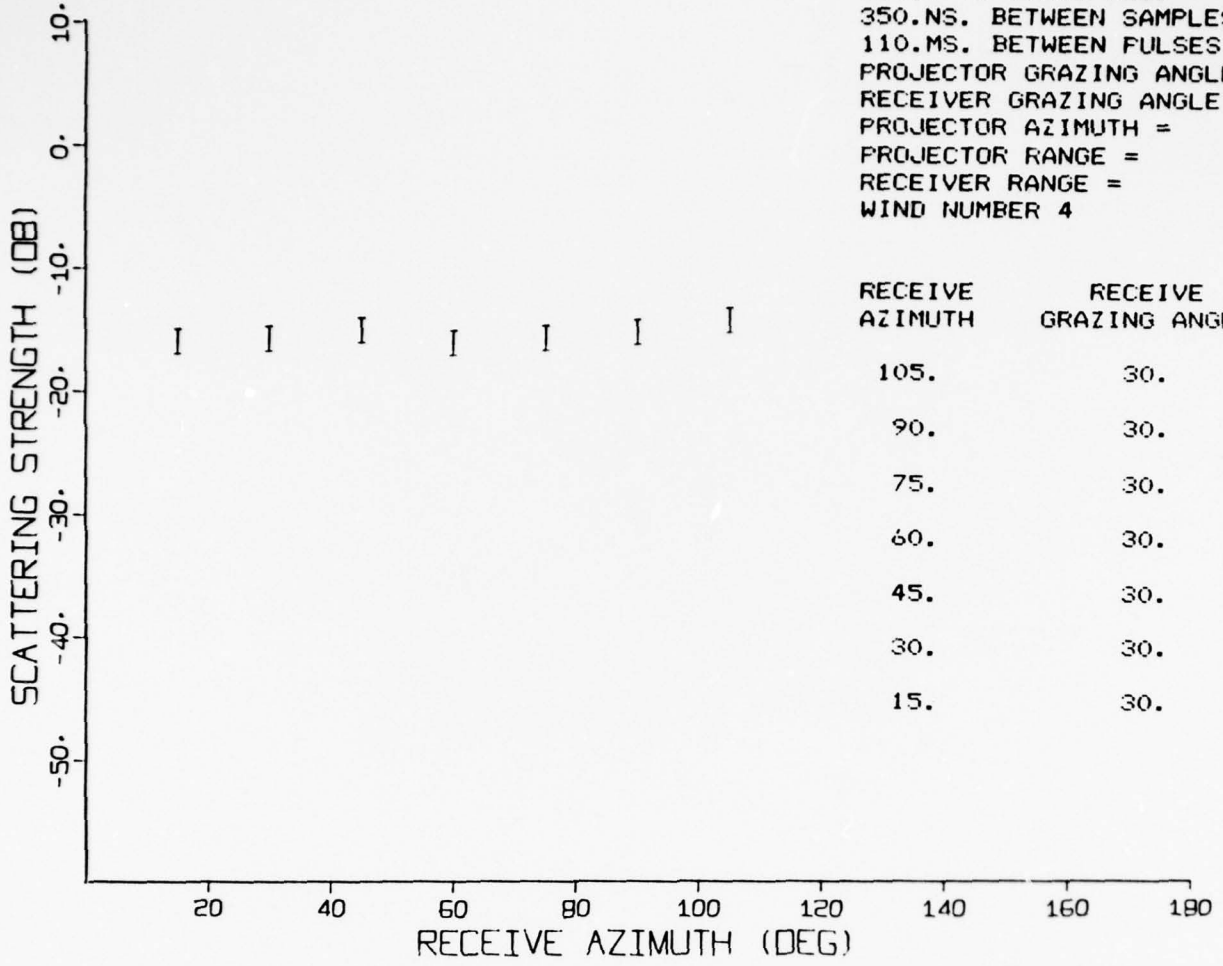

E0015 29JUL79 1 3
LF PWR
0.355 TO 0.360 MHZ.
350.NS. BETWEEN SAMPLES
110.MS. BETWEEN PULSES
PROJECTOR GRAZING ANGLE = 30. DEG.
RECEIVER GRAZING ANGLE = 30. DEG.
PROJECTOR AZIMUTH = 0.DEG.
PROJECTOR RANGE = 36. IN.
RECEIVER RANGE = 36. IN.
WIND NUMBER 4

RECEIVE AZIMUTH	RECEIVE GRAZING ANGLE	SCATTERING STRENGTH
105.	30.	-14.
90.	30.	-15.
75.	30.	-16.
60.	30.	-16.
45.	30.	-15.
30.	30.	-16.
15.	30.	-16.

Figure 16. - Scattering strength measured at 357 kHz., 30 deg. grazing angle, projector facing downwind, wind speed 8.3 m./sec.

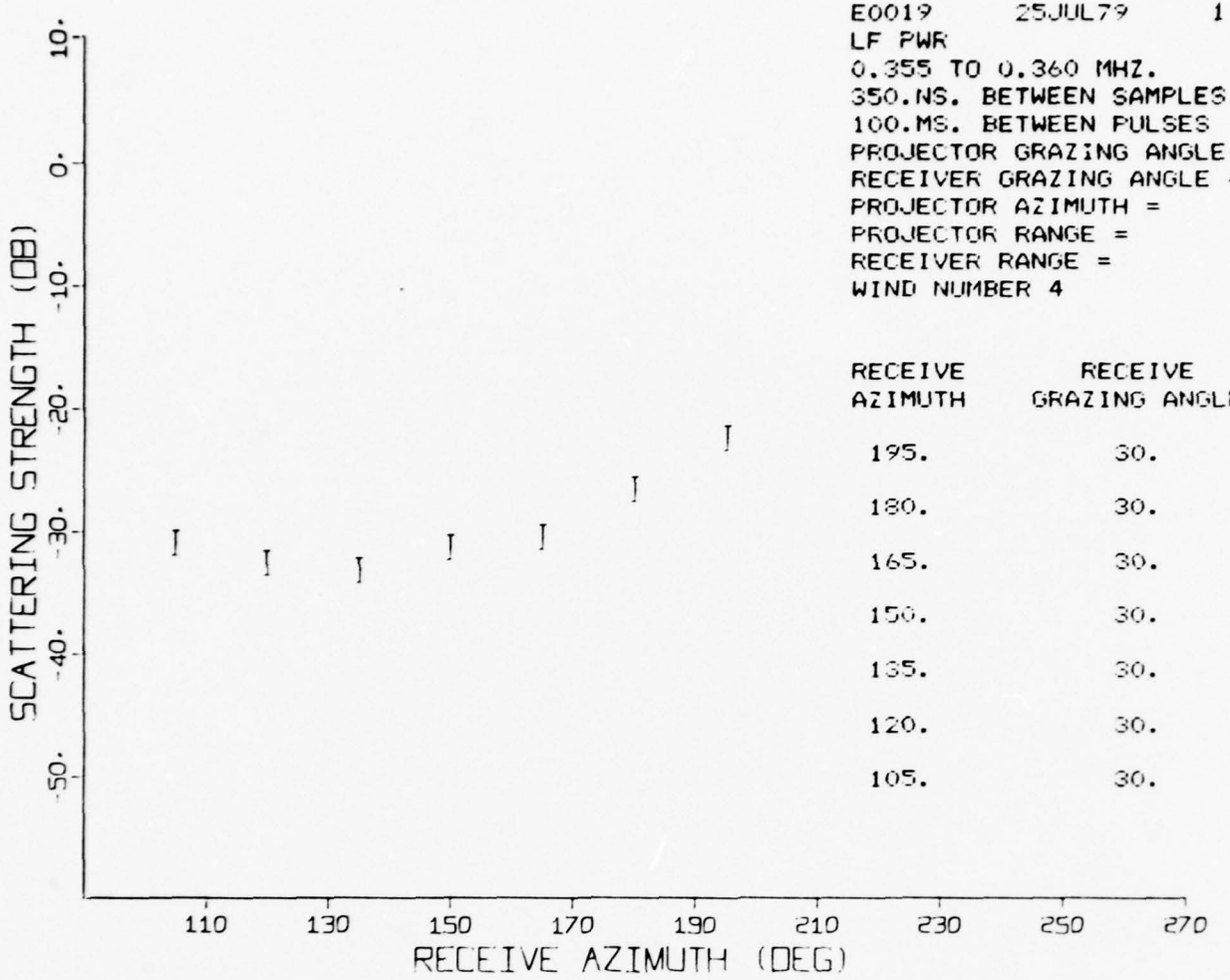

E0019 25JUL79 1 3
LF PWR
0.355 TO 0.360 MHZ.
350.NS. BETWEEN SAMPLES
100.MS. BETWEEN PULSES
PROJECTOR GRAZING ANGLE = 30. DEG.
RECEIVER GRAZING ANGLE = 30. DEG.
PROJECTOR AZIMUTH = 90.DEG.
PROJECTOR RANGE = 36. IN.
RECEIVER RANGE = 36. IN.
WIND NUMBER 4

RECEIVE AZIMUTH	RECEIVE GRAZING ANGLE	SCATTERING STRENGTH
195.	30.	-22.
180.	30.	-27.
165.	30.	-30.
150.	30.	-31.
135.	30.	-33.
120.	30.	-33.
105.	30.	-31.

Figure 17. - Scattering strength measured at 357 kHz., 30 deg. grazing angle, projector facing crosswind, wind speed 8.3 m./sec.

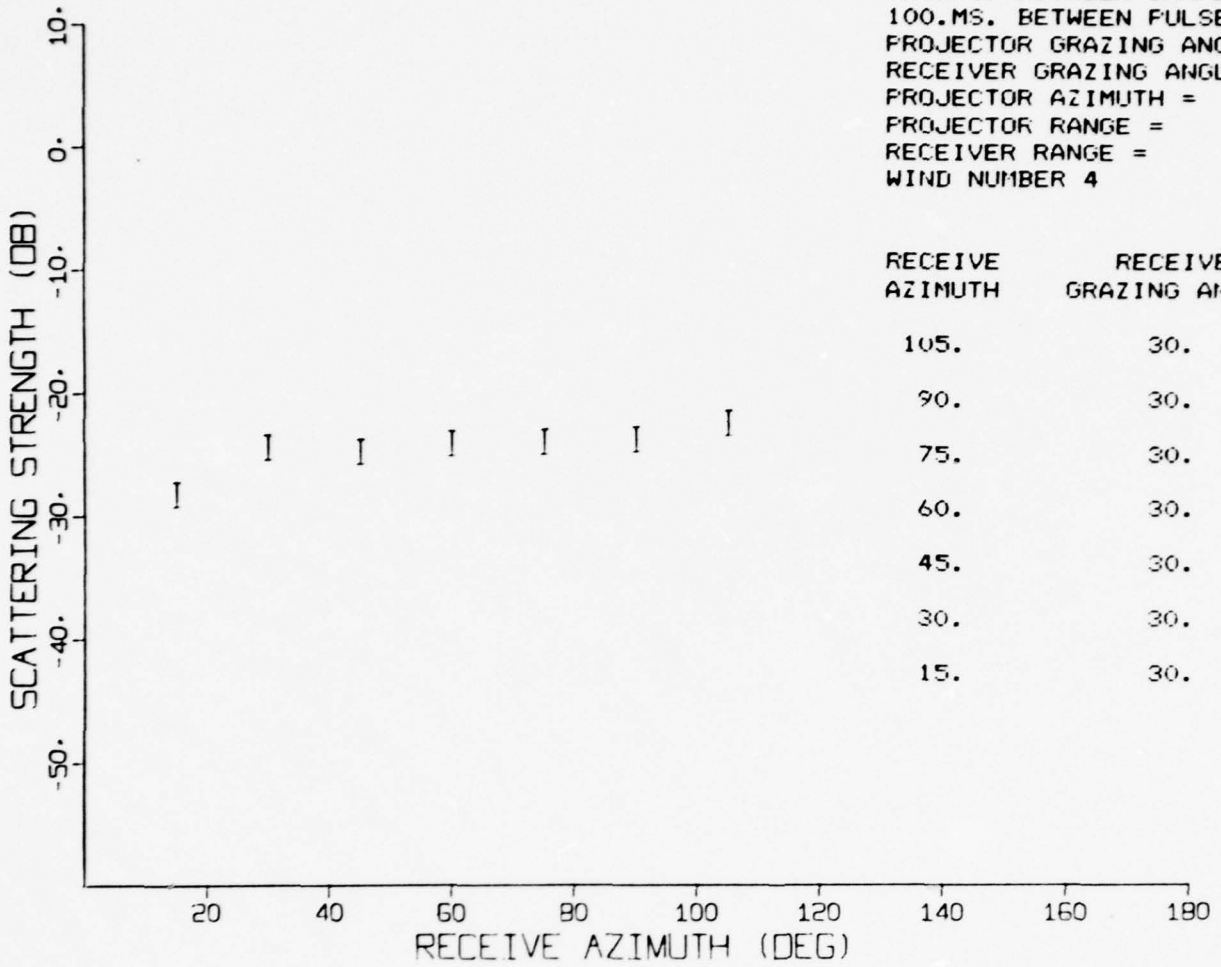

E0016 22JUL79 1 5
LF PWR
0.300 TO 0.305 MHZ.
350.NS. BETWEEN SAMPLES
100.MS. BETWEEN PULSES
PROJECTOR GRAZING ANGLE = 30. DEG.
RECEIVER GRAZING ANGLE = 30. DEG.
PROJECTOR AZIMUTH = 0.DEG.
PROJECTOR RANGE = 36. IN.
RECEIVER RANGE = 36. IN.
WIND NUMBER 4

RECEIVE AZIMUTH	RECEIVE GRAZING ANGLE	SCATTERING STRENGTH
105.	30.	-22.
90.	30.	-24.
75.	30.	-24.
60.	30.	-24.
45.	30.	-25.
30.	30.	-24.
15.	30.	-28.

Figure 18. - Scattering strength measured at 302 kHz., 30 deg. grazing angle, projector facing downwind, wind speed 8.3 m./sec.

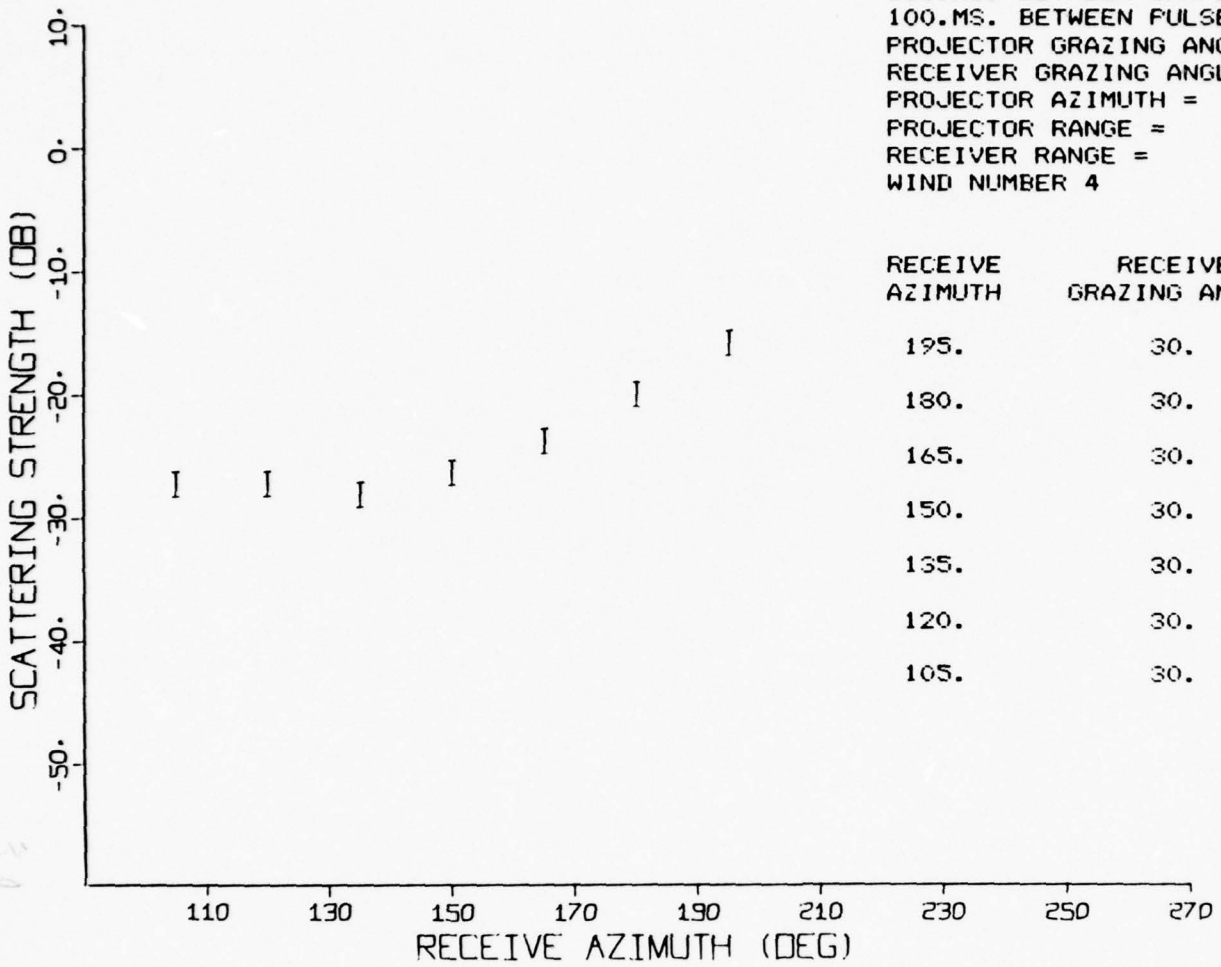

E0017 24-JUL-7 1 5
LF PWR
0.300 TO 0.305 MHZ.
350.NS. BETWEEN SAMPLES
100.MS. BETWEEN PULSES
PROJECTOR GRAZING ANGLE = 30. DEG.
RECEIVER GRAZING ANGLE = 30. DEG.
PROJECTOR AZIMUTH = 90.DEG.
PROJECTOR RANGE = 36. IN.
RECEIVER RANGE = 36. IN.
WIND NUMBER 4

RECEIVE AZIMUTH	RECEIVE GRAZING ANGLE	SCATTERING STRENGTH
195.	30.	-16.
180.	30.	-20.
165.	30.	-24.
150.	30.	-26.
135.	30.	-28.
120.	30.	-27.
105.	30.	-27.

Figure 19. - Scattering strength measured at 302 kHz., 30 deg. grazing angle, projector facing crosswind, wind speed 8.3 m./sec.

ling the wavelength (Fig. 16,17) seems to have had the effect of both raising the scattering strength and reducing the downwind/crosswind difference. This observation is admittedly based on an anomaly in just one run, but it does suggest that further exploration at even longer wavelengths may be worthwhile.

3. The Facet Model: During the past year, in response to the continuing need for a viable theoretical framework on which to hang the considerable mass of data that has been collected, a study has been conducted to determine the possibility of constructing a semiempirical model for reverberant scattering based on the notion of the surface as an ensemble of facet-like scatterers. The notion of modelling a scattering surface as an ensemble of statistically defined scatterers has been championed for some years by Middleton [1977], but has not been used widely due in some part to the difficulty of characterizing the scatterers in terms of measurable characteristics of the physical surface. Patterson [1963,1964] and, more recently, Novarini and Medwin [1978] have presented limited models of the surface based on the notion of plane facets, but these models are relatively primitive and do not in their present condition permit the quantitative prediction of experimental data.

The basic approach of the facet model is to represent the surface as a connected set of plane reflectors of a specific size and shape. In

that way the surface would be simply parameterized and much of its complexity would be eliminated. The connection to the physical surface is made by measurement of surface slope and other surface statistics, permitting the selection of a distribution of facet sizes and slopes in the model. The scattered field is then expressed as the coherent sum of the waves reradiated from each facet to the measurement point. Each facet is treated separately as regards its response to incident field and the coherent summation of reradiated fields is relied upon to account for the dependence between facets. The model is clearly approximate and therefore lacks the elegance of the solution of a scattering integral approach. On the other hand formulations based on such a model can be developed in stages of complexity as needed to arrive at a practical predictor. The principal appeal of the facet model approach is that it preserves to a large extent those scattering phenomena which are assumed away in Helmholtz integral formulations and which show greatest promise in the explanation of low grazing angle reverberation (i.e. diffraction).

The first step in the development of the facet model has been the derivation of an expression for the contribution to the scattered field of one member of the ensemble. The simplest shape for that single facet is a rectangle that is very long in one dimension. A suitable coordinate system is shown in Fig. 20. S and R refer to the source and receiver locations in the Z-X plane and α and β are the angles from the Z axis to the source and receiver directions respec-

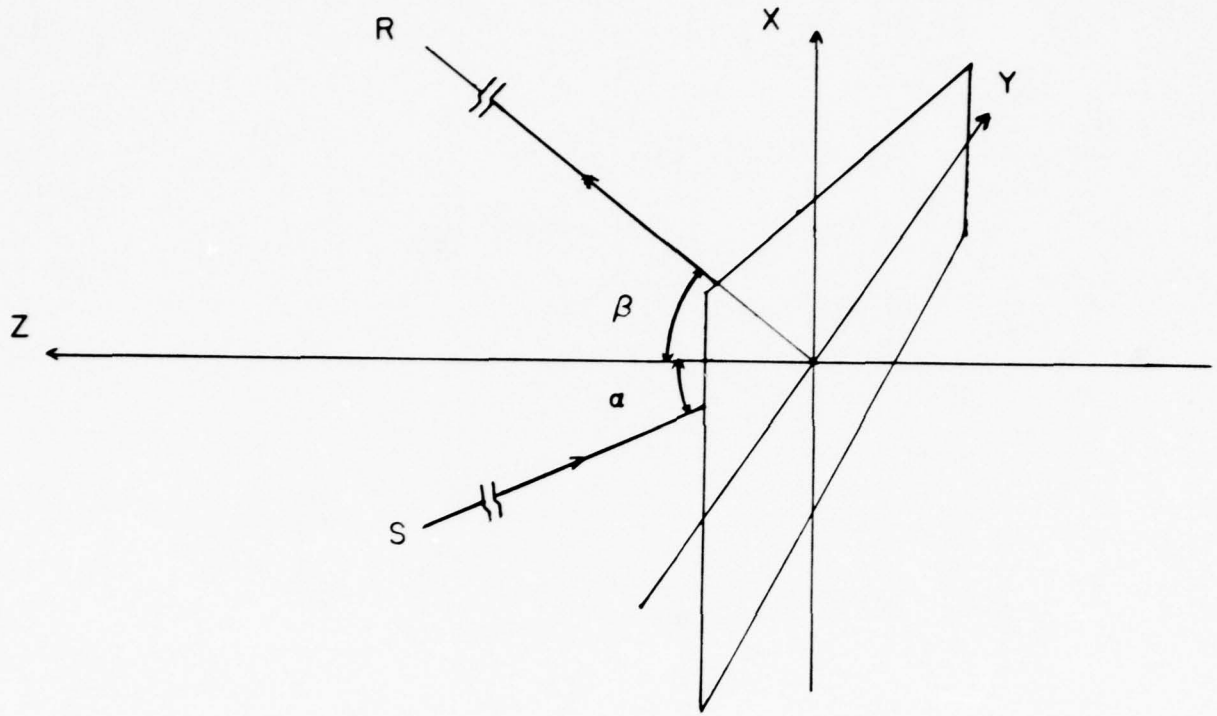

Figure 20. - The geometry of a simple one dimensional facet interaction.

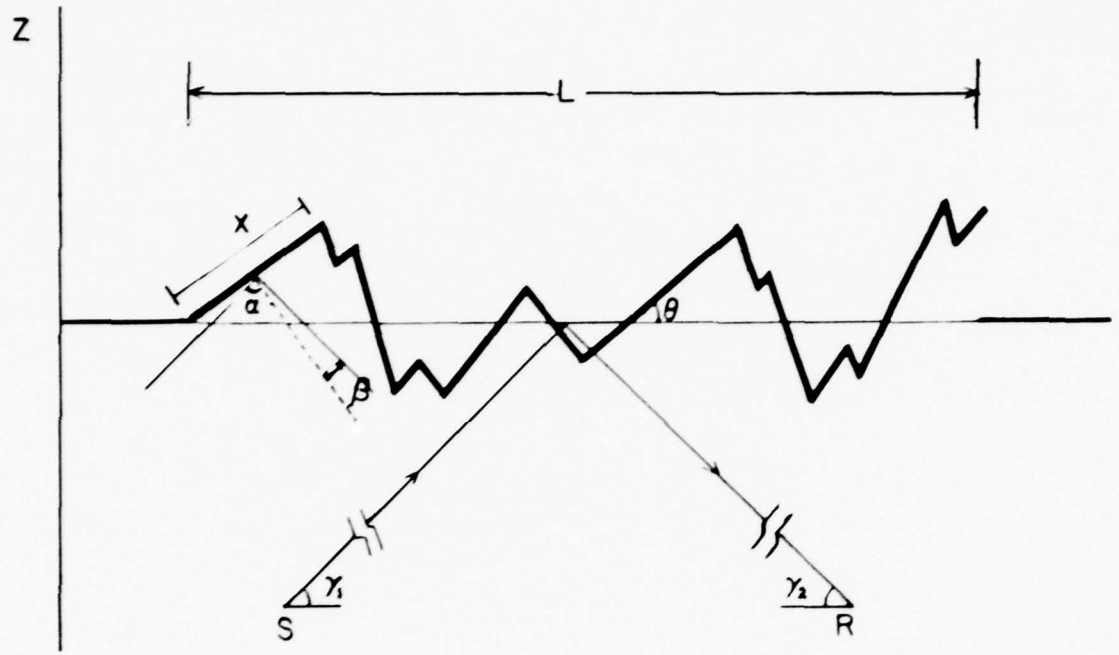

Figure 21. - The construction of a one dimensional surface model from facets. The model is in effect a piecewise linear fit to the actual water surface.

tively. The facet is assumed to extend a great many wavelengths in the Y direction. The source is assumed to be at a distance sufficient so that the insonifying wavefront over the X extent of the facet is essentially plane. This is not a severe restriction given that facets themselves can be expected to be relatively small. The amplitude, phase, and direction of the insonifying wave is determined by the projector orientation and beam pattern.

The reradiated field is calculated under these assumptions for the facet alone. The received pressure is found to be [Kerr, 1951; Goodman, 1968; Patterson, 1963,4]

$$P(\alpha,\beta) = \frac{p_o \cos\beta \sin(\tfrac{1}{2} kX)(\sin\alpha - \sin\beta)}{\cdot \exp(ik(R_1 + R_2))/\tfrac{1}{2} R_2(\sin\alpha - \sin\beta)} \quad (1)$$

where k is the the acoustic wavenumber, X is the facet size, R_1 and R_2 are the facet center to source and receiver distances respectively and p_0 is the pressure incident on the surface. In the forward specular direction $\alpha = \beta$ and the pressure P_{FS} is

$$P_{FS} = P_o\, kX \exp(ik(R_1 + R_2)) \cos\alpha/R_2 \quad (2)$$

In the backscatter direction $\alpha = -\beta$ and the pressure P_{BS} is

$$P_{BS} = P_o \cos\alpha \sin(kX \sin\alpha)\exp(ik(R_1 + R_2))/\sin\alpha \quad (3)$$

For large values of kX the received amplitude can be seen to be very small unless α and β are nearly equal (specular reflection). As kX becomes smaller the facet tends to scatter more omnidirectionally, approaching a point scatterer. In that case the scattered intensity approaches

$$|P^2| = |P_o|^2 \cos^2\alpha \, (kX)^2 \tag{4}$$

The eventual goal of a facet model, of course, is to predict the scattered intensity due to a continuous rough surface. The model represents that surface as an approximation in terms of plane facets parameterized, in this case, by size, slope and position. Additionally, the facets are constrained to be joined at the edges. In the case of a random rough surface the parameters are random variables, not necessarily independent. The scattered field due to this surface is calculated by summing the received fields due to each facet assuming that each is insonified by a plane wave of amplitude a_j and phase ϕ_j determined by the source beam pattern. This way of accounting for the characteristics of the source is similar to the approach used by Clay and Medwin [1970] to include the Fresnel approximation into the Helmholtz integral based formulation.

In the case of a random surface the basis for parameter assignment in

the model will be measurements of surface spatial statistics. From these a model surface can be generated (Fig. 21). In the case of a one dimensional representation, the total received amplitude due to a finite insonified region of the surface having length L can then be expressed as the sum of contributions from the facets.

$$P = \sum_{j=1}^{\ell} a_j \exp(ik(r_{j1}+r_{j2}))(\cos\alpha_j \cos\beta_j)^{\frac{1}{2}} \tag{5}$$

$$\sin \tfrac{1}{2}kX \cdot (\sin\alpha_j \cdot \sin\beta_j)/\tfrac{1}{2}(\sin\alpha_j - \sin\beta_j)$$

The received intensity is then

$$|PP^*| = \frac{1}{R_2^2} \left\{ \sum_{j=1}^{\ell} a_j^2 \cos\alpha_j \cos\beta_j \sin^2[(kX_i/2)(\sin\alpha_j - \sin\beta_j)] \right.$$

$$/(\sin\alpha_j - \sin\beta_j)^2 \tag{6}$$

$$+ 8\, R_e \left\{ \sum_{j=1}^{\ell} \sum_{m=1}^{j-1} a_j a_m \exp[ik(r_{1j} + r_{2j} - (r_{1m} - r_{2m}))] \right.$$

$$\cdot (\cos\alpha_j \cos\beta_j \cos\alpha_m \sin\beta_m)^{\frac{1}{2}} \sin\left[\frac{kX_j}{2}(\sin\alpha_j - \sin\beta_j)\right]$$

$$\left. \left. \cdot \sin\left[\frac{kX_m}{2}(\sin\alpha_m - \sin\beta_m)\right] / (\sin\alpha_j - \sin\beta_j)(\sin\alpha_m - \sin\beta_m) \right\} \right\}$$

The constraints on the generation of the surface are expressed as

$$\sum_{j=1}^{\ell} X_i \cos \theta_i = L \tag{7}$$

$$Z_j + X_j \sin \theta_j = Z_{j+2} - X_{j+1} \sin \theta_{j+1} \tag{8}$$

$$\xi_j + X_j \cos \theta_j = \xi_{j+1} - X_{j+1} \cos \theta_{j+1} \tag{9}$$

where z_j is the vertical displacement of facet center i and ξ_j is the horizontal displacement of the facet. The facet slope is $\tan\theta_j$. The first term in Eq. 6 represents the sum of received intensities from each facet separately. The second term contains the phase dependent interference contribution (constructive or destructive) among facets.

Let us consider the case of a distant projector in which the insonifying wavefront is plane. The angles α_j and β_j are expressed in terms of the source and receiver grazing angles, γ_1 and γ_2, and the facet slope, θ_j, by

$$\begin{aligned} \alpha_j &= \pi/2 - \gamma_1 - \theta_j \\ \beta_j &= \pi/2 - \gamma_2 + \theta_j \end{aligned} \tag{10}$$

For purposes of presenting a simple example we further stipulate that the source and receiver are at the same range, R, and grazing angle, γ. Under these conditions, the intensity measured in the specular direction (forward scatter) is

$$I_{FS} = \frac{|P_o|^2}{R_2^2} \left\{ \sum_{j=1}^{\ell} [\tan^2(\gamma-\theta_j)\sin^2(kX_j \cos(\gamma-\theta_j))] + \right.$$

$$\left. 2 \sum_{j=2}^{\ell} \sum_{m=1}^{j-1} \left[\frac{\cos \Phi_{jm} \sin(\gamma-\theta_j)\sin(\gamma-\theta_m)\sin(kX_j \cos(\gamma-\theta_j)\sin(kX_m \cos(\gamma-\theta_m))}{\cos(\gamma-\theta_j)\cos(\gamma-\theta_m)} \right] \right\} \quad (11)$$

and the monostatic backscattered intensity is

$$I_{BS} = \frac{|P_o|^2}{R_2^2} \left\{ \sum_{j=1}^{\ell} \left[\frac{\sin(\gamma-\theta_j)\sin(\gamma+\theta_j)\sin^2(kX_j \sin\gamma \sin\theta_j)}{\sin^2\gamma \sin^2\theta_j} \right] + \right.$$

$$2 \sum_{j=2}^{\ell} \sum_{m=1}^{j-1} \left[\frac{\cos \Phi'_{jm}(\sin(\gamma-\theta_j)\sin(\gamma+\theta_j)\sin(\gamma+\theta_m)\sin(\gamma-\theta_m))^{\frac{1}{2}}}{\sin^2\gamma \sin\theta_j \sin\theta_m} \cdot \right.$$

$$\left. \left. \sin(kX_j \sin\gamma \sin\theta_j) \sin(kX_m \sin\gamma \sin\theta_m) \right] \right\} \quad (12)$$

The term Φ_{jm} is the phase difference due to path length between facets in backscatter and is given by

$$\Phi_{jm} = k\left\{X_j \cos(\gamma-\theta_j) + X_m \cos(\gamma-\theta_m) + 2 \sum_{n=j+1}^{m-1} X_n \cos(\gamma_j-\theta_n)\right\} \quad (13)$$

Similarly the term Φ'_{jm} for the specular direction is given by

$$\Phi'_{jm} = k \sin \gamma \left\{ X_j \sin \theta_j + X_m \sin \theta_m + 2 \sum_{n=j+1}^{m-1} X_n \sin \theta_n \right\} \qquad (14)$$

The phase term Φ'_{jm} becomes very small when γ or θ and k are small. This occurs in the case of relatively low surface roughness, a virtually smooth surface. In that case the expressions reduce to a Huygen's source representation of a smooth surface.

In the case of monostatic backscatter, the phase term Φ_{jm} depends on the distance between facet centers along the direction of propagation of the incident wave. In the case of small slopes and low grazing angles this is approximately the horizontal distance between facets. If the distance between scatterers is typically much smaller than a wavelength, then one would expect that the contributions from facets would be coherent within Fresnel zones. Also, if the facet sizes are much smaller than a wavelength, then they behave as more or less omnidirectional scatterers. Under these conditions one would expect that the contributions of many Fresnel zones would be roughly of equal amplitude and uniformly distributed phase and would interfere at the receiver. At the other extreme, short wavelengths and relatively large facets, one would expect largely specular reflections from facets adding in a way that is dependent on geometry and surface statistics, but again very little backscatter. In the transition region, however, it seems likely that there exists a regime in which wavelengths are long enough to give rather broad reradiation patterns, but in which facet contributions add somewhat coherently.

This section has presented a preliminary form of a model based on a representation of a rough surface as an ensemble of plane segments. In order to be effective, we expect that the model will have to be refined and extended to 2 dimensions. While some of this may be accomplished analytically, it is expected that the end product will be a partially numerical model. Because of the simple parameterization of the initial form of the model, we expect that numerical experimentation will permit development of the model to be guided by a more or less continuous experimental validation process.

4. Water Surface Statistics: This program of measurements has been motivated by the rather demanding requirements of current analytical models of surface scatter for exact knowledge of the statistics of the scattering surface. One of the principal advantages of model tank studies is that they permit the use of a repeatable calibrated surface. This advantage is greatly reduced if that calibration is only partial or is imprecise. However, measurement of the behavior of a water surface in which there are significant features with sizes on the order of a millimeter is difficult and has been an ongoing effort at this facility since its establishment. A number of current models of underwater acoustic scattering and frequency spreading depend on a knowledge of surface height and surface slope distributions as well as the second order spatial and temporal correlation functions. It has been suggested, for example, that backscatter is due to reflection

from portions of the surface having very steep slopes, and that for similar reasons, observed asymmetry in Doppler spread might be due to asymmetry in the surface slope probability densities. These suggestions, as well as the requirements of the facet model described above, have generated a requirement for a detailed knowledge of surface slope statistics in the model tank facility. Such measurements have in the past been made by optical means [Bobb et al., 1979; Cox and Munk, 1958; Cox, 1958; Schooley, 1960; Sturm and Sorrell, 1973; Wu, 1971, 1977], but data of this sort lacks both the precision and statistical sufficiency for our purposes. This section describes the development of an improved measurement instrumentation and some recent measurements of water surface slopes and time-space covariance functions.

An alternative to optical measurement is the use of wave staffs. In the case of the small scale measurements used in model tank experimentation, the staff is a very fine wire and is normally called a probe wire. The probe wire penetrates the surface vertically and is used to sense the height of the water at that location as a function of time. These time series of wave heights contain information not derivable from glitter photographic measurements and are the basis for the data contained in this section.

As before, the water surface measurements were made in the 8 meter diameter by 1.3 meter deep model tank at the Yale facility. The wind driven waves which are the subject of the measurements are generated

by a collimated fan blowing over the water with approximately 3 meters of fetch. The air velocity is regulated by a combination of fan speed and aperture adjustment. The formation of standing waves in the apparatus is suppressed to a considerable extent by a downwind beach and by irregularities in the skirts of the tunnel used to contain the wind. Wind speeds reported were determined by an anemometer suspended about 18 cm. above the water surface near the measurement site.

Water height measurements were made by measuring the capacitance between the conductor of a .07 mm. uniformly insulated (Formvar insulated magnet) wire and the water in which it is suspended vertically. The capacitance of such a system is linearly proportional to the immersion depth providing that the wire and insulating coating are uniform. In order to develop useful time series of water depth, the capacitance must be sampled at a rate on the order of several hundred times per second. This was accomplished by using the probe as the capacitor in a high pass filter with the water at ground potential as shown in Figures 22 and 23. Measurements of surface slopes were made using two probes with independent electronics. A constant amplitude 5 kHz. sinusoid is applied to the basic probe circuit. The amplified output of the probe, an amplitude modulated signal, is then detected to derive a waveheight signal. A signal proportional to slope is developed by subtracting the detector outputs of two probes of equal calibration. Typically the result is digitized at a rate of 100 times per second to a precision of 12 bits and stored for analysis.

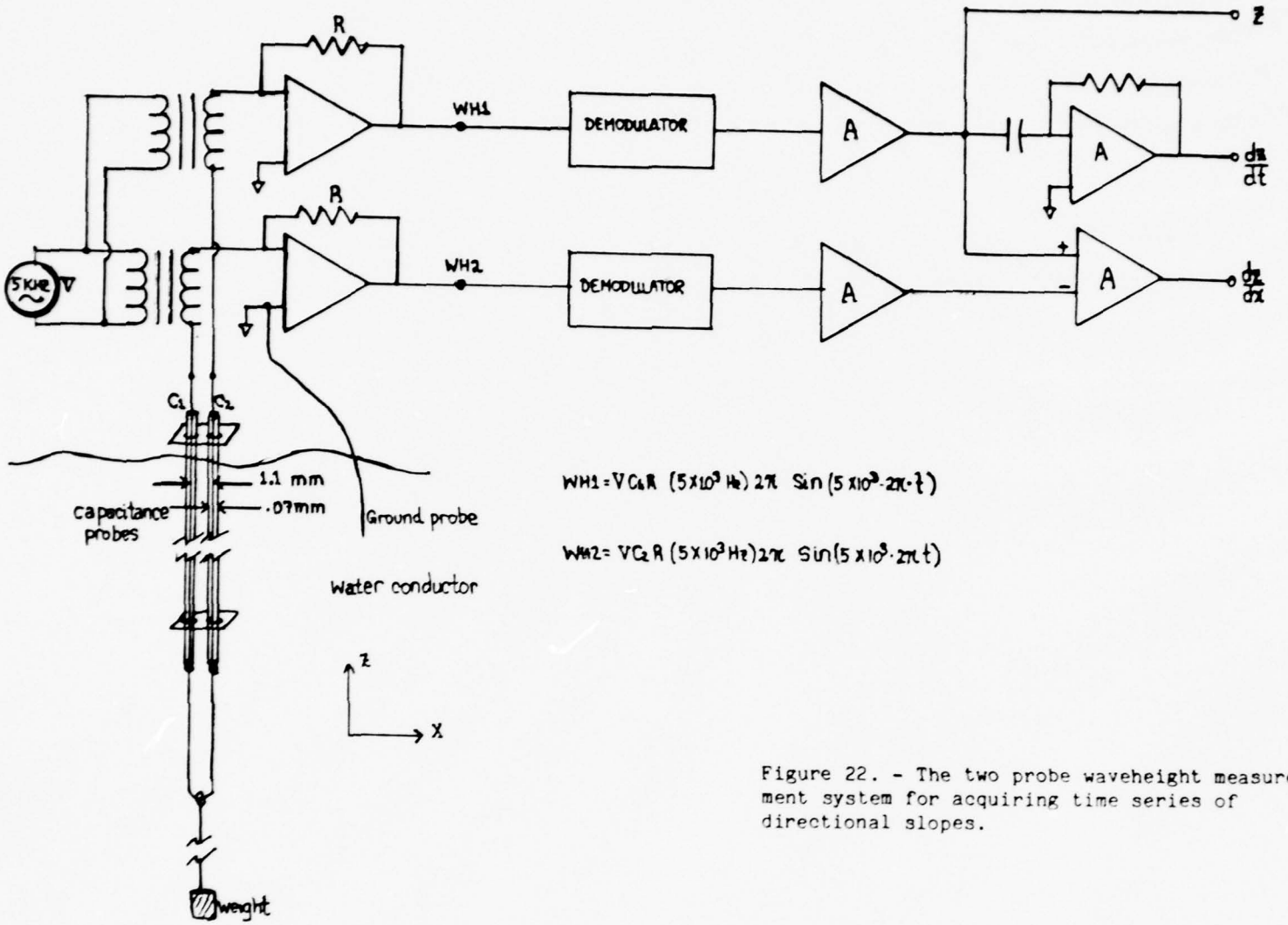

Figure 22. - The two probe waveheight measurement system for acquiring time series of directional slopes.

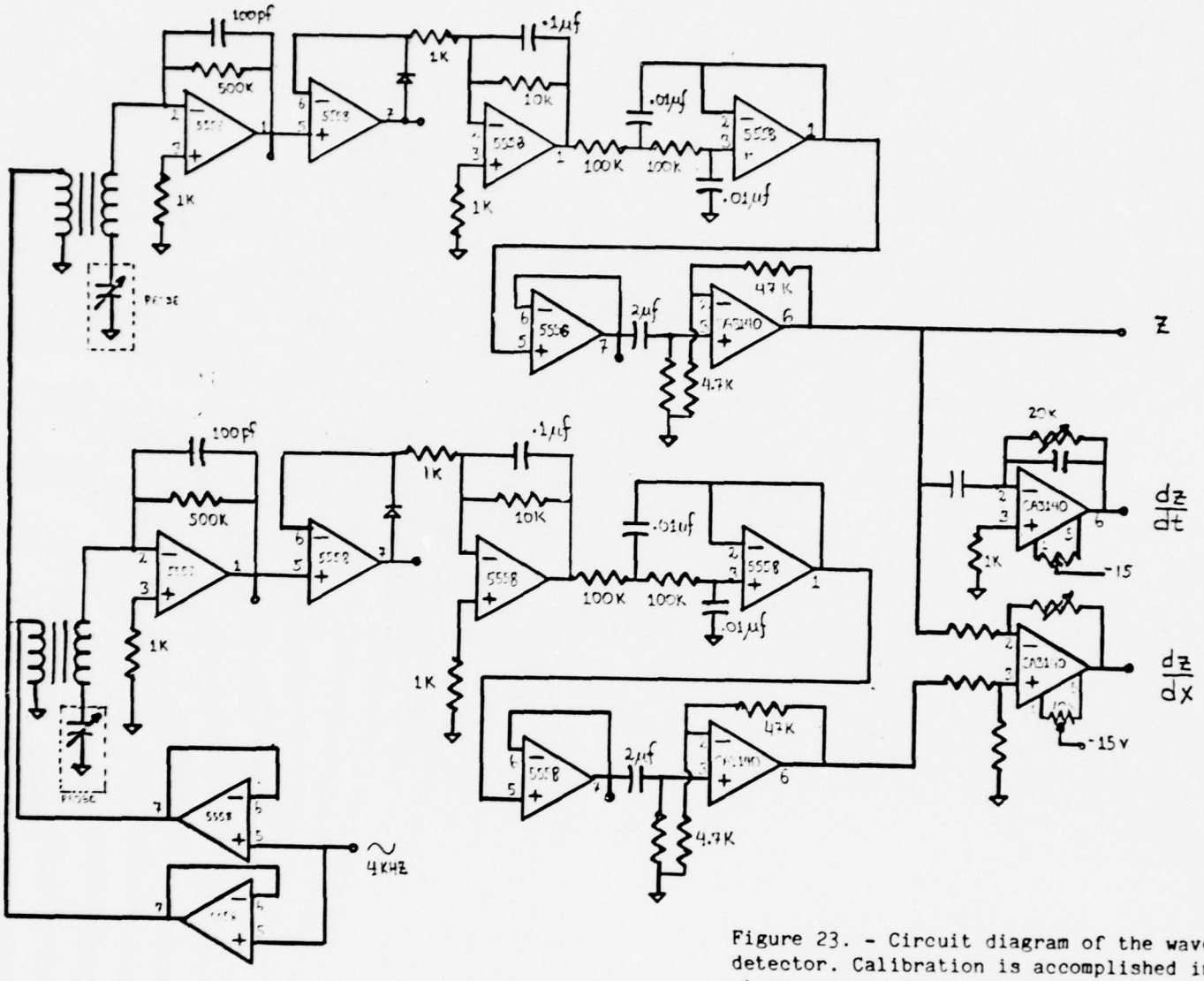

Figure 23. - Circuit diagram of the waveheight detector. Calibration is accomplished in a two stage process described in the text.

The probe electronics are fairly insensitive to small changes in water conductivity (a 10 percent change in conductivity produces a 1 percent change in capacitance). Furthermore, the apparent absence of crosstalk between probe systems makes it possible to make precise two-probe measurements at relatively small separations. In the past, questions have been raised as to the accuracy with which a wire probe system can measure small features of the water surface [Sturm and Sorrell, 1973] It is apparent that the meniscus formed by the water near the wire exhibits a hysteresis which can couple water height and velocity in such a way as to cause an apparent flattening of crests and troughs. This effect is, however, limited in magnitude to roughly twice the wire diameter and was therefore discounted as insignificant. In addition it might be expected that the extent of the meniscus would distort two-probe measurements of wave slope. In order to confirm that these effects were not important in the measurements of slope presented here, trial measurements were made at a variety of probe spacing both greater and smaller than the normal 1 mm. These measurements resulted in essentially identical slope histograms, confirming that the probe spacing was substantially greater than the meniscus effect.

Probe calibration was accomplished by a DC calibration procedure. The probe immersion depth in still water was varied by a known amount and the resulting change in detector output was gain adjusted to an appropriate value. This procedure, while sufficient for simple wave-height measurements was found to be inadequate for the more demanding

differential measurements involved in slope analysis. In order to calibrate two probe systems with sufficient accuracy to permit slope measurement, a method was required which would result in a relative accuracy substantially greater than the absolute accuracy achievable with the immersion calibration. The method used relies on the properties of slope statistics in the following way.

Suppose the conversion gain of probe i is a_i, i = 1,2, and the actual waveheight at each probe location is z_i. The third moment of the voltage difference at the detector output is

$$\mu_3 = \langle (a_1 z_1 - a_2 z_2)^3 \rangle \tag{15}$$

which is proportional to surface slope. Expanding terms one obtains

$$\mu_3 = a_1^3 \langle z_1^3 \rangle - a_2^3 \langle z_2^3 \rangle - 3a_1^2 a_2 \langle z_2 z_1^2 \rangle + 3a_1 a_2^2 \langle z_1 z_2^2 \rangle \tag{16}$$

If the probe positions are now reversed, the same instrumentation gives

$$\mu_3' = a_1^3 \langle Z_2^3 \rangle - a_2^3 \langle Z_1^3 \rangle - 3a_1^2 a_2 \langle Z_1 Z_2^2 \rangle$$

$$+ 3 a_1 a_2^2 \langle Z_1^2 Z_2 \rangle \qquad (17)$$

which is equal to $-\mu_3$ only if $a_1 = a_2$. The calibration method used was to calibrate two probes absolutely using immersion variation, then fine tune the gain of one probe until the sum of the two third moment results went to zero.

Water height and slope signals were sampled and digitized at 10 ms. intervals to 12 bit precision. From 51,200 sample records, histograms of surface slope were constructed to a resolution of .07 in slope. These are given as Figures 24 - 33. These differ substantially from the preliminary results included in the Final Report of 1978 primarily because of improvements in instrumentation and redefinition of coordinates.

Table 1 is a summary of the mean square value and coefficient of skewness of slope at a variety of wind speeds including those which are the facility standards (those with "Wind numbers"). Negative slope is defined, rather arbitrarily, to correspond to a surface rising with the wind direction. We observe that all such distributions are negatively skewed. The skewness rises with wind speed up to a speed of 5 m./sec. and then falls until at wind speeds greater than 11. m./sec. no appreciable skewness is observed. Under these conditions, the most

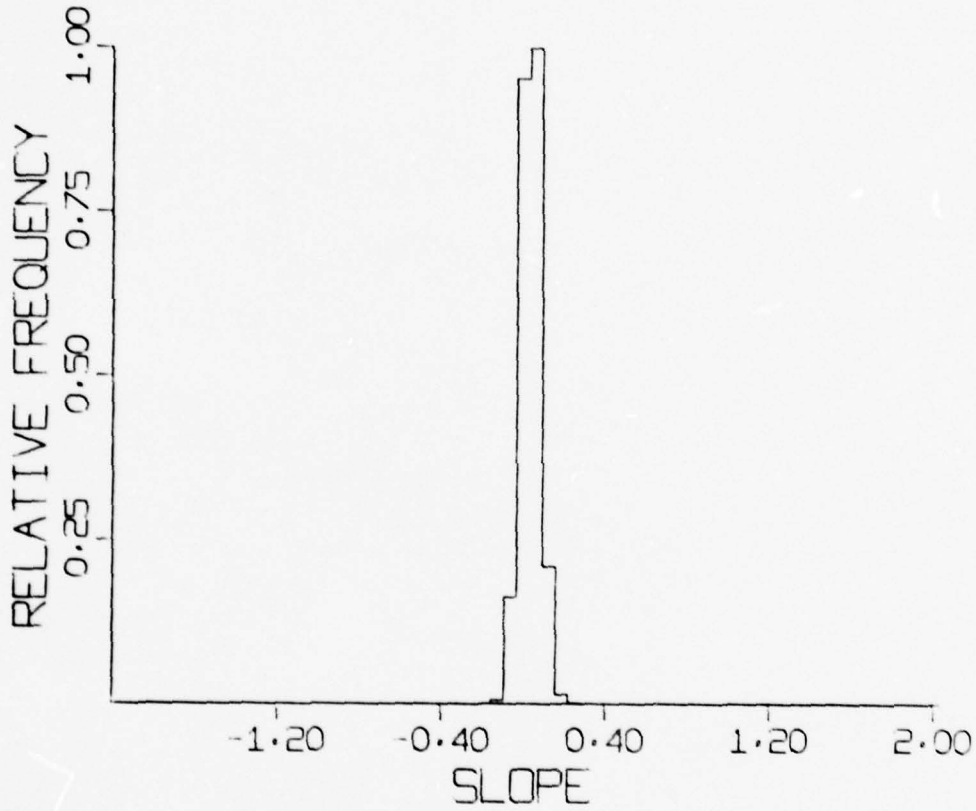

Figure 24. - Histogram of water wave slopes taken crosswind at wind speed 3.8 m./sec.

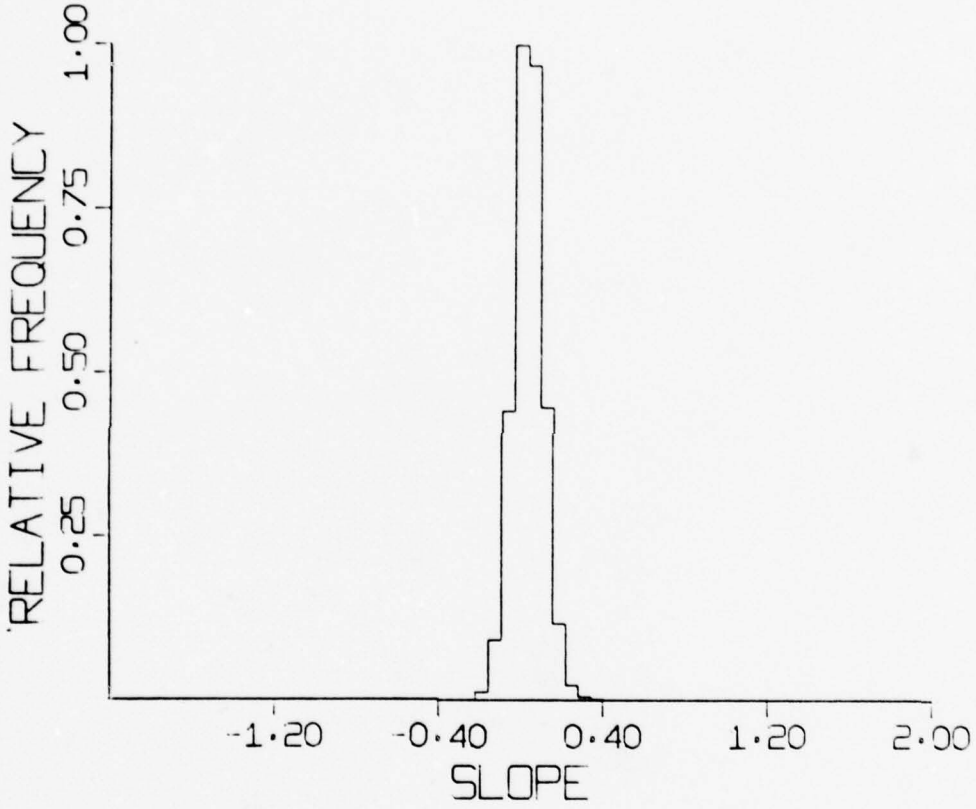

Figure 25. - Histogram of water wave slopes taken crosswind at wind speed 5.4 m./sec.

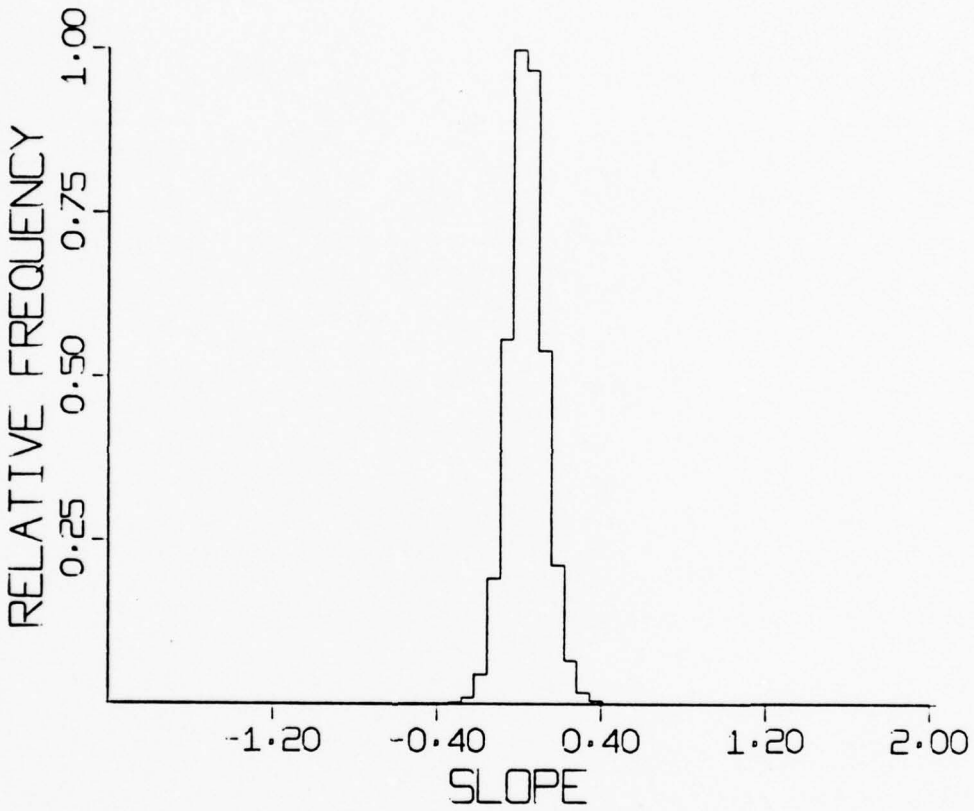

Figure 26. - Histogram of water wave slopes taken crosswind at wind speed 6.7 m./sec.

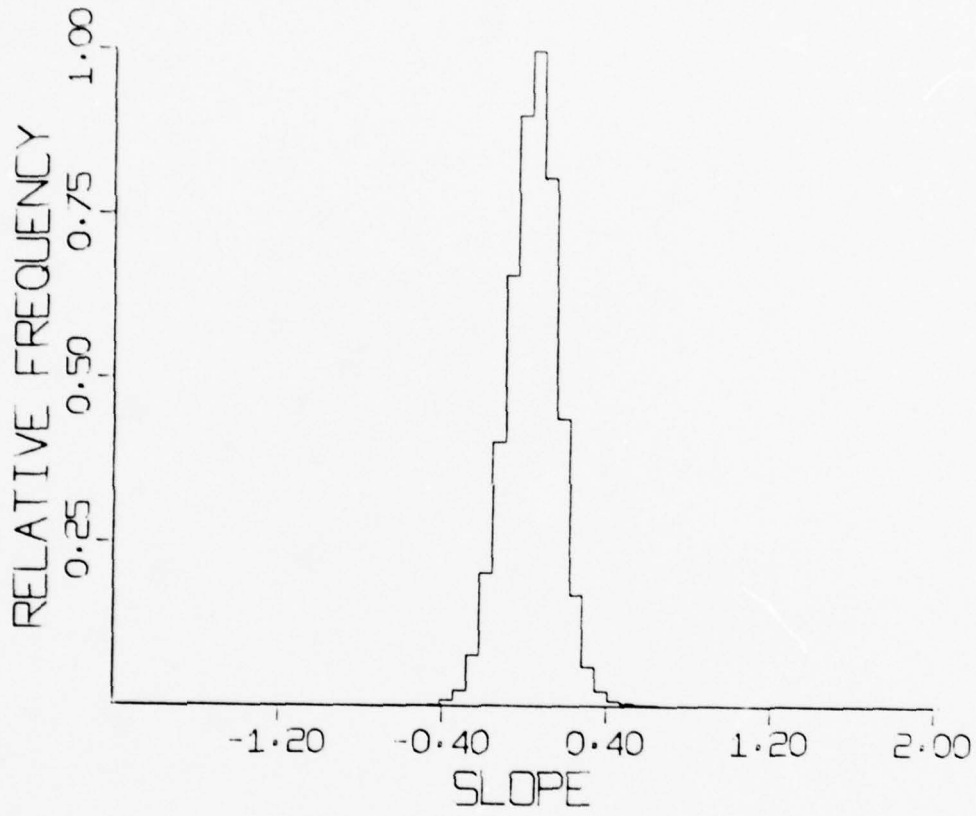

Figure 27. - Histogram of water wave slopes taken crosswind at wind speed 8.3 m./sec.

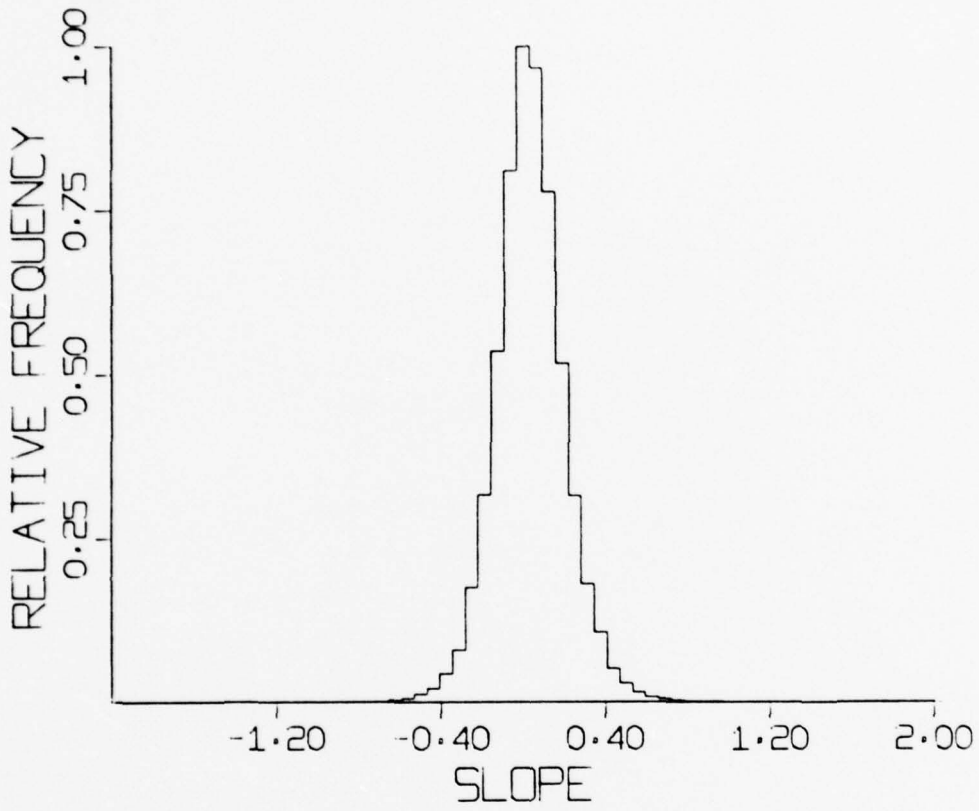

Figure 28. - Histogram of water wave slopes taken crosswind at wind speed 11.2 m./sec.

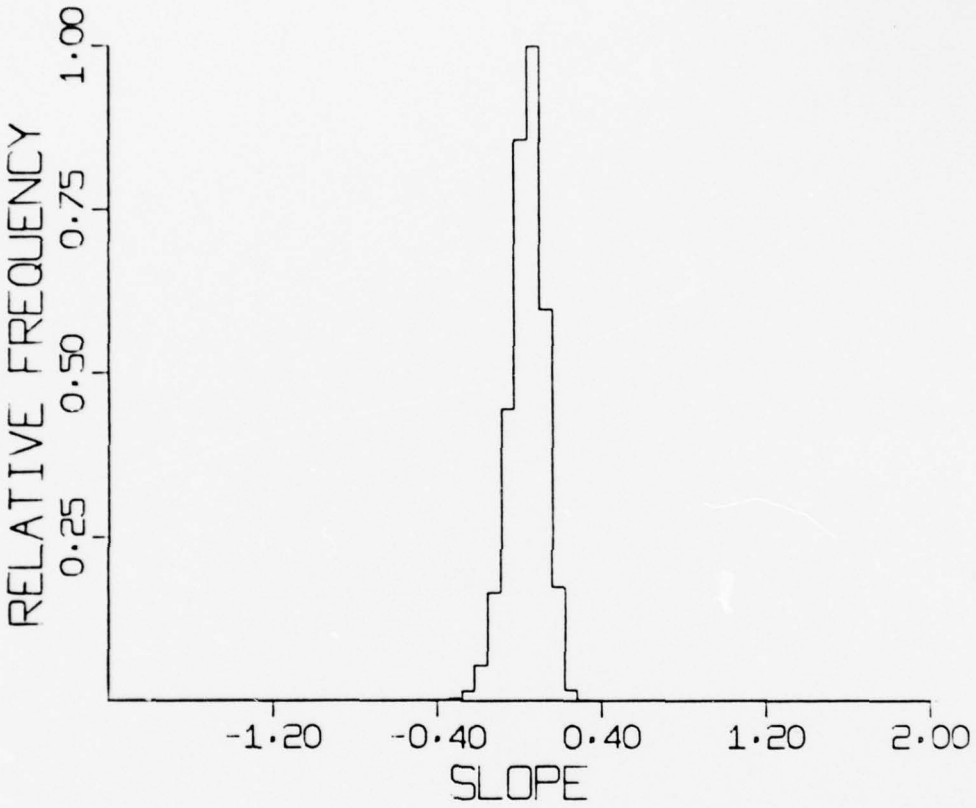

Figure 29. - Histogram of water wave slopes taken downwind at wind speed 3.8 m./sec.

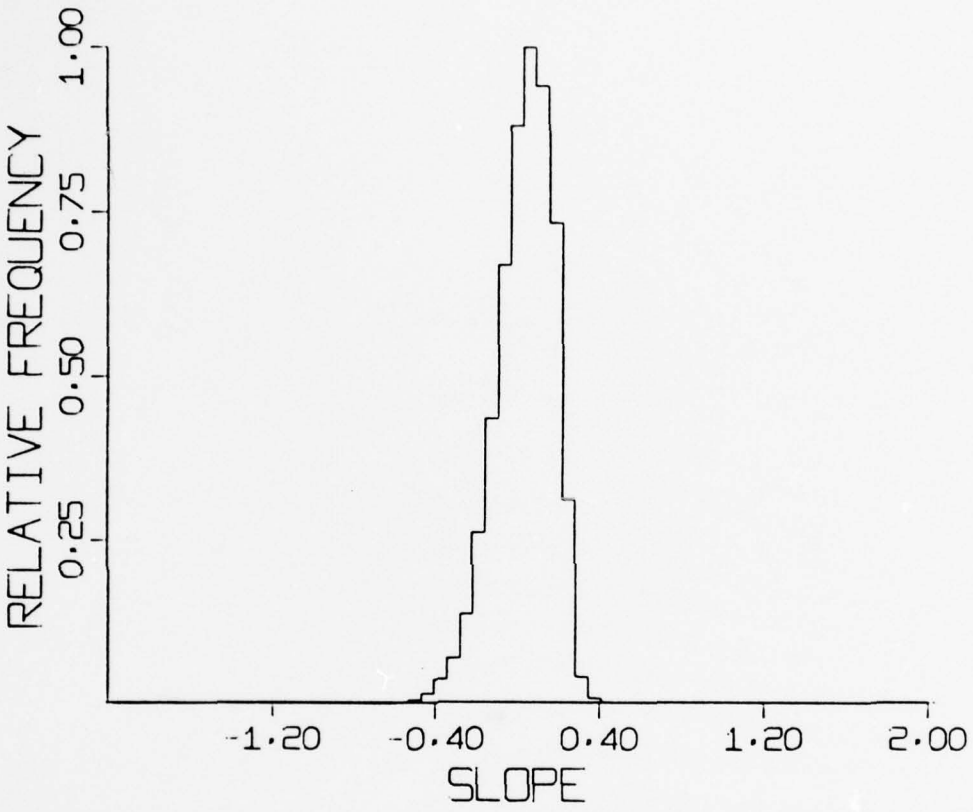

Figure 30. Histogram of water wave slopes taken downwind at wind speed 5.4 m./sec.

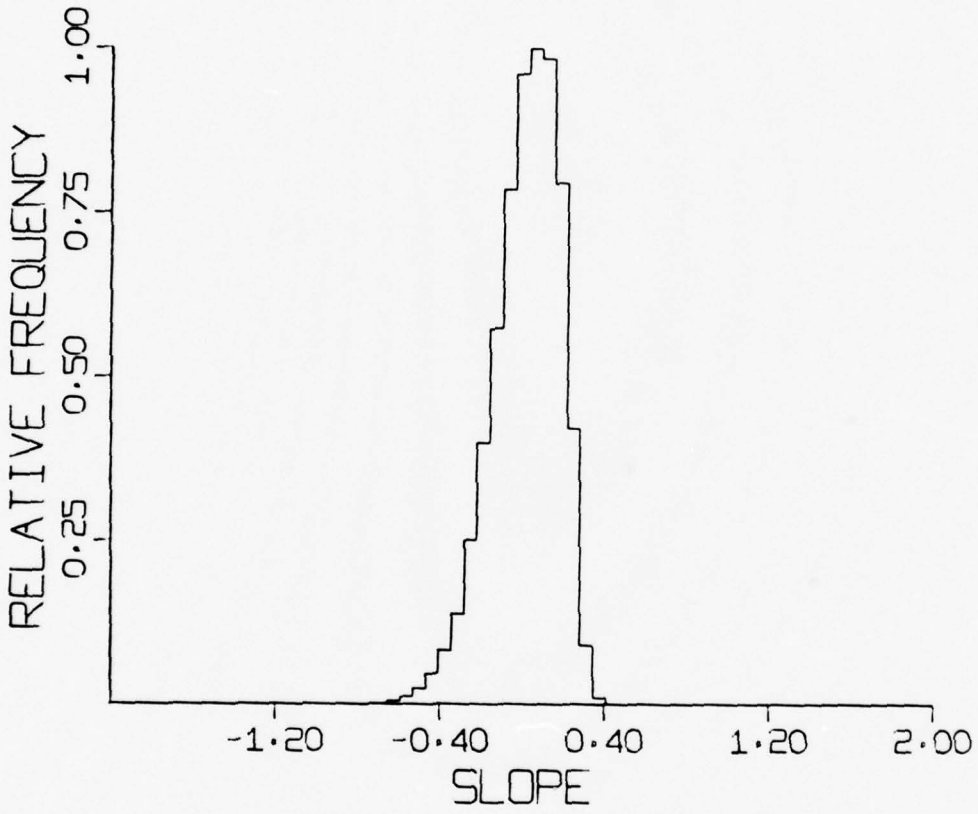

Figure 31. - Histogram of water wave slopes taken downwind at wind speed 6.7 m./sec.

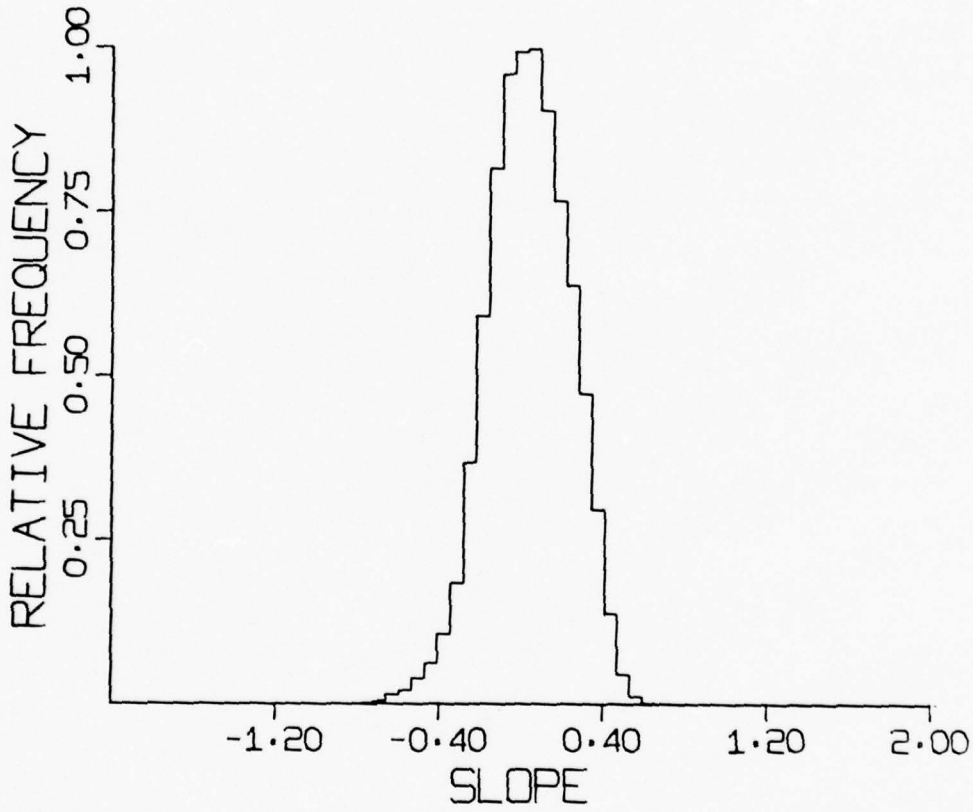

Figure 32. - Histogram of water wave slopes taken downwind at wind speed 8.3 m./sec.

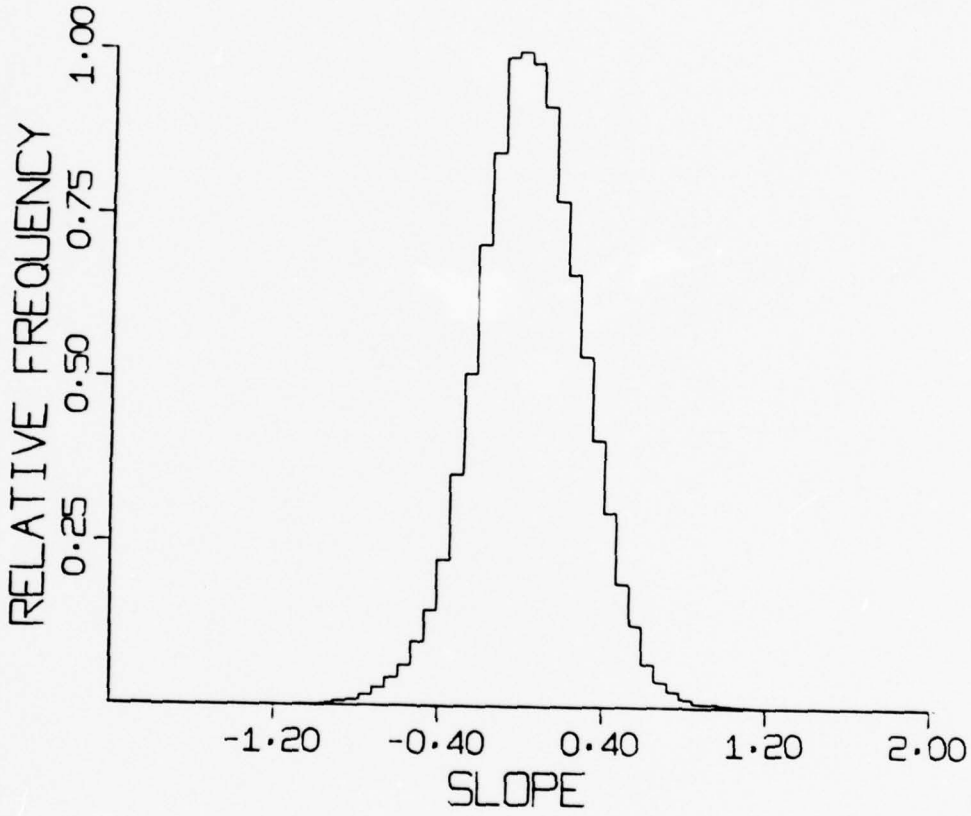

Figure 33. - Histogram of water wave slopes taken downwind at wind speed 11.2 m./sec.

TABLE 1: SLOPE DISTRIBUTION MOMENTS

Orientation	Wind No.	Wind Speed	Mean Sq.	Skewness
Up/Down	1	3.75 m/s	.009	-0.4
"	2	5.4	.020	-0.5
"		6.2	.024	
"	3	6.7	.028	-0.4
"		6.8	.030	
"		7.2	.034	-0.3
"	4	8.3	.040	-0.2
"		9.4	.048	-0.2
"		10.7	.057	-0.2
"	5	11.2	.067	-0.1
Cross	1	3.75	.002	
"	2	5.4	.004	
"	3	6.7	.006	
"	4	8.3	.012	
"	5	11.2	.022	

probable slope is slightly positive and of small magnitude, whereas large slopes are more likely to be negative. This behavior is consistent with results obtained by Wu [1971] and Bobb et al. [1979] in independent model tank measurements. The largest surface tilt angle observed was 60^{o}. Mean square slope increased with wind speed in an almost linear fashion up to 11. m./sec. (see Fig. 34). This is in general agreement with Cox [1958] and Wu [1971,1977] although there are differences in absolute magnitude and the apparent rate of increase with wind speed. The reason for the disagreement is unclear, but could certainly be due to differences in tank construction and effective fetch. Crosswind slope distributions (Figure 34) also exhibited an increase in mean square slope with wind speed, but to much smaller values.

Sample time series of wave height and slope at a wind speed of 8.3 m./sec. are given in Fig. 35. The records are synchronous in time and therefore permit direct comparison. Figure 36 displays a similar comparison with time derivative of waveheight. These examples illustrate the high frequency structure associated with the downwind side of wave crests which has been pointed out by Wu [1977] and others. Figure 37 shows a synchronous comparison of wave slope and negative time derivative. The similarity of these records confirms the notion that even small features of the surface change only slowly with respect to their translation velocity (relatively low dispersion) in the model tank situation.

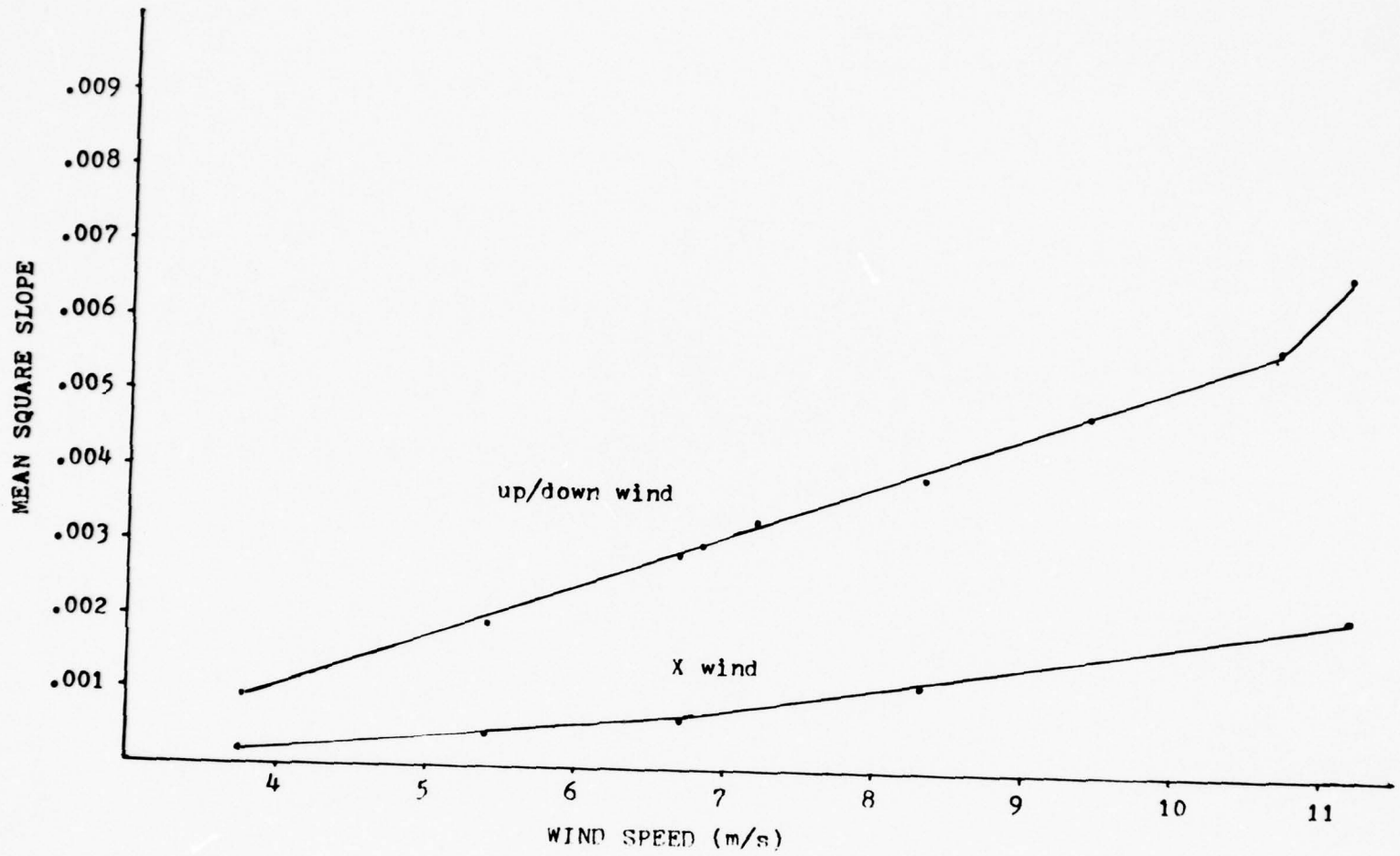

Figure 34. - Mean square slope vs. wind speed for downwind and crosswind orientations. The degree of linearity is substantially greater than that reported by other investigations.

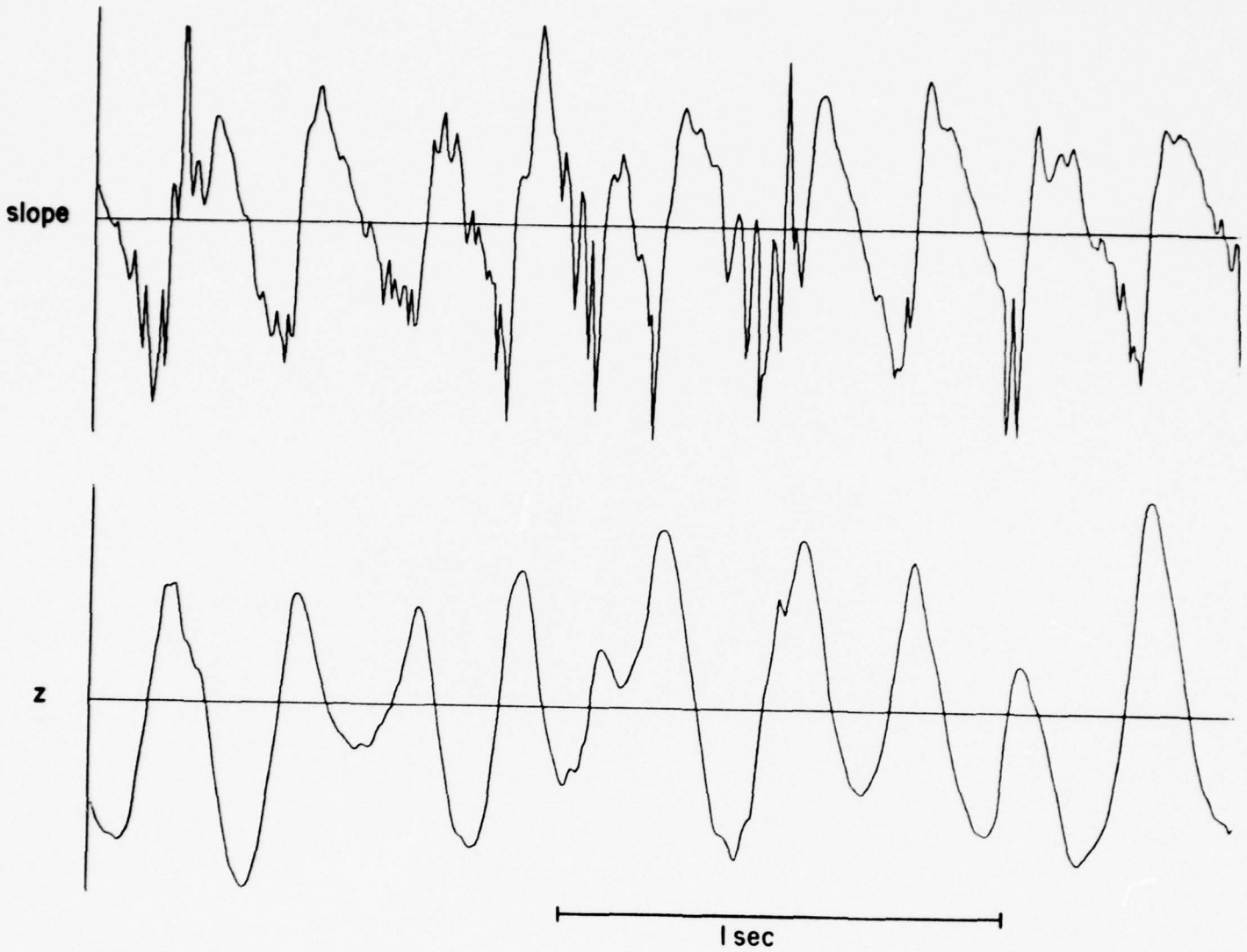

Figure 35. - Synchronous measurements of wave slope and height taken at wind speed 8.3 m./sec. in the downwind direction.

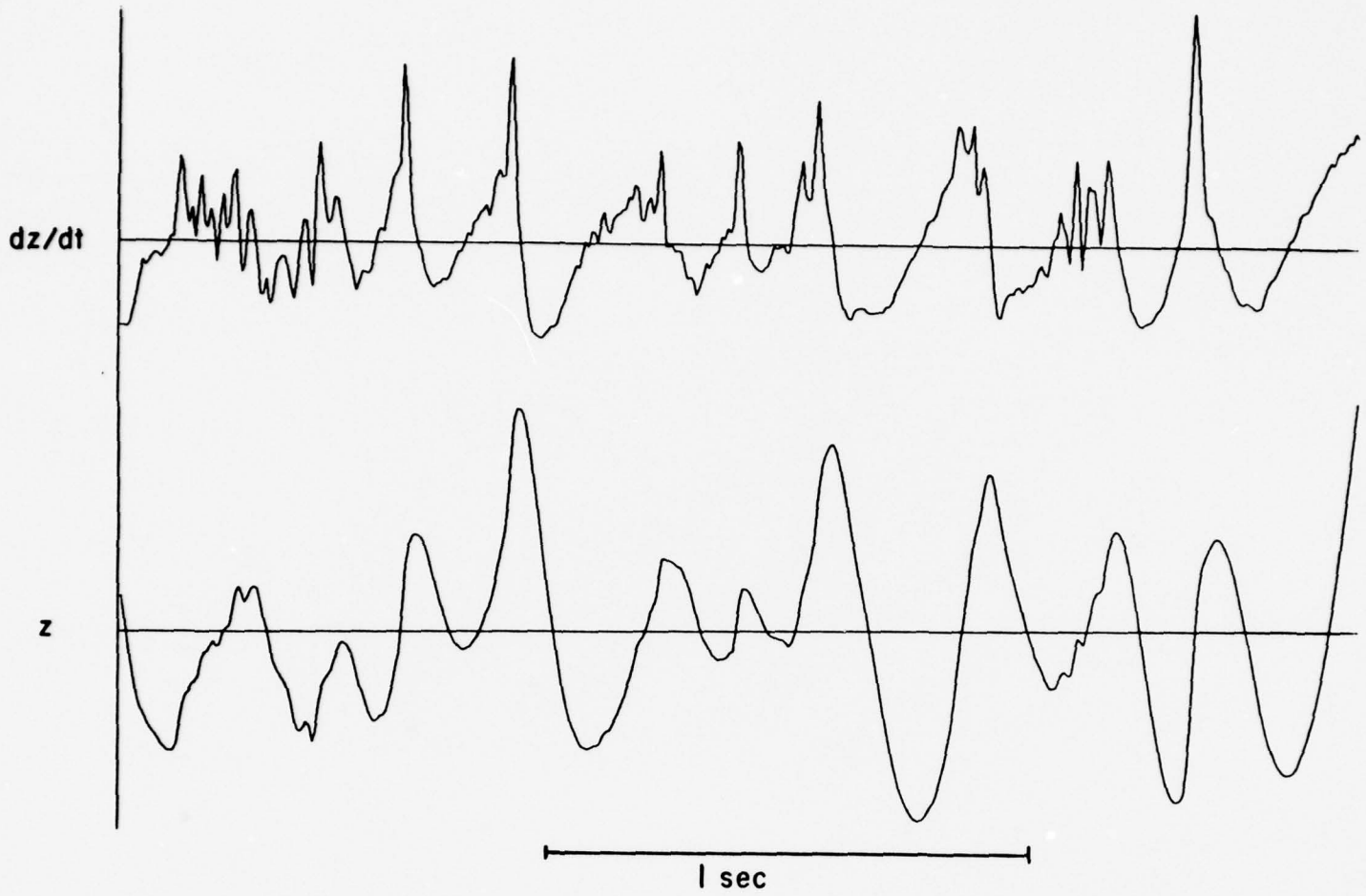

Figure 36. - Synchronous measurements of height and height rate taken at wind speed 8.3 m./sec. in the downwind direction.

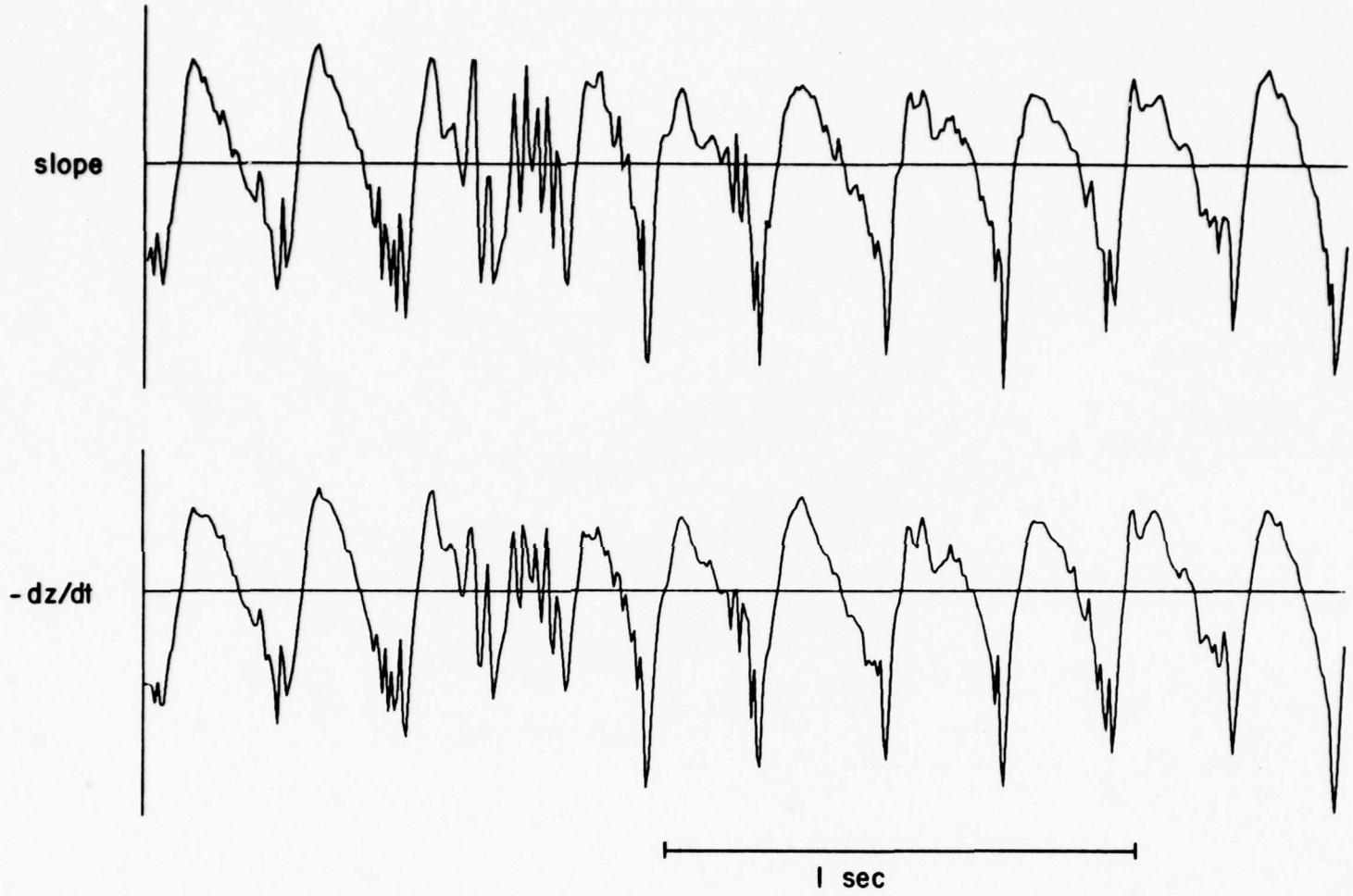

Figure 37. - Synchronous measurements of slope and height rate (displayed as negative) showing the relative lack of dispersion at this scale.

The statistics described above, while they are important in the formulation of the facet model, do not satisfy the requirements of a number of current theoretical formulations predicting Doppler spread in the surface scatter channel. These models generally need a description of the surface in terms of its second order space-time statistics. These are in some cases described by power spectra [Harper and LaBianca, 1975] and in others by the space-time correlation function of the surface [Scharf and Swarts, 1974]. These statistics contain information about the regularity and directionality of the surface waves which are not available from single point statistics and are therefore necessary in order to account for scattering processes in which partial reinforcement (Bragg) mechanisms are important.

During the past year an extensive set of measurements was made of the space-time covariance function of one of the facility standard surfaces (Wind 4). These measurements involved the design and construction of a computer controlled translator and software which permitted the automatic acquisition of covariances for 128 temporal and 32 spatial lags in one run. Because of the relatively low bandwidth of the surface motion and the requirement for good statistical sufficiency in the data, such a run required a very long time (ca. 8 hours). During such a run, no other work could be done in the facility. Therefore the measurements were taken over an extended period of time and are at present limited to an ensemble of 40,000 covariance measurements describing a 32 cm. radius, 90^{o} sector for time lags up to

1.28 seconds. This set of data describes just one wind driven surface condition and must be extended to include at least one or two more. When these measurements are complete they will be reported in a separate technical report.

5. Ultrasonic Array Construction: It has become apparent that the transducers presently available in the facility will not be useful in the characterization of scattering at very low grazing angles. In order to deal in a predictable way with geometries involving low grazing angles, projector and receiver beamwidths must be at least of the same order as and preferably smaller than the proposed grazing angle. During the past year the authors undertook to develop an ultrasonic array to serve the needs of low grazing angle work in future experimentation. This project was undertaken in part because of the recent visit to the facility of Dr. Anthony Pratt of the University of Technology, Loughborough, UK, who made a great number of very useful suggestions based on his own experience which made it possible for the authors to construct the array with a minimum of difficulty.

The array was constructed using rectangular PZT (5400) transducer elements of dimensions 23 mm. x 9.5 mm. and thickness resonant at 320 kHz. The elements were designed to be operated as quarter wave air-backed resonators. The length and width were chosen so as suppress any other resonance modes at operating frequency. The transducers are

mounted in a foam filled polycarbonate (Lexan) housing. Although the acoustic impedance of the foam backing is much higher than that of air, it is still an order of magnitude smaller than that of water and thus suffices as a backing material.

The construction details of the array are shown in Figure 38. The housing is built of 3/8" thick Lexan plate. It is a partitioned rectangular box with both sides, open filled with a self-foaming resin, milled out to accommodate the transducer elements. The elements were mounted on 1 cm. centers in the face of the housing and the front face was sealed with a thin layer of silicone rubber (RTV). Electrical connection was made by soldered connections carried to a cable assembly of 17 - RG174A coaxial cables. The array is amplitude shaded by an assembly of seventeen precision potentiometers (10 turn Helipot) connected directly to the cable assembly.

The array was characterized using sinusoidal bursts about 2 ms. long at 100 ms. intervals. All measurements were taken with the receiver about 3 m. distant from the array. After individual impedance measurements were made to verify the manageability of the design, individual element frequency responses were taken in the finished array. A selection of these is given as Figure 39. Using this information the shader was adjusted to give an effectively uniform shading function at the resonant frequency. The frequency response of the array on axis under these conditions is given as Figure 40.

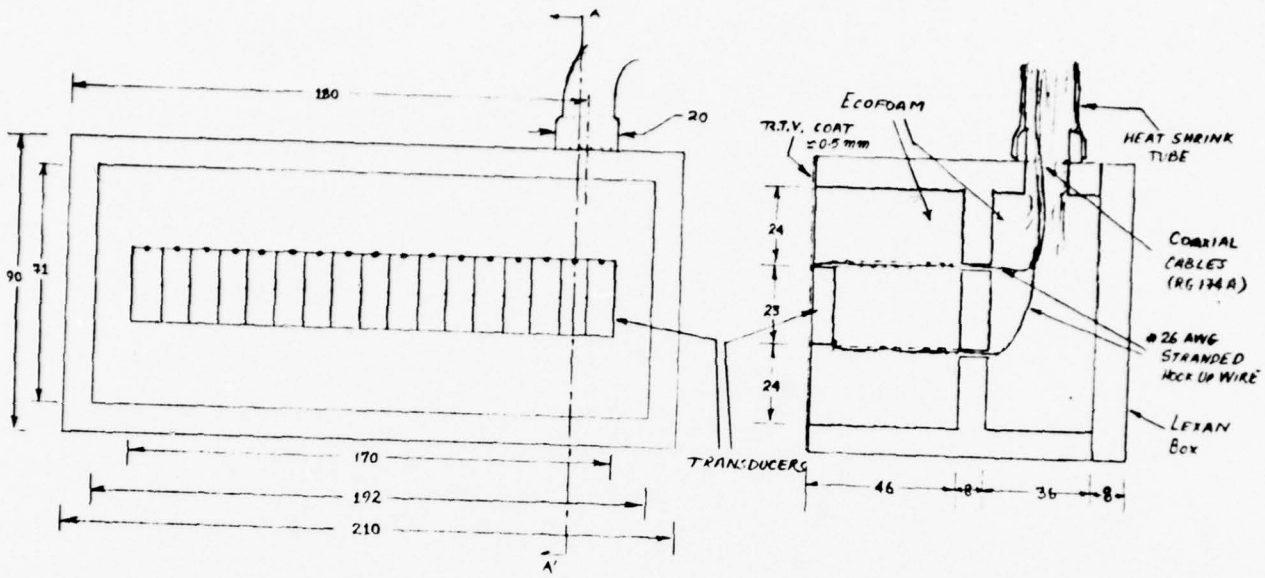

(ALL DIMENSIONS IN MM.)

Figure 38. - Details of construction of the 17 element 320 kHz. array. The transducer elements are PZT (5400).

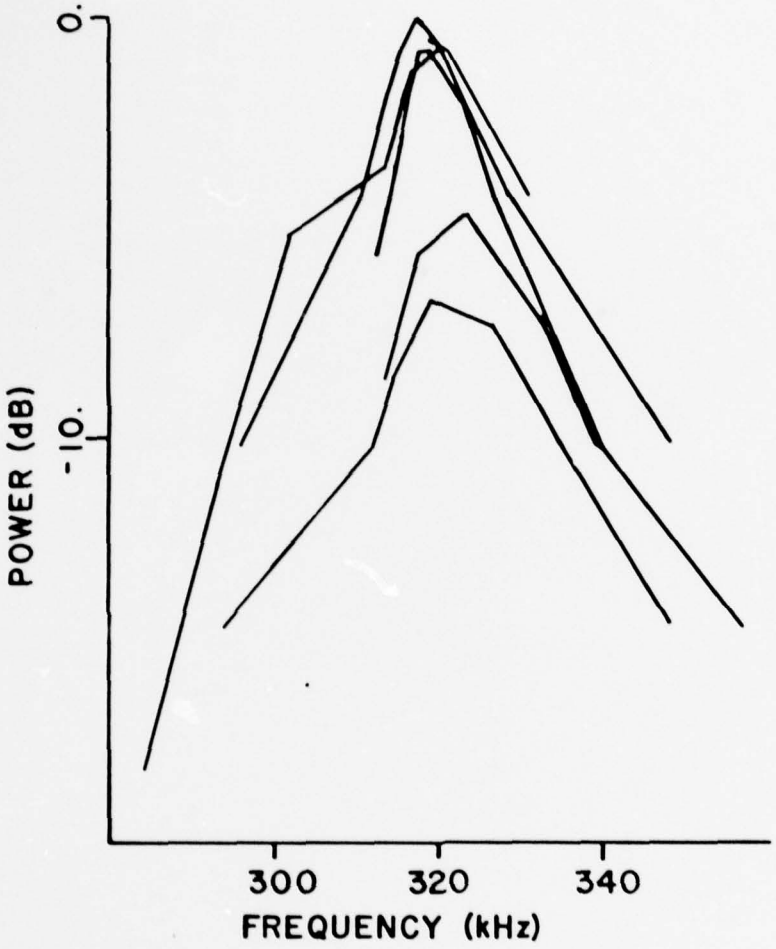

Figure 39. - Responses of a selection of five transducer elements. Some portion of the non-uniformity could have been due to construction imperfections.

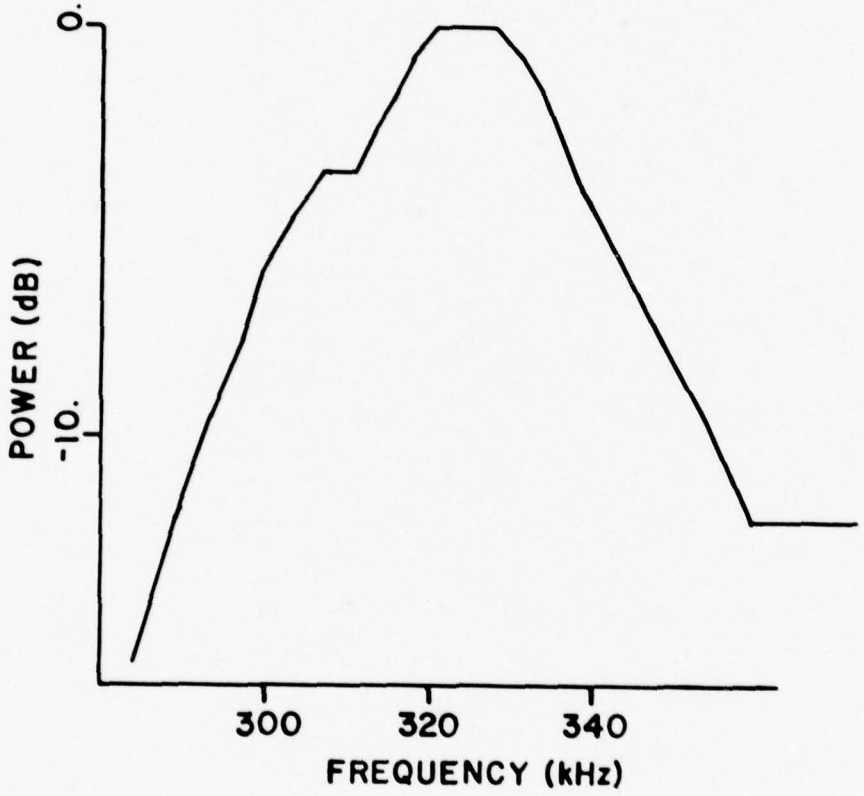

Figure 40. - Overall response of the finished array with all elements driven so as to generate equal output.

Figure 41. gives the polar response at resonance along the axis of the array of a single element. The -10 dB. beam width is seen to be 35^{o}. Figure 42. gives the polar response of the uniformly shaded array at 322.6 kHz. Under these conditions the main lobe -10 dB. beam width is 5^{o}, but there are sidelobes at 29^{o} at only 5 dB. below the main lobe. In addition the power radiated between the principal lobes is only 17 dB. down. The pattern perpendicular to the principal axis of the of the array is shown in Figure 43.

Several experiments with shading were made to test the effect of shading on the pattern of the array. The first of these was a cosine shading function used as a basis for comparison with more complicated shading functions. The result is given in Figure 44. As can be seen the simple shading function resulted in a reduction of main lobe width to 4^{o} and a substantial reduction in the near sidelobe power to at most - 21 dB. A second attempt at shading was the application of the Dolf-Chebychev method for a predicted sidelobe rejection of 30 dB. The result of this experiment is given as Figure 45. The actual reduction obtained was only -23 dB., possibly because of approximations made in adjusting the shading potentiometers. Again the mainlobe width was about 4^{o}.

The general result of this adventure in array design was the acquisition of a new and useful tool for narrow beam probing of scattering surfaces. The array appears to have sufficient efficiency and band-

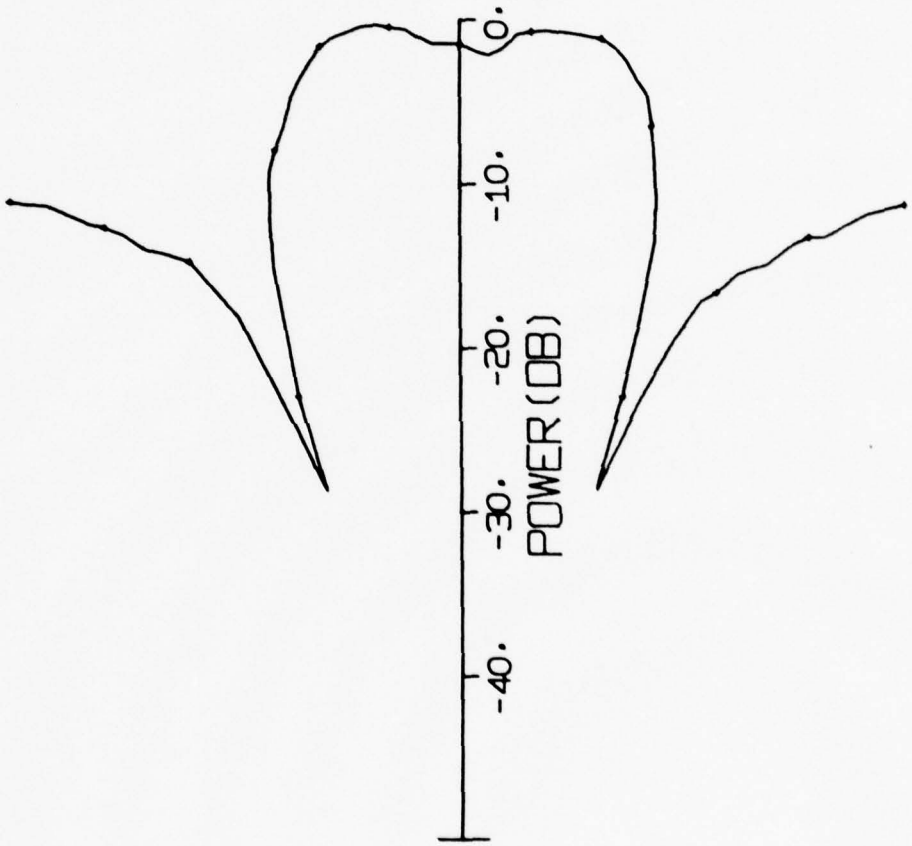

Figure 41. - Polar response of a single transducer element along the principal axis of the array.

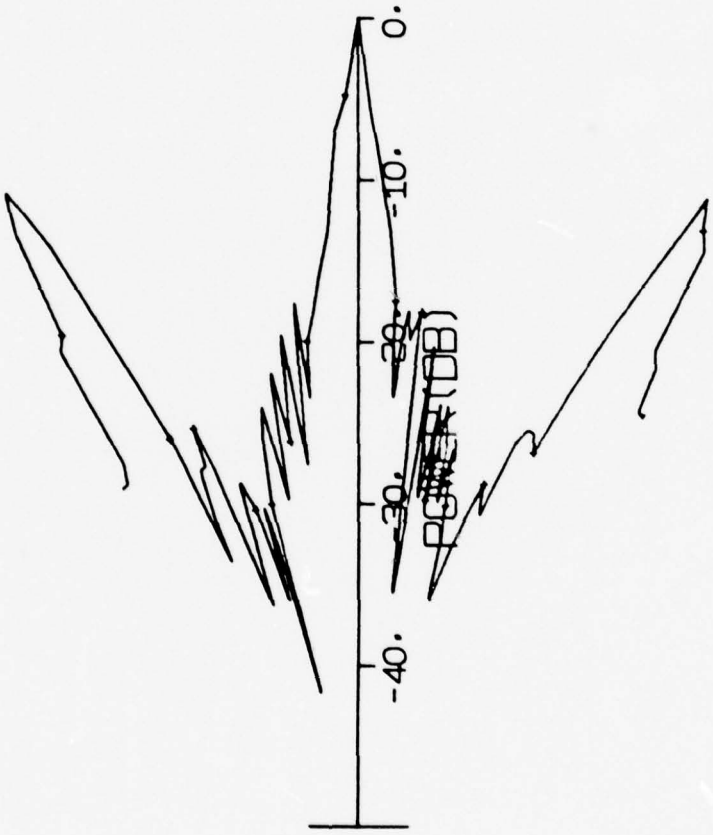

Figure 42. - Polar response of the completed array uniformly shaded as in Fig. 40.

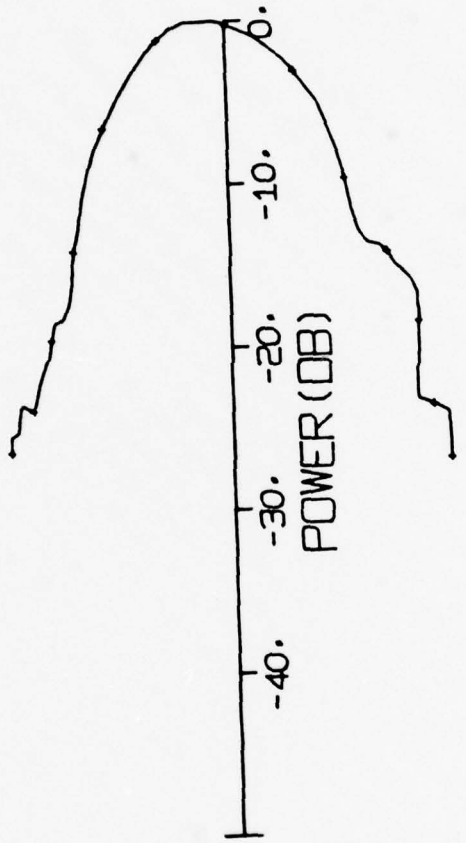

Figure 43. - Polar response of the array perpendicular to the pricipal axis.

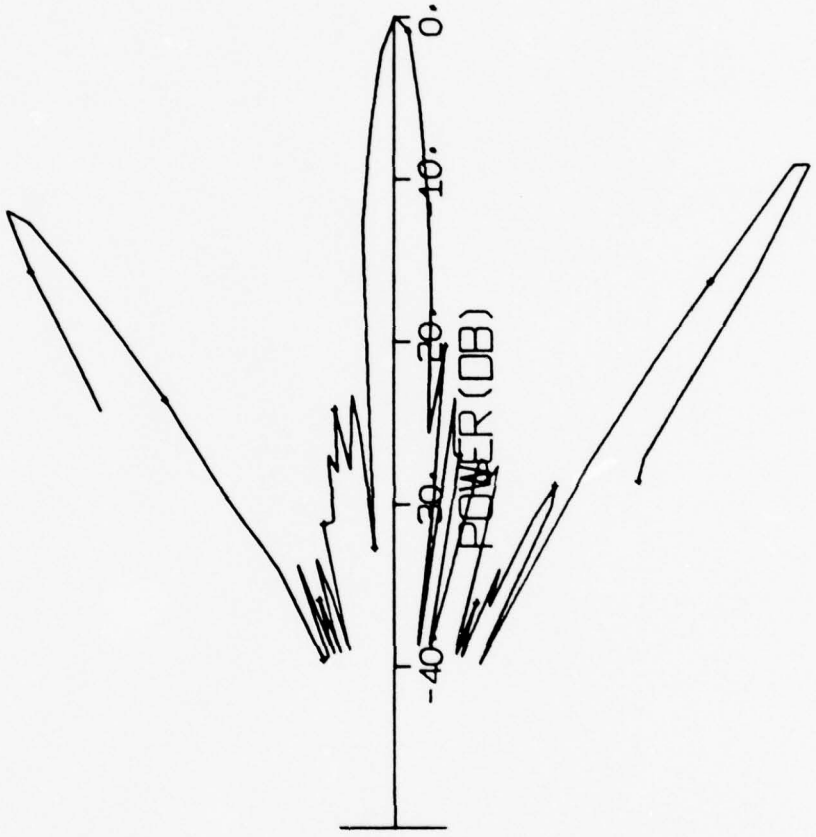

Figure 44. - Polar response of the array along the principal axis with cosine shading.

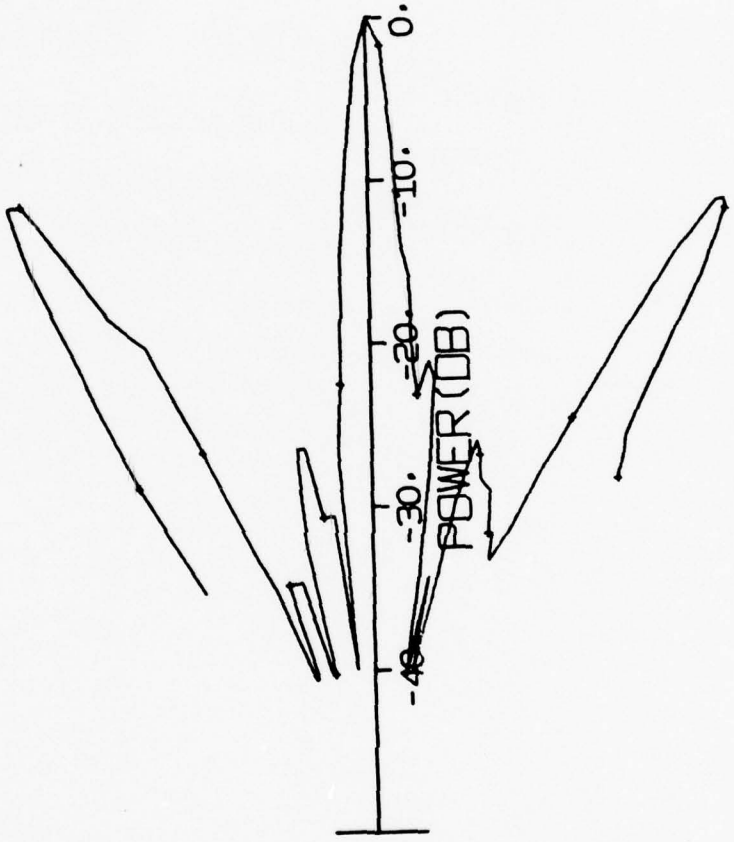

Figure 45. - Polar response of the array with Dolf-Chebychev shading. Not a great deal of improvement was realized.

width for pulsed monochromatic probing of the surface at low grazing angles. Not surprisingly, the patterns achieved with shading do not appear terribly sensitive to the choice of shading function.

6. Frequency Spreading Studies: Rather independently of the above work, previous studies of frequency spreading in forward scatter have been continued in order to explore an anomalous shift in mean received frequency under conditions of geometric symmetry [Zornig, 1978]. These results are as yet not fully explained. However, a theory explaining some of the effects observed is in the process of publication [Tuteur et al., 1979] and will be available in the near future.

The experiment conducted was basically the same as that described in the above referenced work. A preemphasized probing signal s(t) is designed and synthesized. This signal is applied to a projector, interacts with the surface, is received by a hydrophone and is digitized at the sampling rate used in its synthesis. Because of the linearity of the process, it is assumed and has been demonstrated [Zornig and McDonald, 1974] that the signal waveform received after digitization is equal to the convolution of the original probing signal, the impulse responses of the two transducers, and the time varying impulse response of the surface. Since the surface impulse response is slowly varying with respect to the time scale of the signal itself, it is possible to represent this process after trans-

formation to the signal frequency domain as follows:

$$R(\omega_n,t) = S(\omega_n)\, P_0(\omega)\, H(\omega,t)\, P_1(\omega) \qquad (18)$$

where $S(\omega_n)$ is the probing signal applied to the projector

$P_0(\omega)$ is the projector transfer function

$P_1(\omega)$ is the receiver transfer function

$H(\omega,t)$ is the time varying transfer function of the surface

$R(\omega_n,t)$ is the signal out of the hydrophone and amplifiers

The data collection instrumentation removed a fixed time delay from the received signals which is reflected in the notation here in the use of the same t in both $H(\omega,t)$ and $R(\omega_n,t)$ and the suppression of time dependence in $S(\omega_n)$. The representation of $S(\omega_n)$ and $R(\omega_n,t)$ as defined on a finite domain of frequencies is based on the fact that both waveforms are wholly contained in relatively short time windows and are analyzed in terms of discrete Fourier transforms.

In this representation, $H(\omega,t)$ is a stationary ergodic random process expressing the amplitude and phase response of the surface to frequency ω at time t. Care was taken, of course, to sample in t at rates in excess of the Nyquist rate of the process; the actual sampling rate used varied between 50 and 300 per second. In practice, sampling in t was limited to 64 contiguous samples in a burst. This limit was imposed by memory availability in the data acquisition computer, and is

equivalent to CW pulse lengths of from 850 to 20,000 cycles of the carrier. The recorded samples of $H(\omega,t)$ were then Fourier transformed on the variable t to give an ensemble of instantaneous spreading functions.

$$\Phi(\omega_n,\nu_k) = < F(\omega_n,\nu_k) * W(\nu_k) > \tag{20}$$

Ensembles of roughly 200 measurements of $F(\omega_n,\nu_k)$ were then windowed and averaged to give the frequency spreading function,

$$F(\omega_n,\nu_k) = (S(\omega_n)P_0(\omega_n)\ P_1(\omega_n))^{-1} \cdot (\Delta t \sum_{m=o}^{N-1} R(\omega_n,t_m)e^{-j\nu_k m\Delta t}) \tag{19}$$

In previous work, a systematic shift of the frequency of the maximum of the frequency spreading function had been observed under some symmetric geometries. Since a number of theoretical formulations predicted that under conditions of symmetric transducer location Doppler spread would be symmetric, it was suggested that the observed asymmetries could be due to small misalignments of the experimental apparatus. Therefore a careful set of experiments was performed in which transducer alignment was surveyed to a high degree of precision and then varied so as to test the sensitivity of the results to alignment error. Figure 46. gives a set of Doppler spread spectra taken crosswind at 4 harmonically related frequencies and relatively high roughnesses. The apparatus was exactly aligned both with with respect to itself and to the wind direction. It can be seen that a

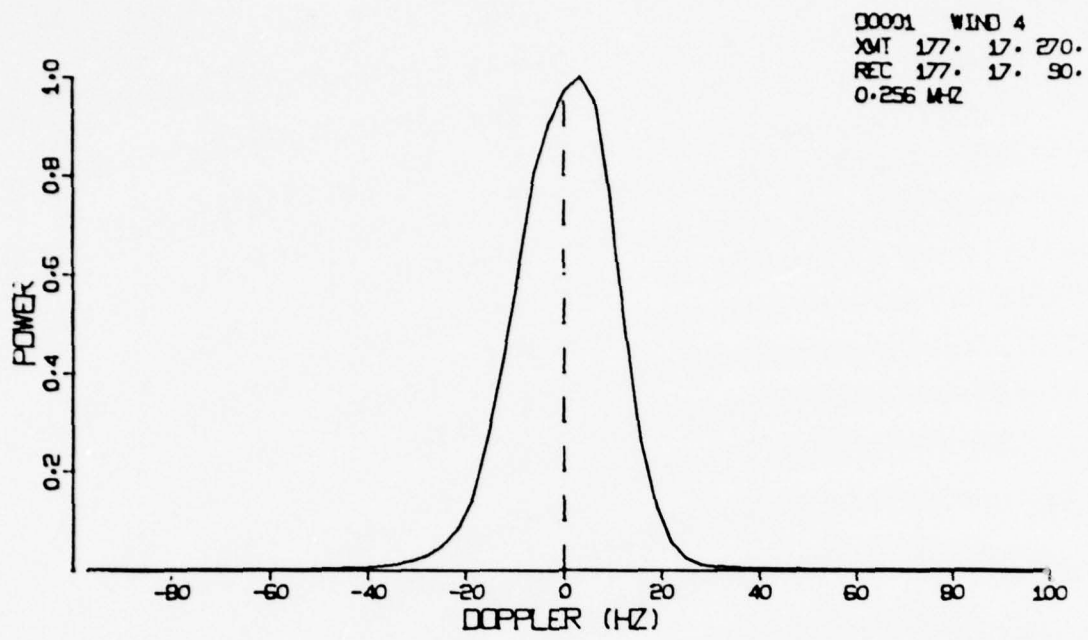

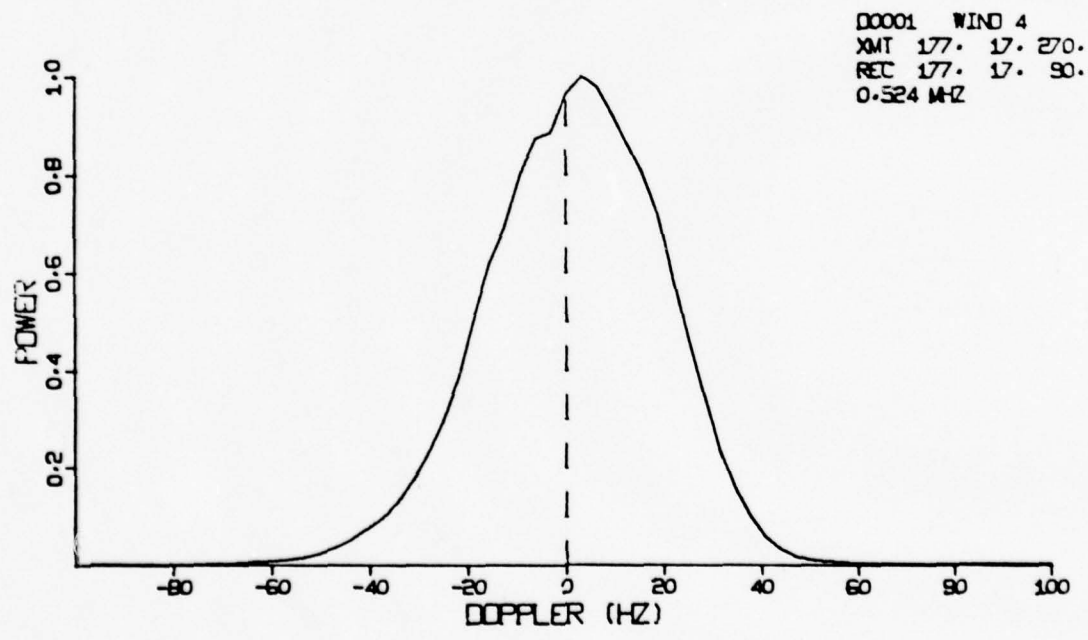

Figure 46(a): - Frequency spread spectrum taken at 17 deg. grazing angle and well surveyed crosswind orientation.

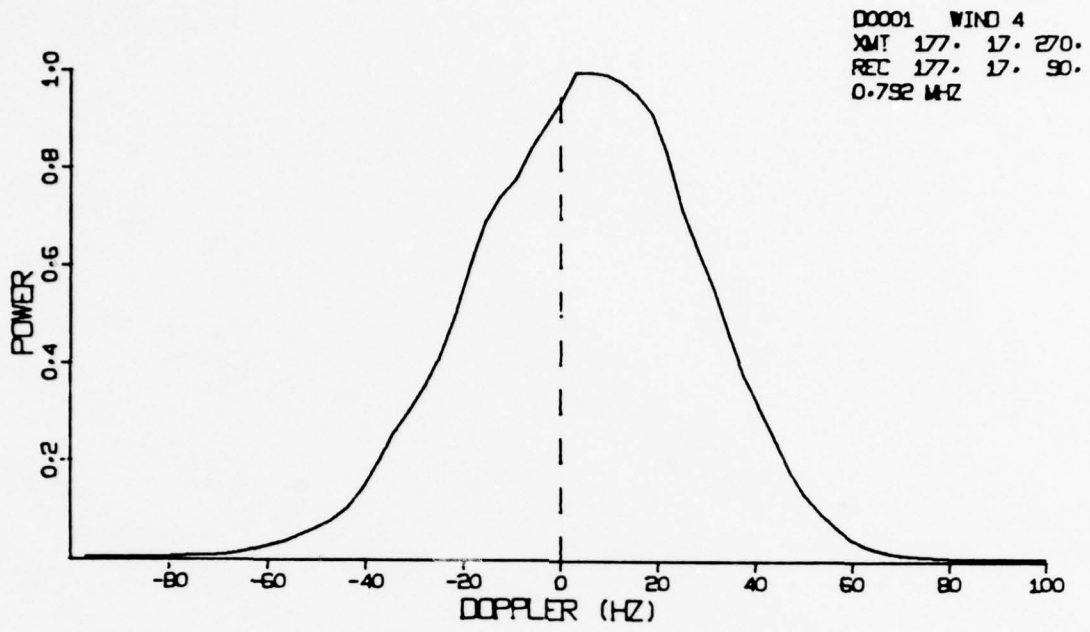

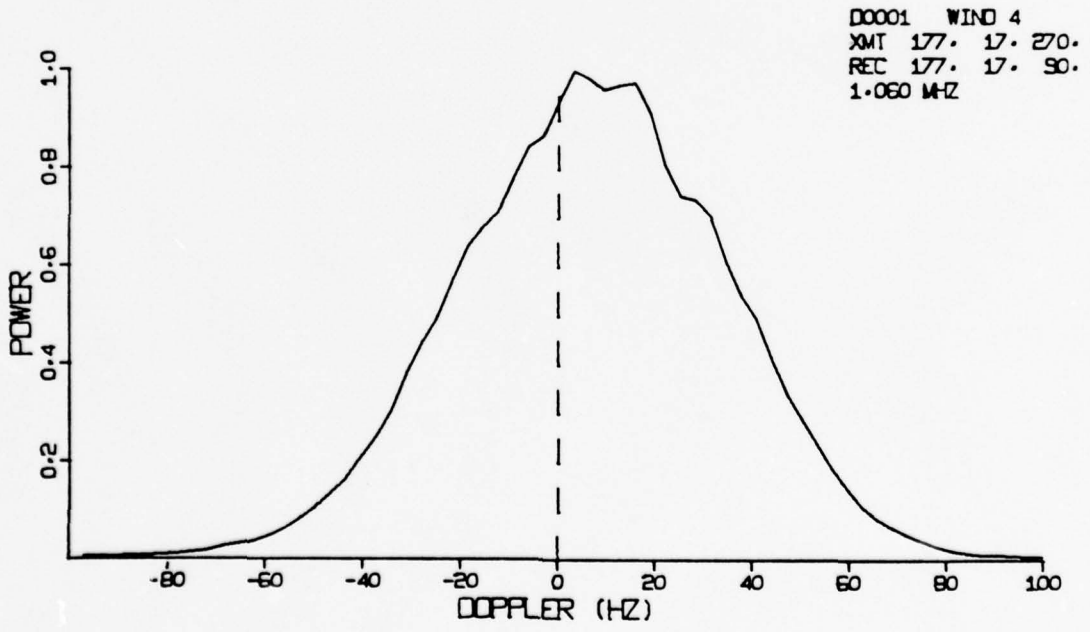

Figure 46(b): - Frequency spread spectrum taken at 17 deg. grazing angle and well surveyed crosswind orientation.

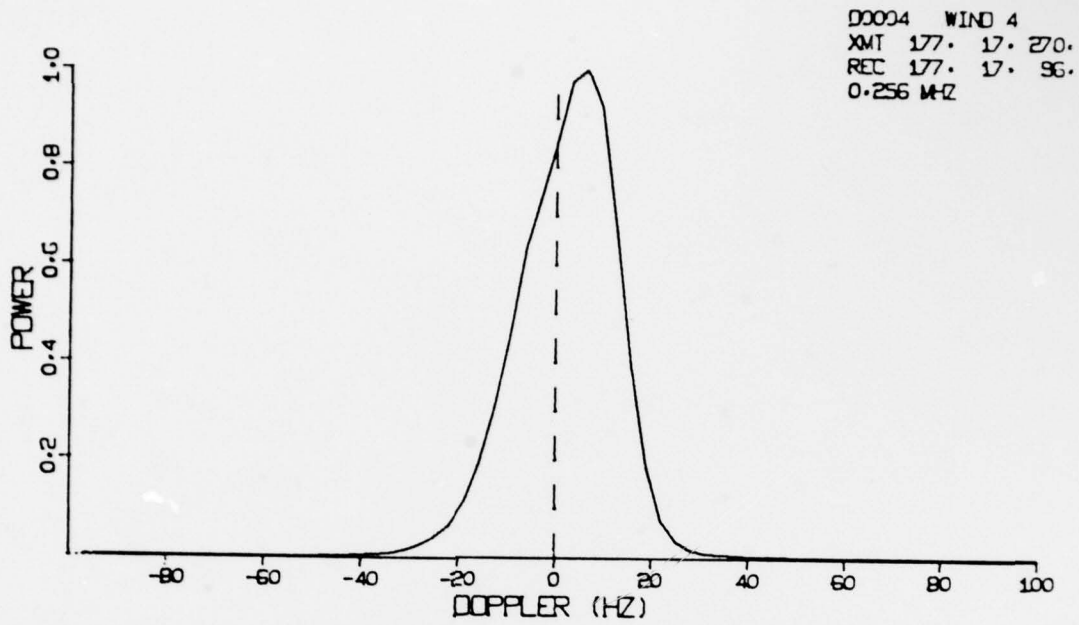

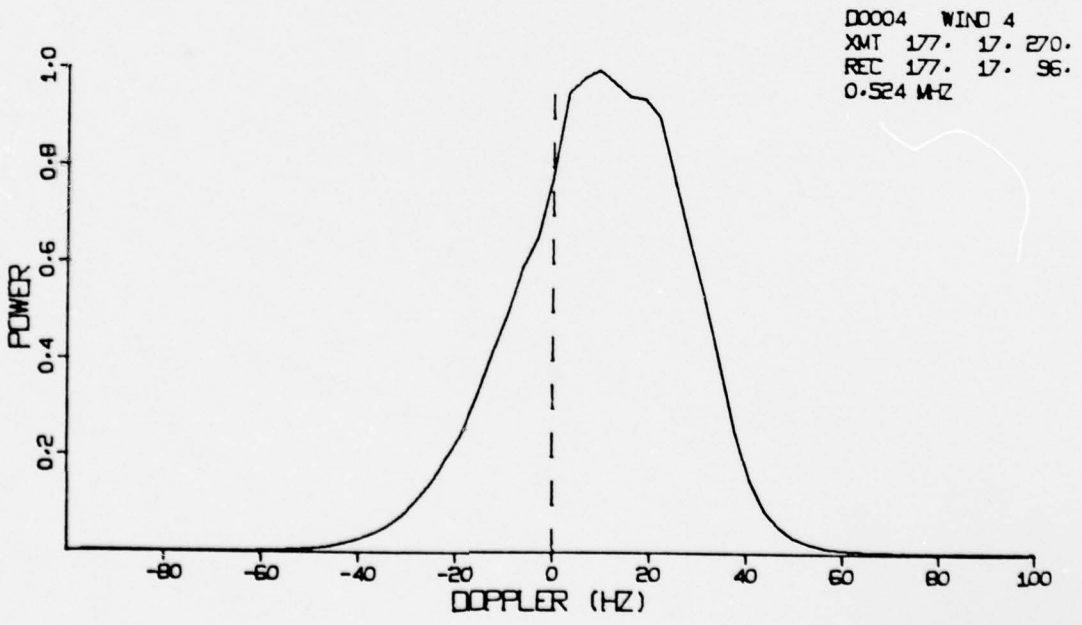

Figure 47(a): - Frequency spread spectrum taken at 17 deg. grazing angle and a 6 deg. "dogleg" alignment shift from a crosswind orientation.

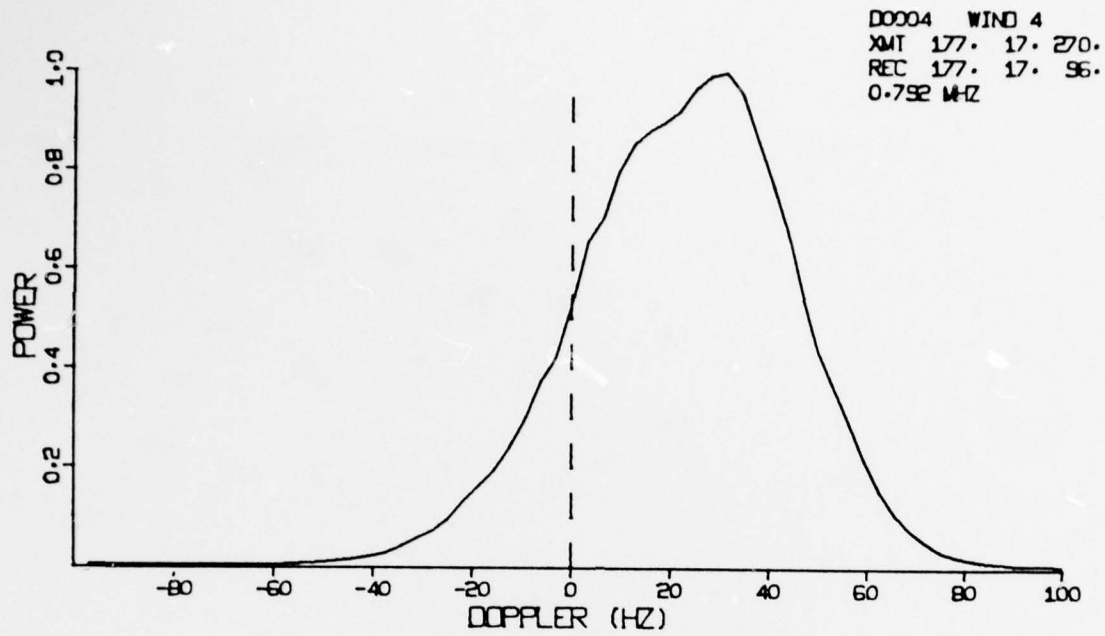

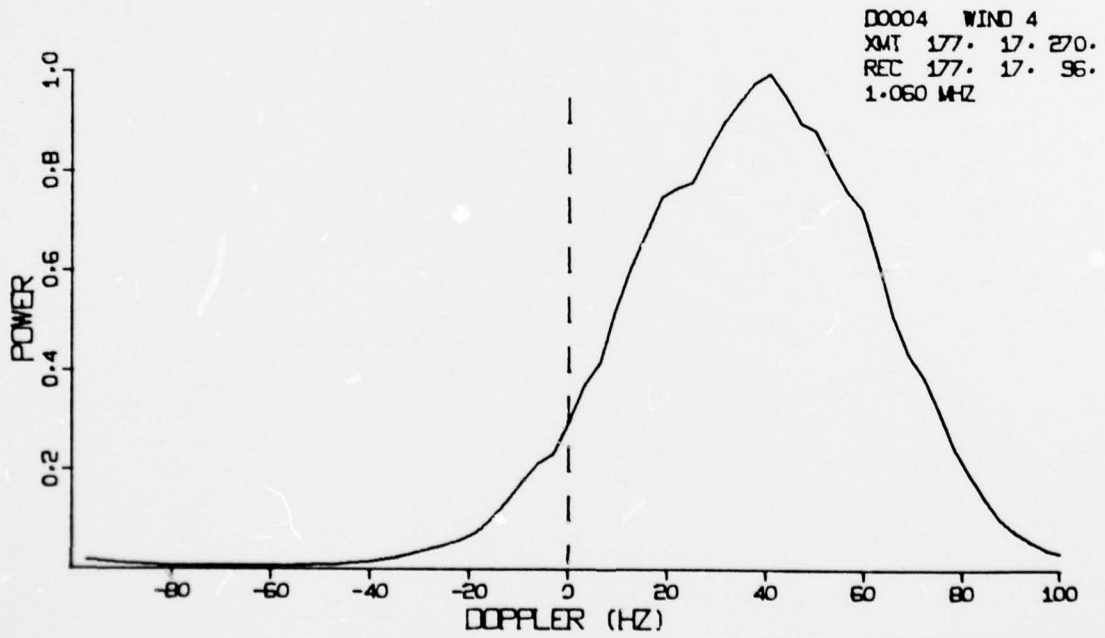

Figure 47(b): - Frequency spread spectrum taken at 17 deg. grazing angle and a 6 deg. "dogleg" alignment shift from a crosswind orientation.

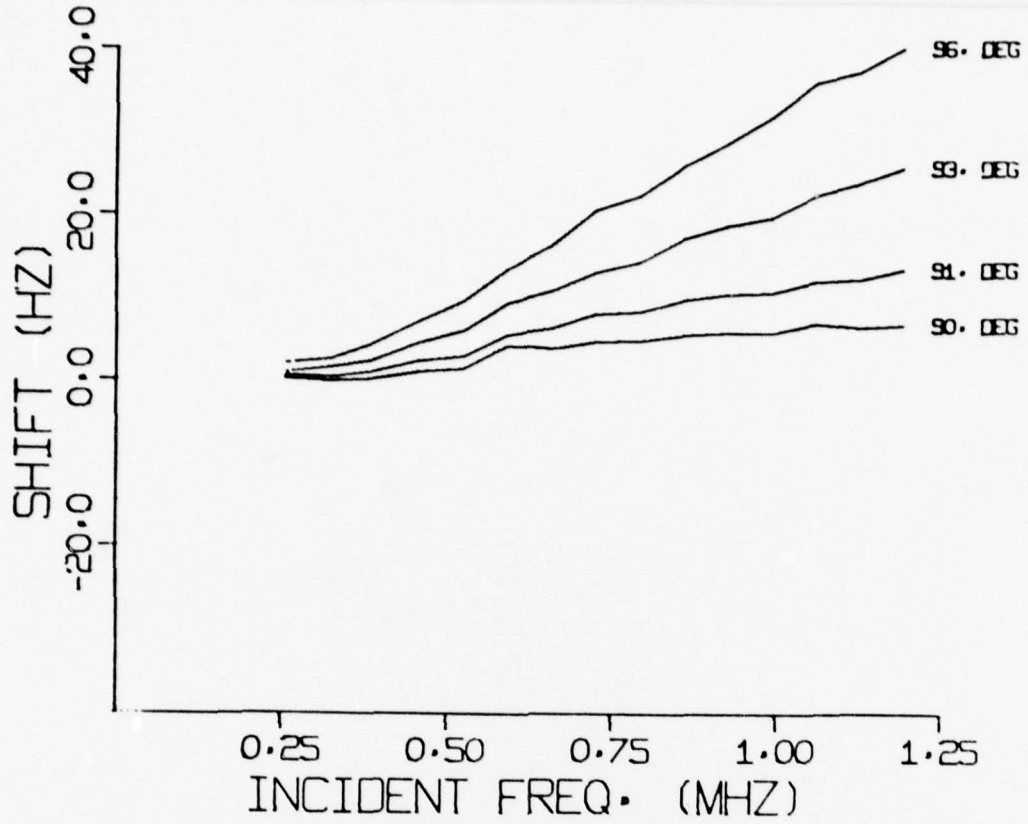

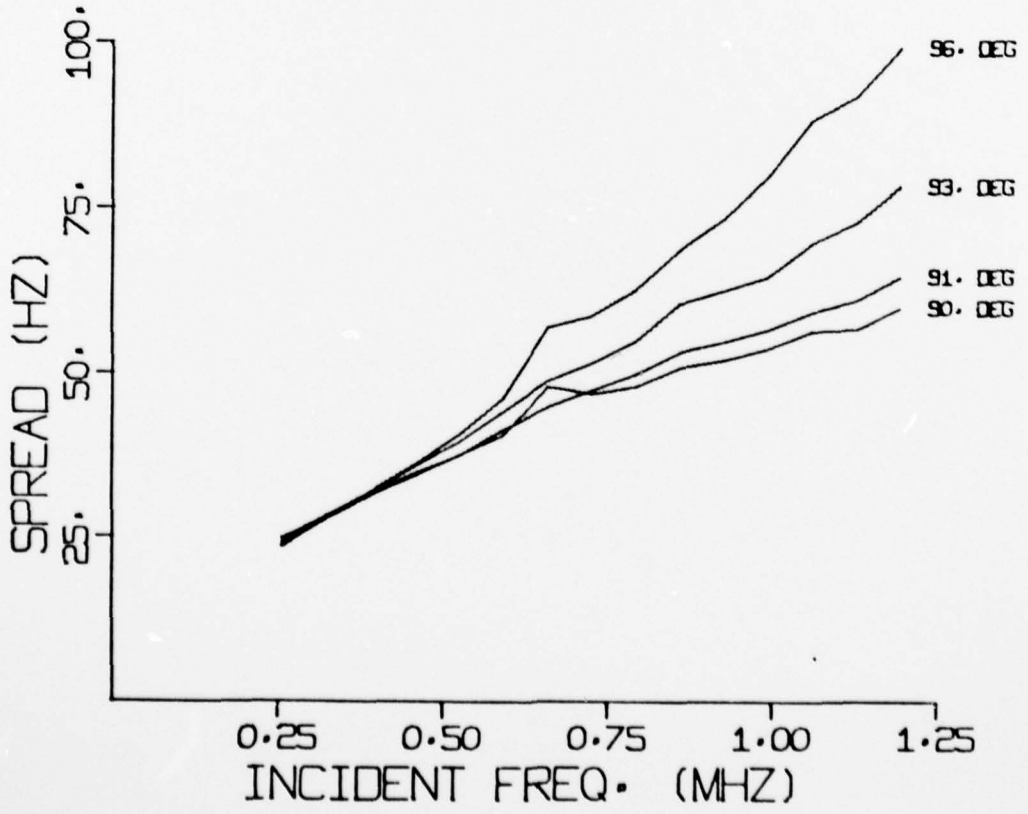

Figure 48: - Mean frequency shift and RMS spread at 17 deg. grazing angle for several clockwise "dogleg" alignment shifts from a crosswind orientation.

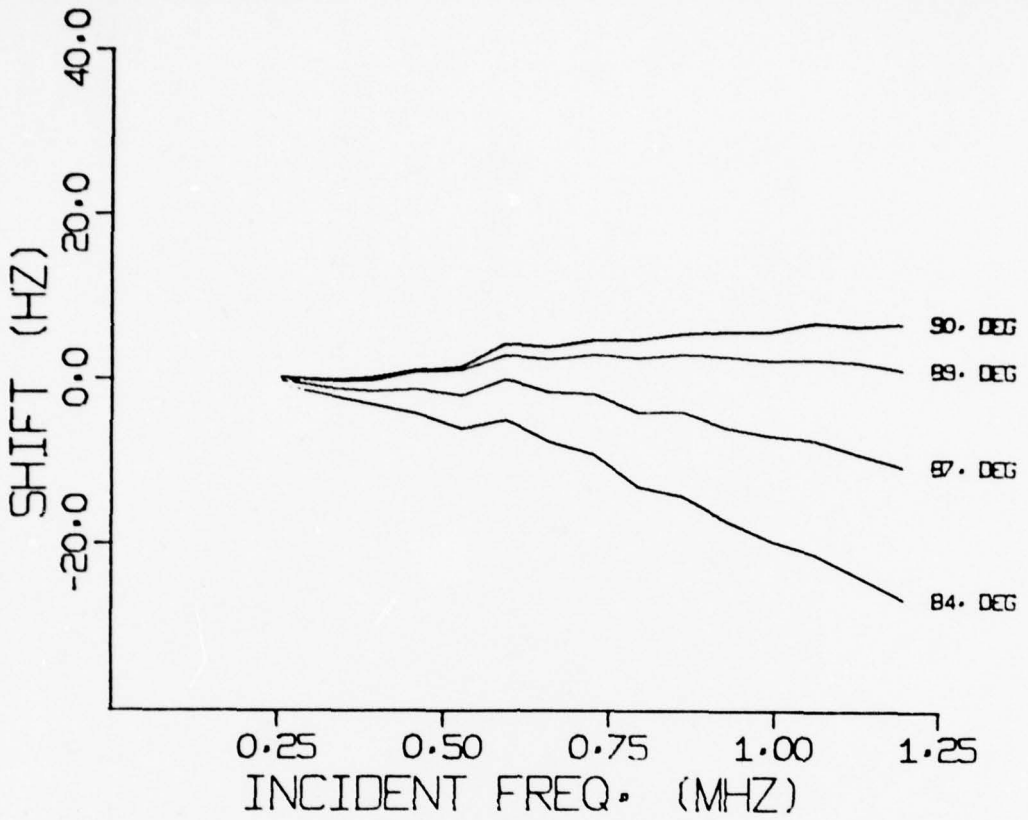

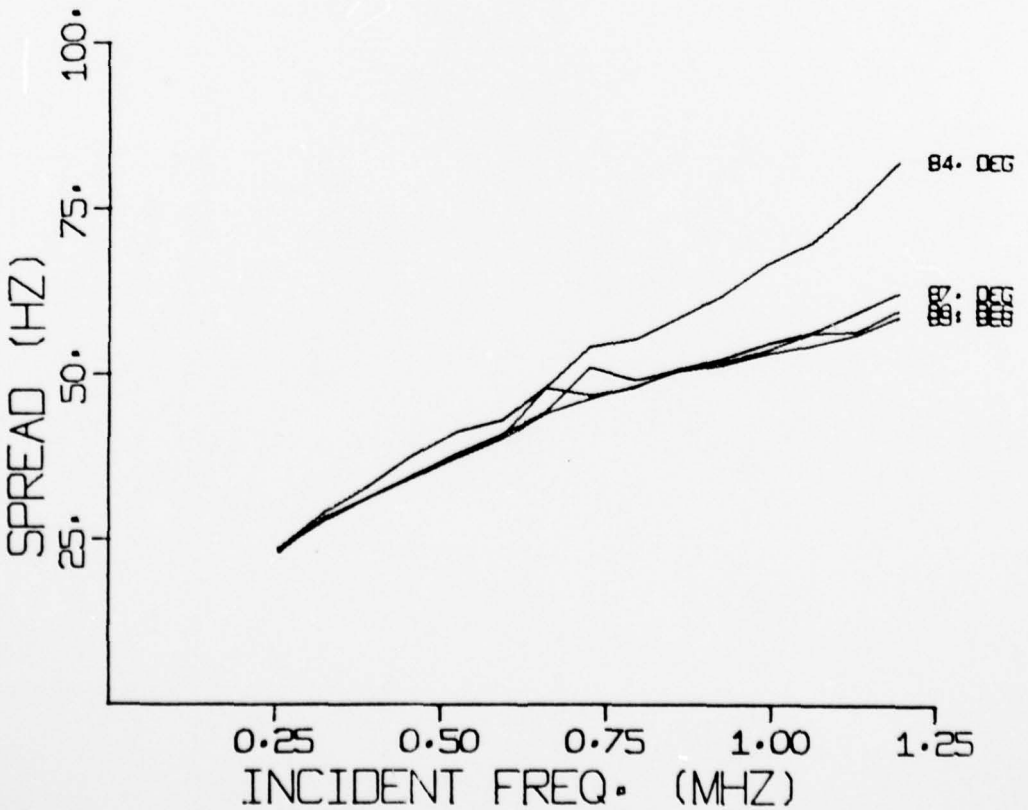

Figure 49: - Mean frequency shift and RMS spread at 17 deg. grazing angle for several counterclockwise "dogleg" alignment shifts from a crosswind orientation.

small up shift is apparent, increasing with carrier frequency.

In order to test sensitivity to alignment, the receiver was moved 6° in azimuth while maintaining grazing angle and range. This type of misalignment has the effect of shifting the center of the Fresnel zones on the surface, the specular point, out of the center of the transducer beam patterns and of shifting the specular path with respect to the wind direction, but only slightly. The results, shown in Figure 47, demonstrate the very large change in Doppler shift produced by a misalignment of this type. When carefully surveyed, the transducers are oriented to within a small fraction of a degree. A summary of this experiment repeated for several "dogleg" angles is given as Figures 48 - 49. As can be seen the results are quite regular.

In order to test the sensitivity of the spreading to wind direction a number of runs were taken at specular alignment, but at various orientations to the wind. Several of these are given as Figure 50 for a single carrier frequency. As can be seen, the neither the spread nor the shift is sensitive to the exact wind direction.

Finally, the transducer alignment experiment was repeated in the up/down wind orientation. The result, Figures 51 - 55, showed only a very small sensitivity.

The particular sensitivity in the crosswind direction, the authors

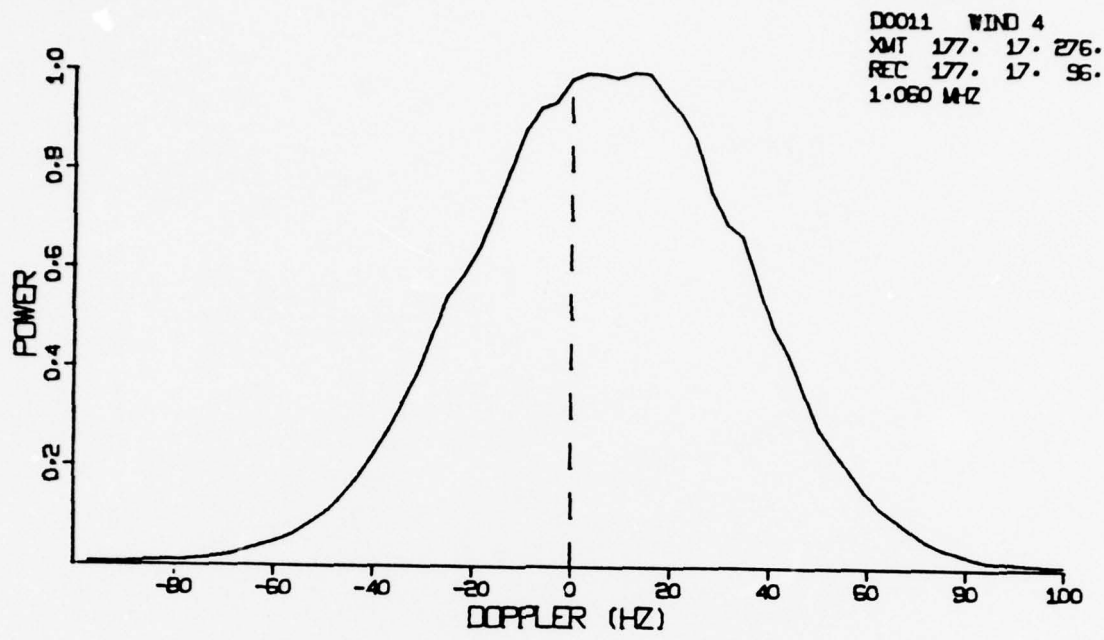

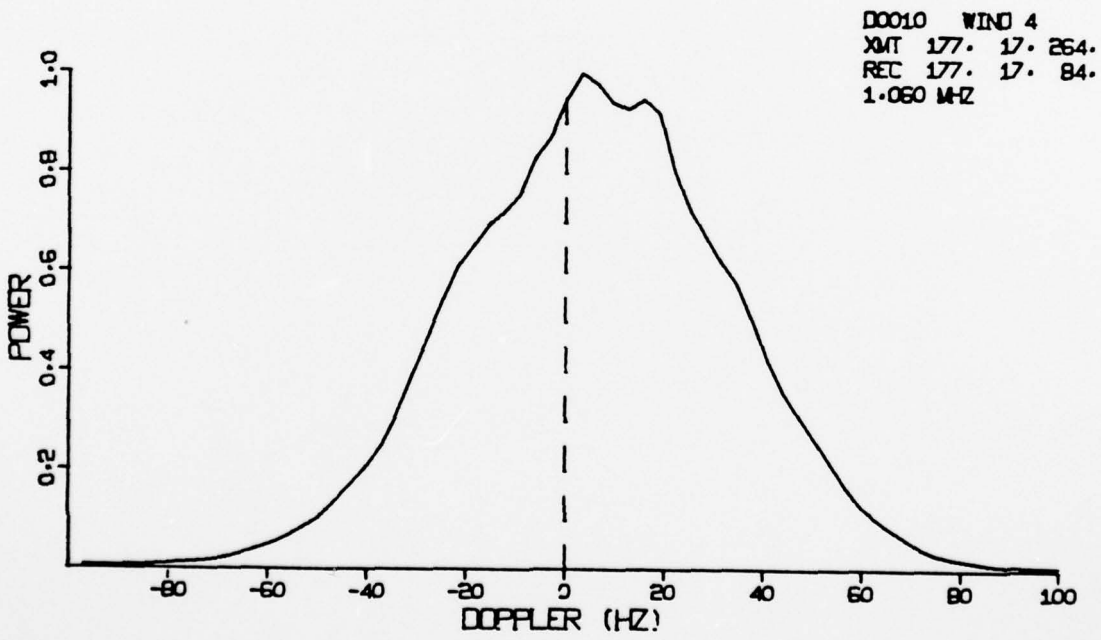

Figure 50(a): - Frequency spread spectrum at 1.06 mHz. for 6 deg. rotations of the transmitter - receiver pair clockwise (above) and counterclockwise (below) with respect to the wind.

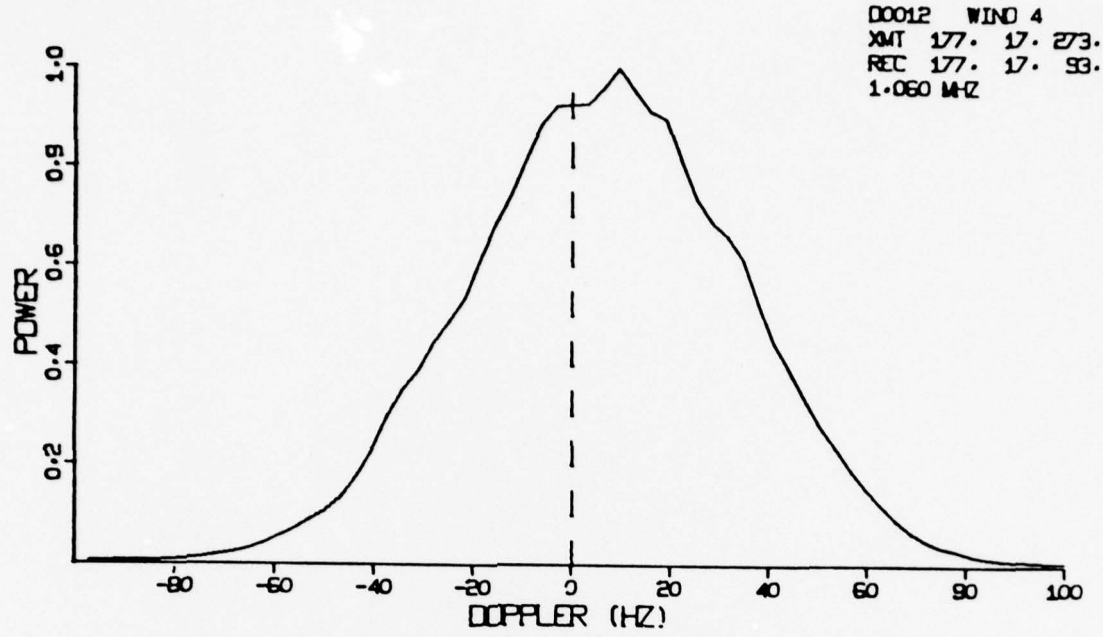

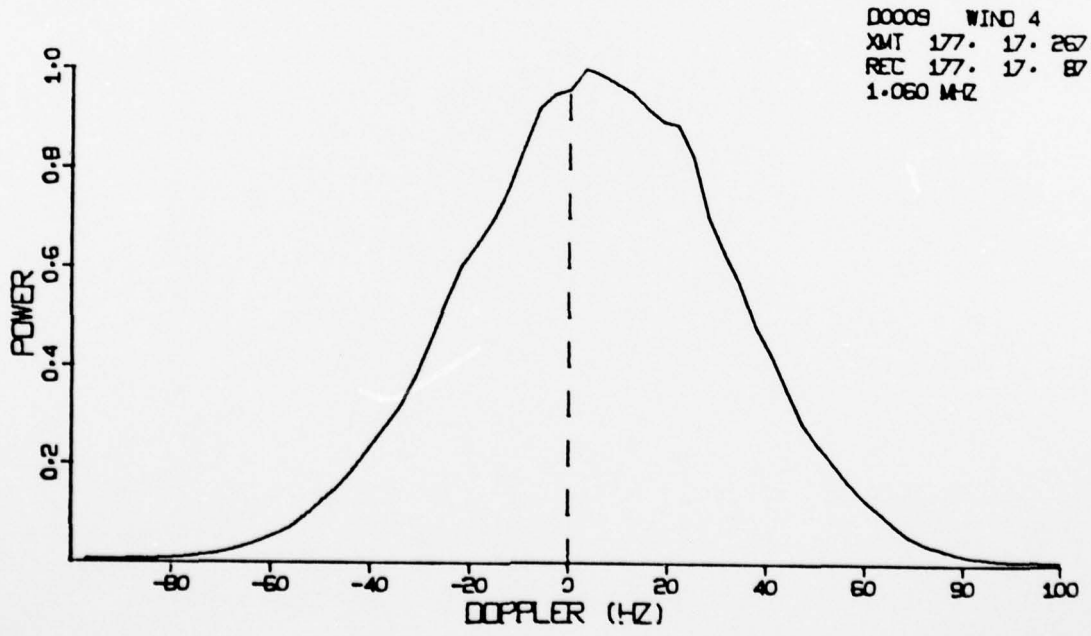

Figure 50(b): - Frequency spread spectrum at 1.06 mHz. for 3 deg. rotations of the transmitter - receiver pair clockwise (above) and counterclockwise (below) with respect to the wind.

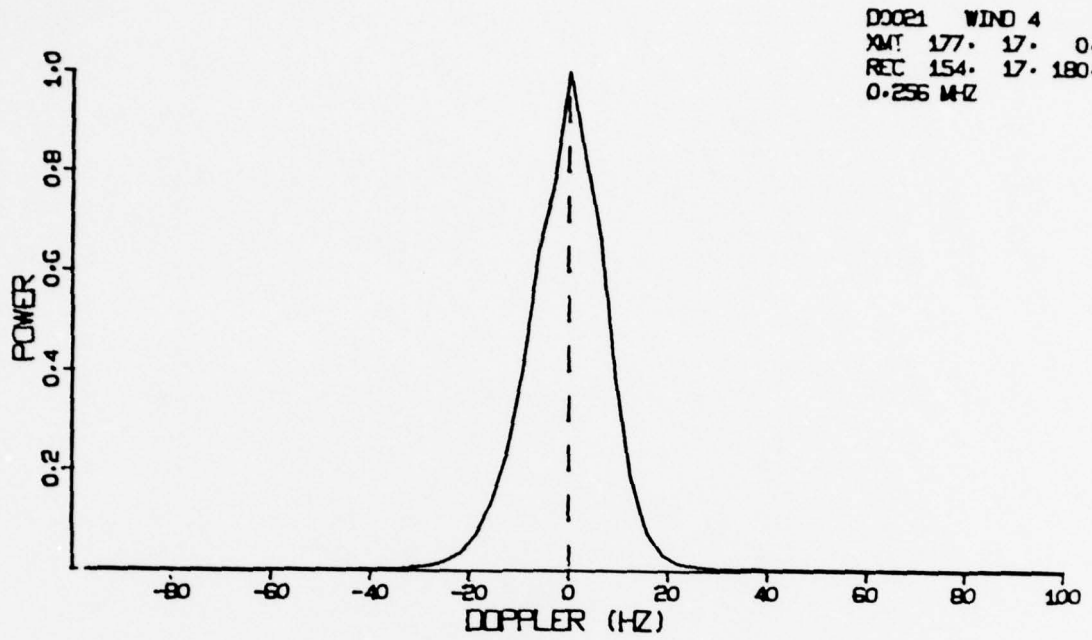

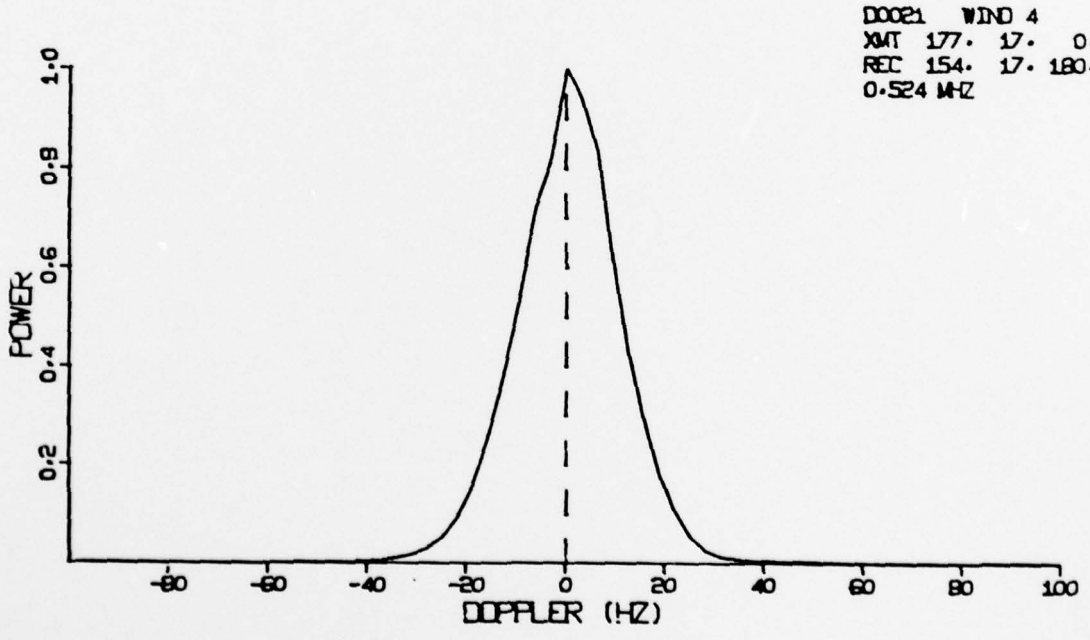

Figure 51(a): - Frequency spread spectrum taken at 17 deg. grazing angle and well surveyed downwind orientation.

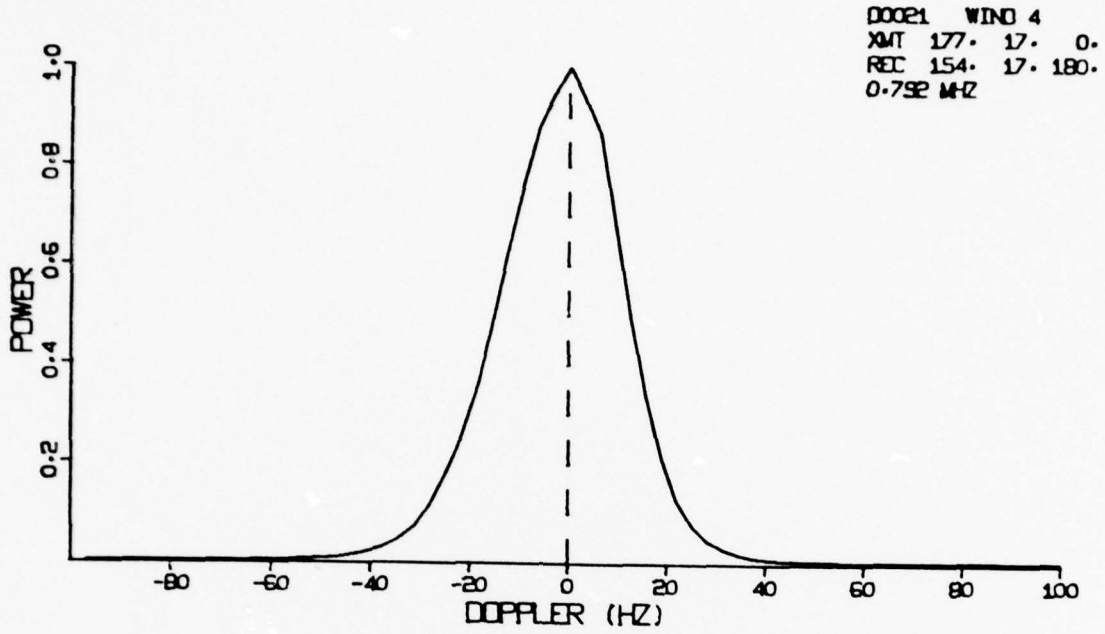

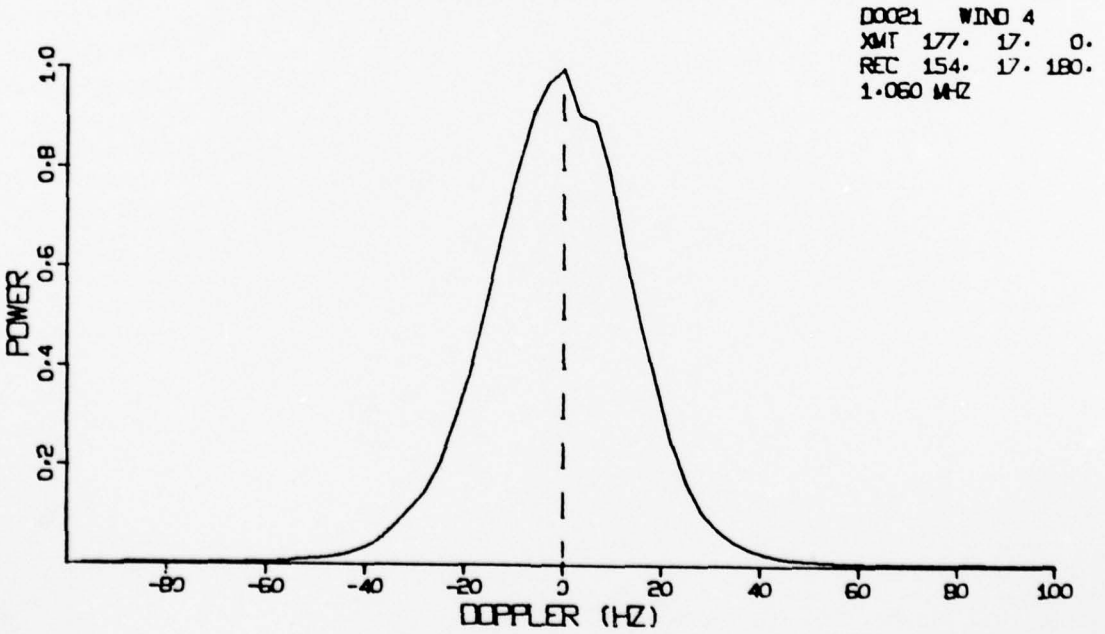

Figure 51(b): - Frequency spread spectrum taken at 17 deg. grazing angle and well surveyed downwind orientation.

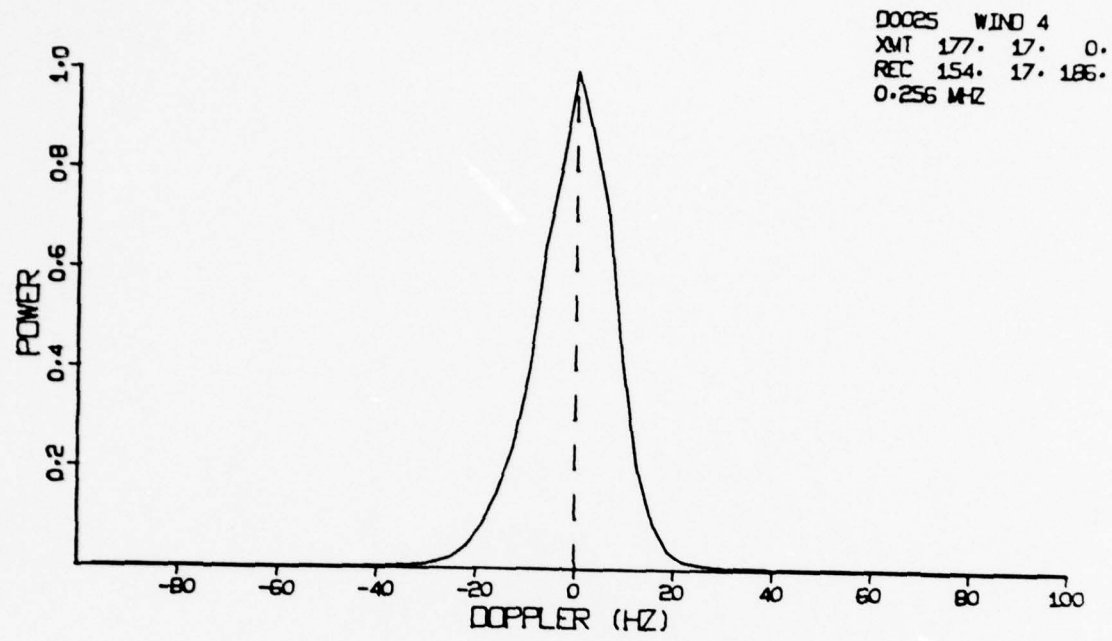

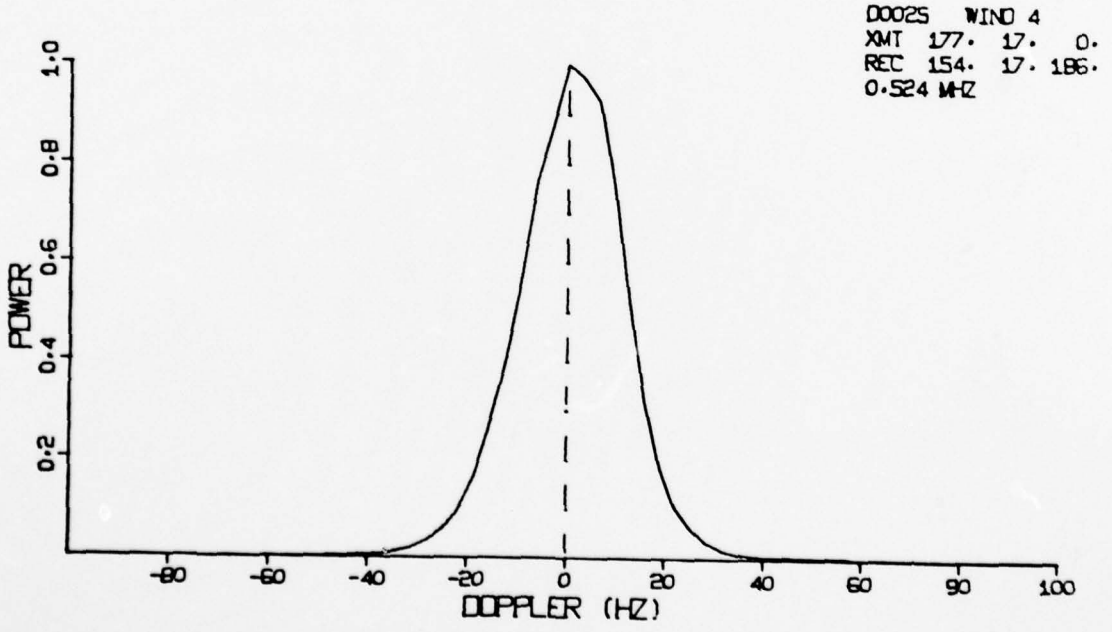

Figure 52(a): - Frequency spread spectrum taken at 17 deg. grazing angle and a 6 deg. "dogleg" alignment shift from a downwind orientation.

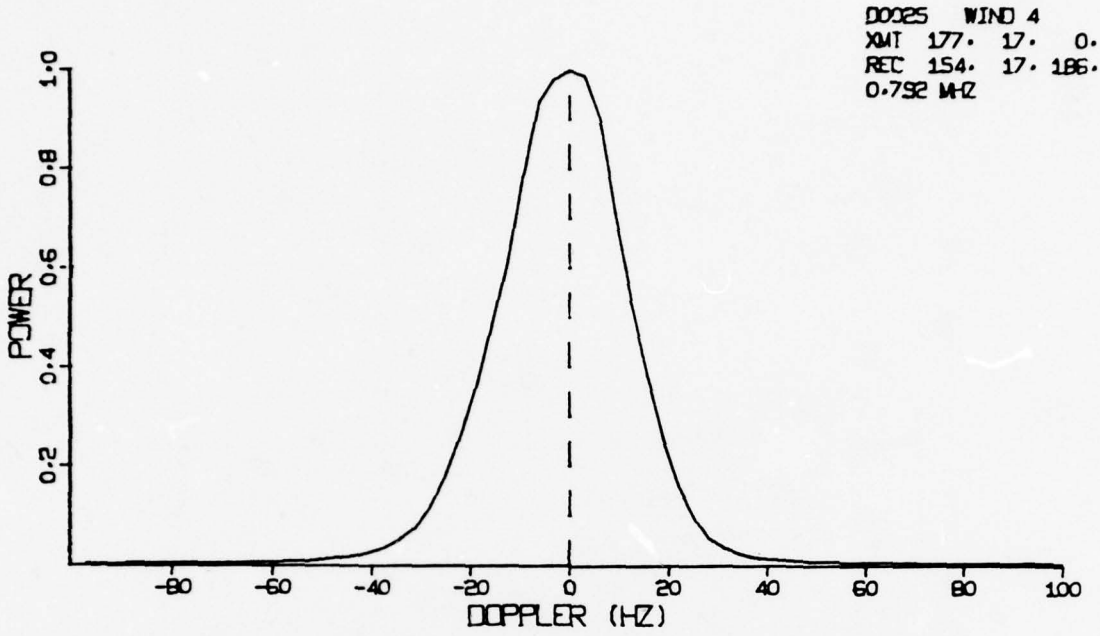

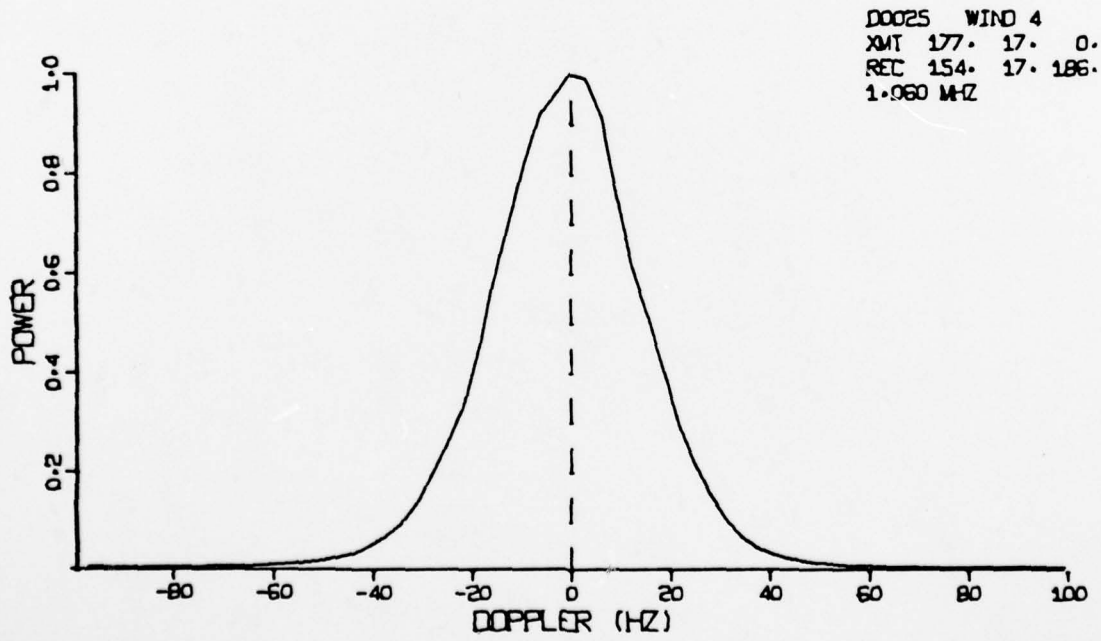

Figure 52(b): - Frequency spread spectrum taken at 17 deg. grazing angle and a 6 deg. "dogleg" alignment shift from a downwind orientation.

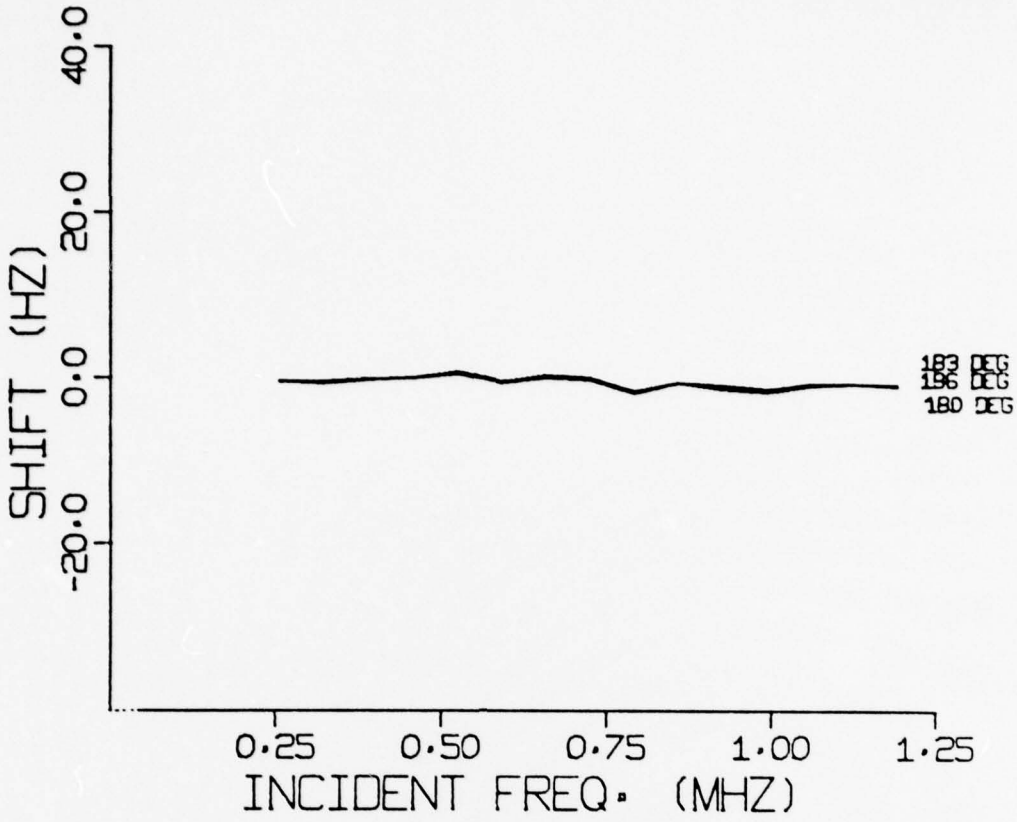

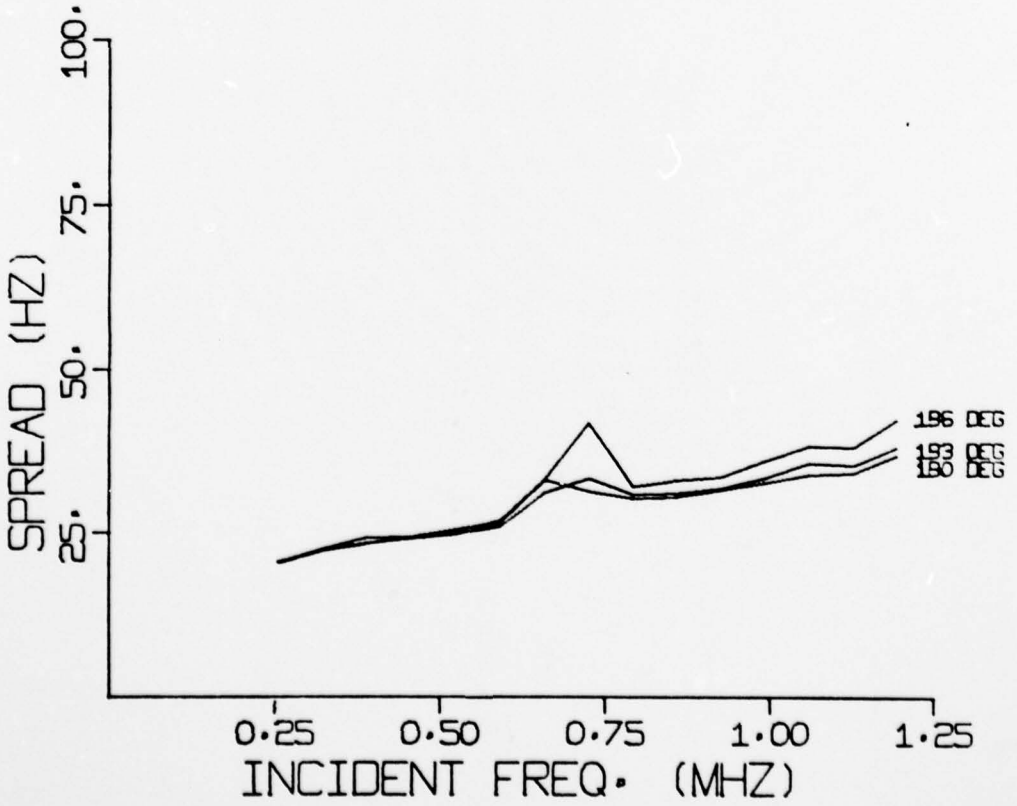

Figure 53: - Mean frequency shift and RMS spread at 17 deg. grazing angle for several clockwise "dogleg" alignment shifts from a downwind orientation.

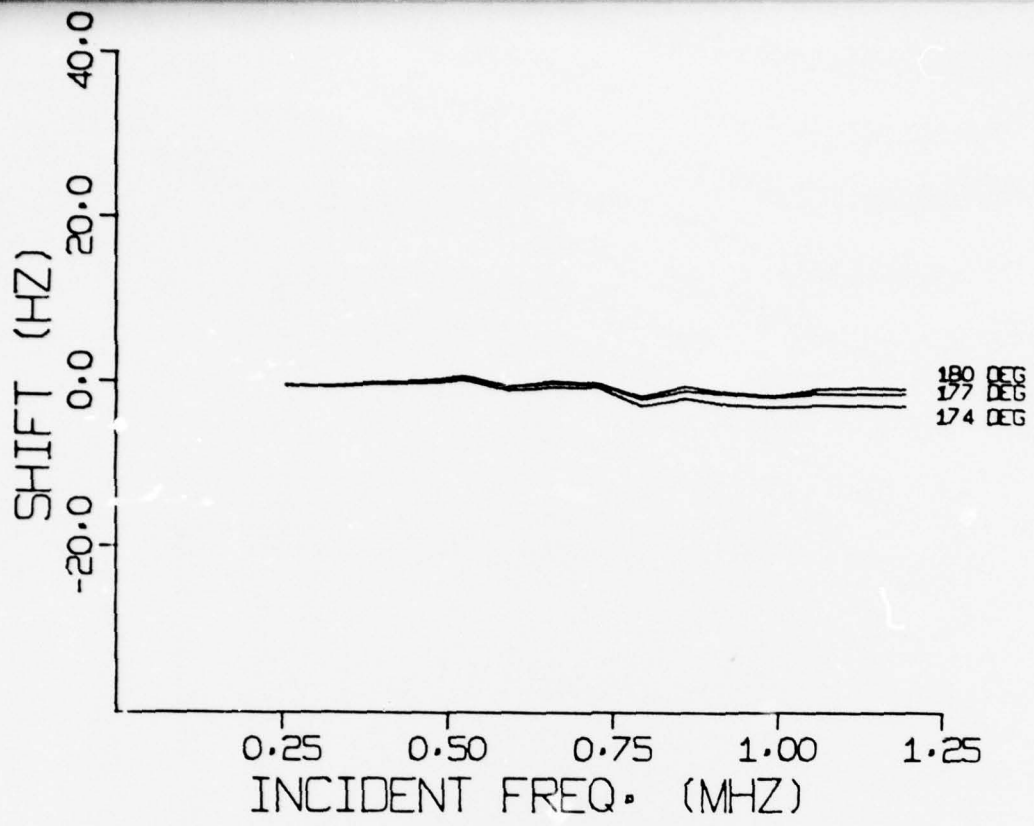

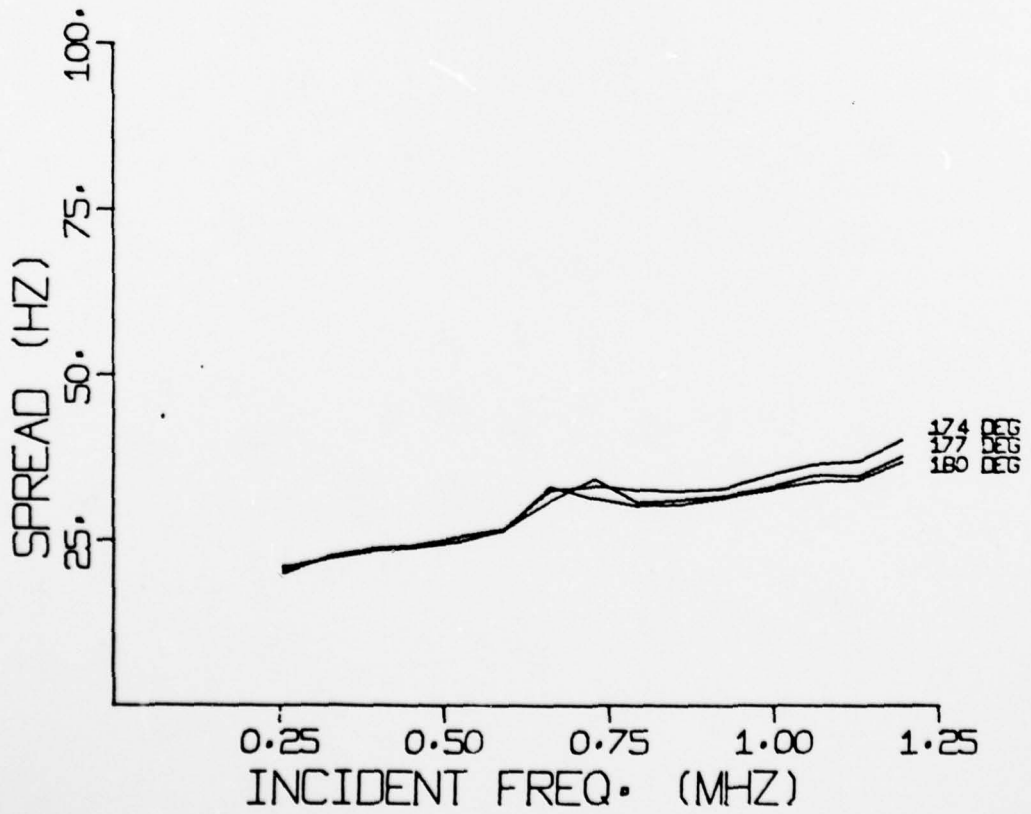

Figure 54: - Mean frequency shift and RMS spread at 17 deg. grazing angle for several counterclockwise "dogleg" alignment shifts from a downwind orientation.

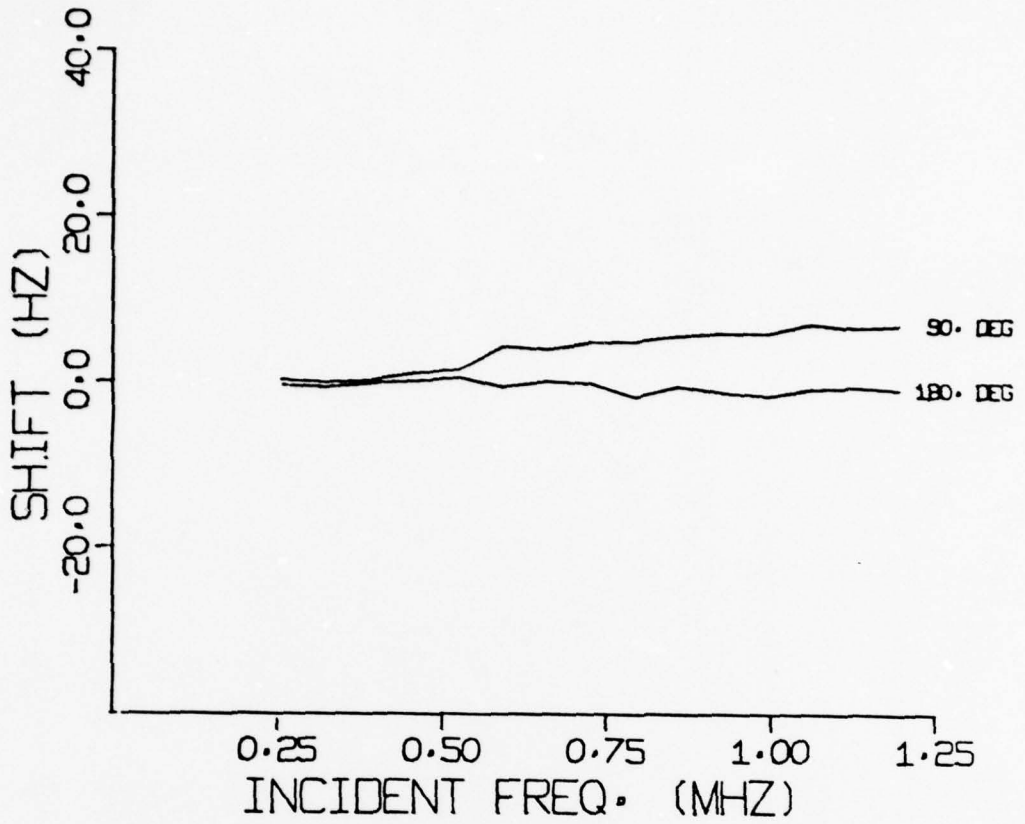

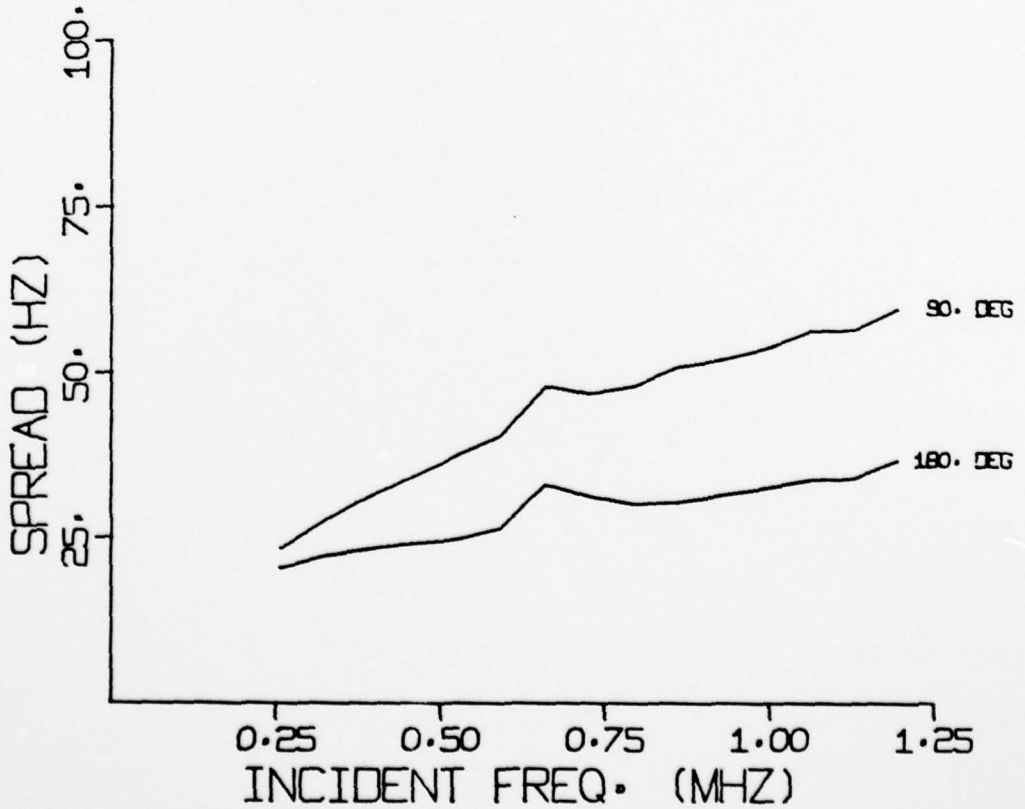

Figure 55: - Comparison of frequency shift and spread observed at exact transducer alignment in crosswind and up_/downwind orientation.

believe, can only be attributed to asymmetry in the wind driven surface. The exact mechanism is the subject of the theoretical investigation referred to above. In general qualitative terms the shift in the case of exact alignment can be seen as the result of unequal contribution to the scattered signal from portions of the surface up and down wind from the specular point. This unequal contribution, we suggest, is due to the asymmetry of the shape of the surface that result from the fact that it is wind stressed. In the case of misalignment, the shift probably results from asymmetric weighting of contributions from the surface due to the transducer pattern misalignment; wind direction has apparently little effect.

7. Conclusion: It can readily be seen that this report is a summary of the current state of a number of projects in progress. The main thrust of the contract under which this work has been supported has been a better understanding of the reverberation from rough surfaces, especially in bistatic configurations and at low grazing angles. The scattering strength measurements, surface slope measurements and facet model development have led us to believe that the primary mechanism involved in low angle backscatter is diffraction and that the model has a high probability of developing into a useful predictive tool. However, at present there are substantial analytical obstacles to the development of a full facet model which must either be overcome or sidestepped. It seems clear that the scattering strength observed at

AD-A078 434 YALE UNIV NEW HAVEN CT SYSTEMS AND INFORMATION SCIENCES F/G 20/1
SURFACE SCATTERING STUDIES.(U)
AUG 79 J G ZORNIG , P M SCHULTHEISS N00014-75-C-1014
UNCLASSIFIED S/IS-7905 NL

2 OF 2
AD
A078434

END
DATE
FILMED
1-80
DDC

long wavelengths has turned out to be considerably higher than that measured at very short wavelengths. However, additional measurements at a variety of wavelengths both intermediate and much longer are feasible and desirable as guidance in testing the model.

The nature of frequency spreading behavior has become somewhat clearer as a result of the sensitivity tests, but a full explanation is still not available. Recently, two ocean experiments have been conducted which will provide an additional basis for comparison with theory. In addition, the availability of a complete second order description of the model tank surfaces used in these studies will permit comparison with general Helmholtz integral formulations. The authors wish to point out that the data presented in this report are representative of a large base of data obtained through experimentation and analysis which has not been included for reasons of clarity and economy. These data are, however, available to interested researchers on request.

REFERENCES:

L. C. Bobb, G. Ferguson, and M. Rankin: "Capillary wave measurements," Applied Optics 18, 1167-1171, 1979

C. Cox and W. Munk: "Statistics of the sea surface derived from sun glitter," J. Mar. Res. 13, 198-227, 1954

C. Cox: "Measurements of slopes of high-frequency wind waves," J. Mar. Res. 16, 199-225, 1958

C. S. Clay and H. Medwin: "Dependence of spatial and temporal correlation of forward-scattered underwater sound on the surface statistics: Part I," J. Acoust. Soc. Amer. 47, 1412-1418, 1970

D. E. Kerr (ed.): "Propagation of short radio waves," M.I.T. Radiation Laboratory Series 13, pp. 445-469, McGraw Hill, NYC, 1951

J. W. Goodman: "Introduction to Fourier optics," McGraw Hill, NYC, 1968

E. Y. Harper and F. M. LaBianca: "Perturbation theory for scattering of sound from a point source by a moving rough surface in the presence of refraction," J. Acoust. Soc. Am. 57, 1044-1051, 1975

David Middleton: "Doppler effects for randomly moving scatterers and platforms," J. Acoust. Soc. Am. 61, 1231-1250 (1977)

E. E. Mikeska and C. M. McKinney: "Range dependence of underwater echoes from randomly rough surfaces," J. Acoust. Soc. Amer. 63, 1375-1380, 1978

J. C. Novarini and H. Medwin: "Diffraction, reflection, and interference during near-grazing and near-normal ocean surface backscattering," J. Acoust. Soc. Amer. 64, 260-268, 1978

R. B. Patterson: "Backscatter of Sound from a Rough Boundary," J. Acoust. Soc. Amer. 35, 2010-1013, 1963

R. B. Patterson: "Model of a Rough Boundary as a Backscatterer of Wave Radiation," J. Acoust. Soc. Amer. 36, 1150-1153, 1964

L. L. Scharf and R. L. Swarts: "Acoustic scattering from a stochastic sea surface," J. Acoust. Soc. Am. 55, 247-253, 1974

A. H. Schooley: "Double, triple, and higher-order dimples in the profiles of wind-generated water waves in the capillary-gravity transition region," J. Geophys. Res. 65, 4075-4079, 1960

V. Sturm and F. Y. Sorrell: "Optical wave measurement and experimental

comparison with conventional wave height probes," Applied Optics 12, 1928-1933, 1973

F. B. Tuteur, H. Tung and J. G. Zornig: "Asymmetric doppler amplitudes in the surface scatter channel, crosswind transmitter-receiver geometry," (to be published, 1979)

J. Wu: "Slope and curvature distributions of wind disturbed water surface," J. Optical Soc. Amer. 61, 852-858, 1971

J. Wu: "Directional slope and curvature distributions of wind waves," J. Fluid Mech. 79, 463-480, 1977

J. G. Zornig, J. F. McDonald: "Direct measurement of surface-scatter channel coherence by impulse probing," J. Acoust. Soc. Am., 55, 1205-1211 (1974)

J. G. Zornig: "Bistatic surface scattering strength measured at short wavelengths," J. Acoust. Soc. Am. 63, 758-767, 1978

J. G. Zornig: "Physical model studies of forward surface scatter frequency spreading," J. Acoust Soc. Am. 64, 1492-1499, 1978